Zeitschrift: IABSE congress report = Rapport du congrès AIPC = IVBH Kongressbericht

Band: 13 (1988)

Rubrik: I. Structural response under exceptional circumstances

SEMINAR

I

Structural Response under Exceptional Circumstances

Comportement des structures dans des circonstances exceptionnelles

Verhalten von Bauwerken unter aussergewöhnlichen Umständen

Chairman: A.L. Bouma, the Netherlands

Technical Adviser: R. Fechtig, Switzerland

Leere Seite
Blank page
Page vide

Die Theorie der Brauchbarkeit veränderter Tragwerke

Theory concerning the application of changed structures

Possibilité d'utilisation d'une construction modifiée

Karel CHOBOT
Prof.Ing.DrSc.
TU Prag
Prag, ČSSR

Karel Chobot, geboren 1929, promovierte als Bauingenieur auf der Fakultät für Bauingenieurwesen TU Prag. Seit 1951 arbeitet am Lehrstuhl für Baumechanik der Baufakultät TU Prag, zur Zeit als Professor.

ZUSAMMENFASSUNG
Bei Rekonstruktionen oder Havarien von Stabtragwerken ändert sich das statische Modell des Tragsystems und dadurch auch die Beanspruchung von einzelnen Elementen. Der Einfluss der Abschaffung eines Stabes des ursprünglichen Systems auf die Veränderungen der inneren Kräfte in den restlichen Stäben ist analysiert worden. Es hat sich herausgestellt, dass bestimmte Gesetzmässigkeiten der Ausbreitung dieser Veränderungen festgestellt und die entsprechenden Veränderungsbereiche geometrisch definiert werden können.

SUMMARY
In reconstructions or during failure of frame systems the statical model of the bearing structure and thus also the stress state in the individual elements undergoes a change. An analysis has been carried out of the influence of releasing one of the beams of the original system on the changes of the internal forces in the remaining beams. It has been shown that certain rules governing the distribution of these changes can be determined and their range of applicability defined.

RÉSUMÉ
A la suite de reconstruction ou de dommage sur des ossatures, le modèle statique du système porteur change de même que l'état de contraintes des différents éléments. L'influence de la disparition d'un élément du système original est étudiée avec les modifications des efforts intérieurs dans le reste du système. Certaines règles relatives à la distribution de ces efforts peuvent être détérminées de façon géométrique.

1. EINLEITUNG

Bei Rekonstruktionen oder Havarien von Rahmen ändert sich das statische Modell des Tragsystems. Die Beanspruchung von einzelnen Elementen wird also auch geändert. Jedenfalls ist das modifizierte Tragsystem neu zu berechnen. Für grosse und komplizierte Tragwerke kann die neue Berechnung sehr zeitraubend und kostspielig sein. Die Beurteilung der Tragfähigkeitsverminderung oder die Entscheidung, ob ein Teil des Tragsystems rekonstruiert werden soll, kann durch eine vorläufige Abschätzung von Beanspruchungsveränderungen wesentlich erleichtert werden. Dadurch werden Zeit und Kosten gespart. Wir haben uns deswegen bemüht, die Gesetzmässigkeiten der Ausbreitung von Beanspruchungsveränderungen in einzelnen Stabelementen nach der Abschaffung eines Stabes zu finden. Die Berechnungen haben wir für mehr als vierzig ebene und räumliche Stabtragwerke durchgeführt. Die Ergebnisse wollen wir an zwei Beispielen von ebenen Tragwerken demonstrieren. Es werden dabei zwei Gruppen von Tragsystemen unterschieden: sgn. "hohe" Systeme und "breite" Systeme (nach der Proportion der Geschossanzahl und der Anzahl der Felder). Wir haben nur prismatische Stäbe, gleichmässige Belastung der Querriegel und einseitige Windbelastung in Betracht gezogen. Systeme, die nach der Abschaffung eines Stabes instabil werden, haben wir ausser Betracht gelassen (d.h. statisch bestimmte Systeme oder Systeme mit nur einem Feld, in dem z.B. eine Stütze im ersten Geschoss beseitigt ist usw.).
Es hat sich herausgestellt, dass für die Veränderung von Biegemomenten und Normalkräften bestimmte Gesetzmässigkeiten festgestellt werden können. Bei der Auswertung von Veränderungen wurden prozentuale Differenzen benutzt. Es wurden die Differenzen von 2%, 5% und 10% im Vergleich mit dem ursprünglichen Zustand ausgewertet. Es ist dabei zu unterscheiden, ob eine innere oder äussere Stütze oder ein Querriegel beseitigt wurde.
In den Bildern sind die Veränderungsbereiche in folgender Weise markiert: Volle Linien schliessen Bereiche der Veränderungen von mehr als 10%, gestrichelte Linien von mehr als 5%, punktierte Linien von mehr als 2% ein. In den restlichen Stäben ergeben sich nur bedeutungslose Veränderungen. In Fig. 1-3 bezeichnet das Symbol x positive Veränderungen von Biegemomenten in Endquerschnitten, das Symbol + positive Veränderungen von Normalkräften, in den restlichen Stäben des Bereiches sind die Veränderungen negativ. Der beseitigte Stab wird durch Pfeile bezeichnet.

2. VERAENDERUNGEN VON BIEGEMOMENTEN

2.1. Erste Gruppe

Es wurde eine äussere Stütze beseitigt. In diesem Fall erfolgt die 10% Veränderung der Biegemomente im ganzen oberen Bereich des Tragwerkes über der beseitigten Stütze. Unterhalb dieser Stütze traten die Veränderungen höchstens in einem Geschoss ein. Die Bereiche von 5% und 2% Veränderungen verlaufen analog. Die graphische Darstellung des Veränderungsbereiches hat eine ovale Form. Der beseitigte Stab befindet sich im rechten oder linken Teil eines Ovals, das sich über das ganze Tragwerk oberhalb des beseitigten Stabes erstreckt. Dieser Bereich wird als "Ovalbereich" bezeichnet (Fig. 1)

2.2. Zweite Gruppe

Die Lage eines beseitigten Querriegels in der Konstruktion spielt keine Rolle. Unabhängig von ihr hat der Veränderungsbereich von Biegemomenten eine näherungsweise elliptische Form. Diese Ellipse schliesst höchstens ein Geschoss oberhalb und ein Geschoss unterhalb des beseitigten Stabes ein. Die Breite der Ellipse ist gleich der Breite des gesamten Tragwerkes. Dieser Bereich wird "der elliptische Bereich" genannt (Fig. 2).

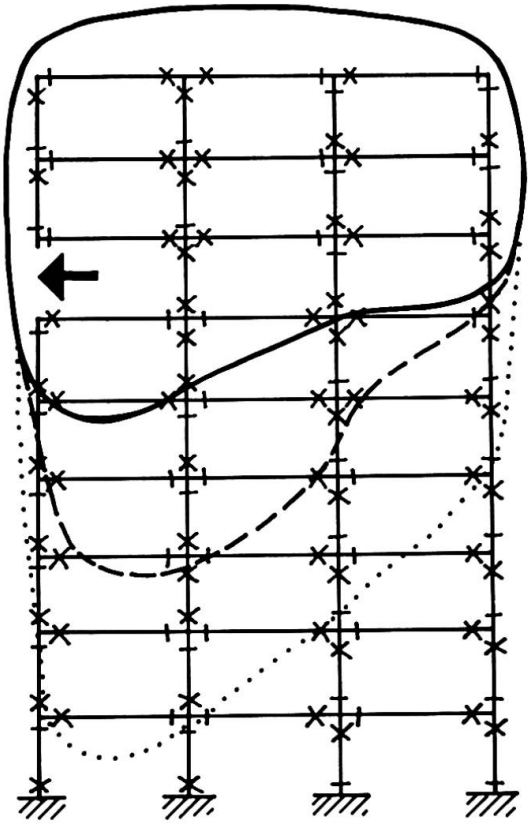

Fig.1 Der Ovalbereich

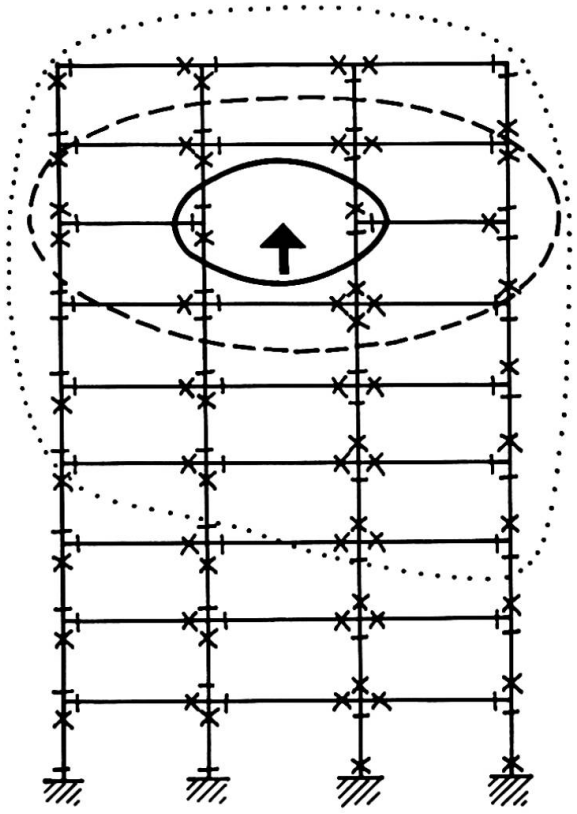

Fig.2 Der elliptische Bereich

2.3. Dritte Gruppe

Es wurde eine innere Stütze beseitigt. In diesem Fall ist der Veränderungsbereich der Biegemomente am interessantesten. Die beseitigte Stütze befindet sich in der Achse der Gebiete, die sich nur in unmittelbar benachbarten Feldern erstrecken. Die Höhe des Bereiches reicht bis zu den letzten Etagen. Unter dem entfernten Stab erfolgen die Veränderungen nur etwa zwei Etagen unterhalb des Stabes. Es ist erstaunlich, dass die unmittelbar benachbarten Stützen unter und über der Stütze kaum beeinflusst werden. Diesen Bereich bezeichnen wir als "Flügelbereich" (Fig. 3).
Alle bisher diskutierten Ergebnisse sind nur für regelmässige Tragwerke gültig. Für Tragwerke mit z.B. nicht durchlaufenden Stützen oder Querriegeln gelten die obigen Schlussfolgerungen nicht.

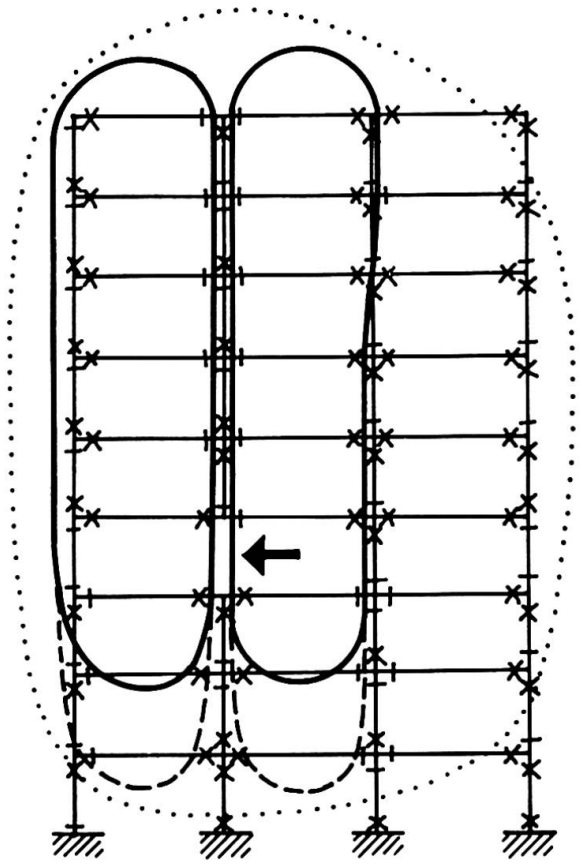

Fig. 3 Eine innere Stütze wurde beseitigt - der Flügelbereich

Für räumliche Stabwerke sind ähnliche Schlussfolgerungen gültig. Nach den Abbildungen ist klar sichtbar, dass man auch für die Vorzeichenveränderungen bestimmte Regeln finden kann. Z.B. für den elliptischen Bereich (Fig. 2) ändern sich die Differenzvorzeichen nach einem "Diagonalsystem".

3. VERAENDERUNGEN VON NORMAL-KRAEFTEN

Um die Bereiche der prozentualen Veränderungen von Normalkräften analog den Veränderungen von Biegemomenten definieren zu können, sind die Veränderungen von Normalkräften getrennt in Stützen und in Querriegeln zu untersuchen.

3.1. Erste Gruppe

Beim Ausfall eines der Querriegel kann der Veränderungsbereich der Normalkräfte in Säulen als ein "Rechteckbereich" bezeichnet werden. Die Normalkräfte ändern sich in den Stäben unter dem entfernten Querriegel (Fig. 4). Bei hohen Systemen können auch zusätzliche Veränderungen auftreten. Diese Anomalien sind dadurch verursacht, dass gleichzeitig eine senkrechte und eine waagrechte Belastung aufgenommen werden (Fig. 5).
Die Veränderungen von Normalkräften in Querriegeln beschränken sich auf einen "elliptischen Bereich" (Fig. 6). Bei breiten Tragsystemen befindet sich der beseitigte Stab ungefähr im Brennpunkt (Stäbe in den Mittelfeldern) der Ellipse. Normalkräfte ändern sich im Bereich von ca. zwei Etagen oberhalb und unterhalb des beseitigten Querriegels. Wenn ein Querriegel im Randfeld beseitigt wird, können die Veränderungen bis in vier Feldern erscheinen. Für hohe Tragsysteme sind praktisch die gleichen Schlussfolgerungen gültig (Fig. 7).

3.2. Zweite Gruppe

Die Lokalisierung der Veränderungsbereiche im Falle einer beseitigen Stütze ist ziemlich kompliziert. In diesem Fall ändern sich die Normalkräfte in den meisten Stäben des Systems. Trotzdem können bei breiten Tragsystemen die Veränderungsbereiche als "Rechteck"- oder "Doppelrechteckbereiche" charakterisiert werden. Dies hängt davon ab, ob eine innere Stütze beseitigt wird. Die Veränderungen erfolgen in zwei bis drei Etagen und Feldern. Die Veränderungen von Normalkräften in Querriegeln erfolgen in mehreren Feldern (Fig. 8, Fig. 9).

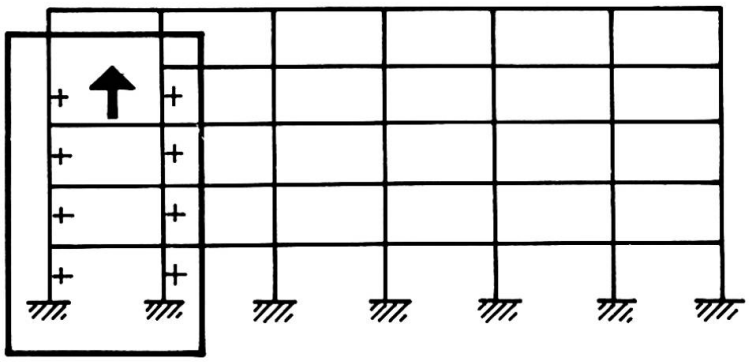

Fig.4 Der Rechteckbereich der Veränderungen von Normalkräften in Säulen bei "breiten" Konstruktionen

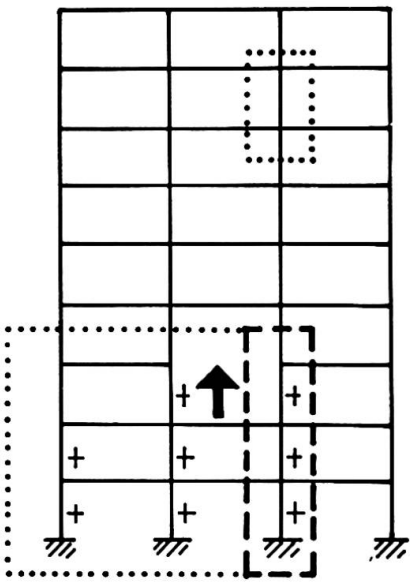

Fig.5 Der Rechteckbereich der Veränderungen von Normalkräften in Säulen in "hohen" Konstruktionen

Aus den Schemen ist sichtbar, dass die Gesetzmässigkeiten der Vorzeichenveränderungen von Normalkräftedifferenzen leichter zu verfolgen sind als diejenigen bei den Biegemomenten. Die angegebenen Kriterien können selbstverständlich die genaue Berechnung des modifizierten Tragsystems nicht ersetzen, die Veränderungsbereiche können jedoch katalogisiert werden. Man kann jedoch auf diese Weise z.B. im Falle einer Beschädigung der Tragwerke schnell beurteilen, welche Teile der Konstruktion sofort zu sichern sind, um eine weitere Beschädigung zu vermeiden. Angaben über die Topologie und Steifigkeit des Tragwerkes und über die Lage des beschädigten Stabes sind dafür ausreichend.

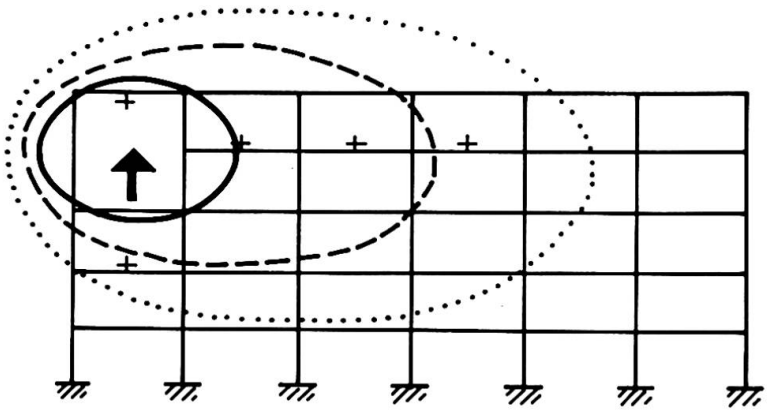

Fig.6 Der elliptische Bereich der Veränderungen von Normalkräften in Säulen in "breiten" Konstruktionen

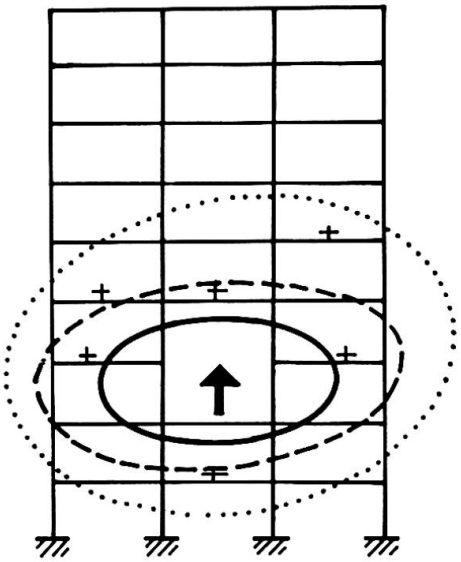

Fig.7 Der elliptische Bereich der Veränderungen von Normalkräften in Riegeln in hohen Konstruktionen

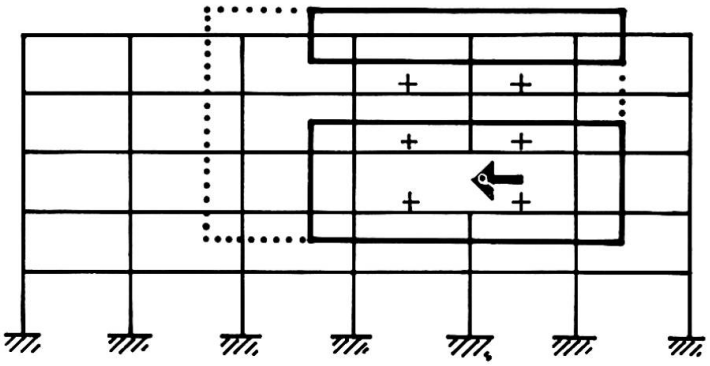

Fig.9 Der Doppelrechteckbereich der Veränderungen von Normalkräften in Riegeln in breite Konstruktion

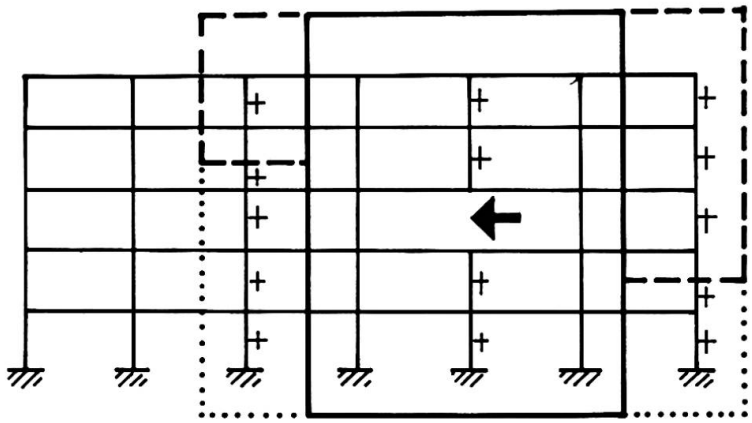

Fig.8 Der Rechteckbereich der Veränderungen von Normalkräften in Säulen in breite Konstruktion

Alternative Bridging Systems in Precast Concrete Structures

Systèmes porteurs alternatifs dans les structures préfabriquées en béton armé

Alternative überbrückende Systeme in Gebäuden aus Stahlbeton-Fertigteilen

Björn ENGSTRÖM
Research Ass.
Chalmers Univ. of Technol.
Göteborg, Sweden

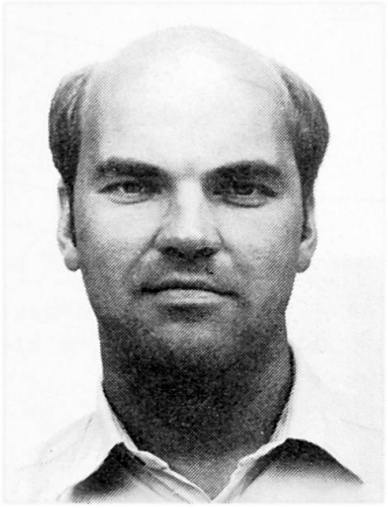

Björn Engström, born 1950, received his M.Sc. degree in Civil Engineering 1974 at Chalmers University of Technology. He is now responsible for a research project on structural connections in precast concrete structures.

SUMMARY
Building structures should be designed to prevent progressive collapse. Primary damage of the structural system can be accepted as long as the overall stability remains and an alternative load-bearing system bridges over the damaged area. An approach for the design and analysis of alternative bridging systems in precast structures is exemplified by means of rotation mechanisms. It is shown how the non-linear behaviour of tie connections affects the dynamic resistance.

RÉSUMÉ
Il faut construire les structures des bâtiments en vue d'éviter un rupture progressive. Un dégât primaire du système structural peut êtère accepté si la stabilité générale est garantie et si un système porteur alternatif peut remplacer la partie détruite. Une méthode pour la construction et l'analyse des systèmes porteurs alternatifs dans les structures du béton armé est illustrée par des mécanismes rotatifs. On montre comment la résistance dynamique est influencée par le comportement non-linéaire des assemblages.

ZUSAMMENFASSUNG
Gebäude müssen so dimensioniert werden, dass ein fortschreitender Zusammenbruch verhindert wird. Primäre Schäden am Tragsystem können akzeptiert werden solange die Gesamtstabilität erhalten bleibt und ein alternatives lasttragendes System den Schaden überbrückt. Eine Methode der Dimensionierung und Analyse von alternativen überbrückenden Systemen in Gebäuden aus Stahlbeton-Fertigteilen ist mit Hilfe von Rotationsmechanismen erklärt. Damit kann gezeigt werden, wie die nichtlineare Wirkungsweise der Zugverbindungen die dynamische Tragfähigkeit beeinflusst.

1. INTRODUCTION

For a certain presupposed local damage in a precast structure, possible collapse mechanisms and the corresponding alternative bridging systems will be determined by the actual joint locations and detailing. The deformations which follow the primary failure may be concentrated to the joints. Accordingly, the resistance of the bridging system will mainly depend on the behaviour of the structural connections which are strained during the transition, for instance tie connections across joints which open up, see Fig. 1.

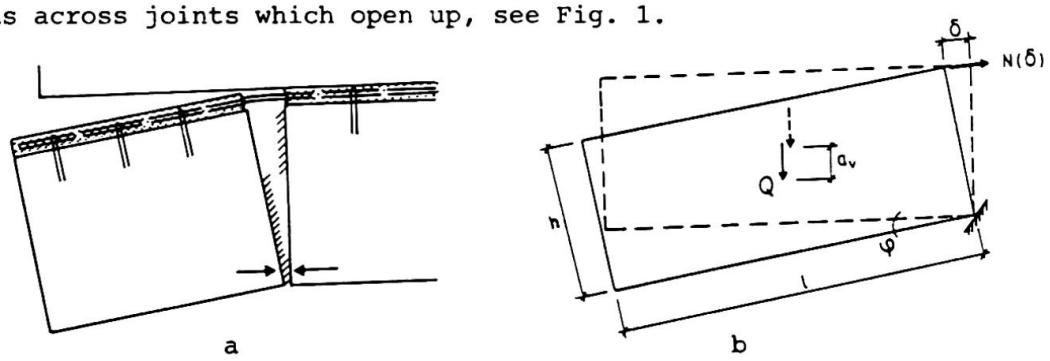

Fig. 1 A wall panel forming an alternative load-bearing system by cantilever action at large plastic deformations of a tie connection
a) example of detailing
b) model for the collapse mechanism

In this paper an approach for the design and analysis of alternative load-bearing systems in precast concrete structures is presented. The aim is to show how the non-linear behaviour of tie connections will affect the dynamic resistance of alternative load-bearing systems. The presentation is limited to systems which can be characterized as rotation mechanisms, as in Figs. 1 and 3. The resistance of the system should be determined by the tensile action of tie connections only. The imposed elongations of the tie connections should be caused by the rotation of the system around one well-defined axis.

It is important to design and detail elements, connections, anchorages etc. in consequence with the intended collapse mechanism. By that means the behaviour can be controlled to a considerable extent. Anchorage failures and brittle ruptures of other components than the ductile ones should be prevented by a proper design and detailing.

When the system is composed from interacting structural elements, as in Fig. 3, the connections between the elements must have sufficient strength and rigidity to keep the integrity of the system.

The design approach, as it is presented, is not applicable on collapse mechanisms including joint slips or suspension action, as in catenary systems. However, the method can be extended to cover also those cases if the design formulas are expressed in accordance. The design of catenary systems with the proposed method is exemplified in [2].

2. NON-LINEAR BEHAVIOUR OF TIE CONNECTIONS

The basic behaviour of different types of tie connections between concrete elements has been examined in previous investigations at Chalmers University of Technology [1]. It was then of special interest to study the connections at large imposed deformations resulting in a non-linear behaviour. The test methods and test results are presented in [1] together with proposed formulas which can be used for estimation of the ultimate deformation capacity of tie connections.

It was concluded that the behaviour of simple tie connections could be characterized by schematic bilinear relationships between the tensile force N and the elongations δ, as exemplified in Fig. 2a. The relationships are valid for tie connections where the fractural load of the tie bar is wholly anchored by bond or by end-anchors.

The area which is bounded by the tensile force graph in the load-displacement relationships represents the strain energy W_{int}. The efficiency of tie connections under imposed elongations will depend on the strain energy development. The efficiency for a certain elongation δ can be expressed by a dimensionless parameter $\xi(\delta)$.

$$\xi(\delta) = \frac{W_{int}(\delta)}{N_{max} \cdot \delta} \qquad (1)$$

where N_{max} = fractural load of the tie bar.

For the schematic load-displacement relationships presented in Fig. 2a, the corresponding efficiency functions are illustrated in Fig. 2b.

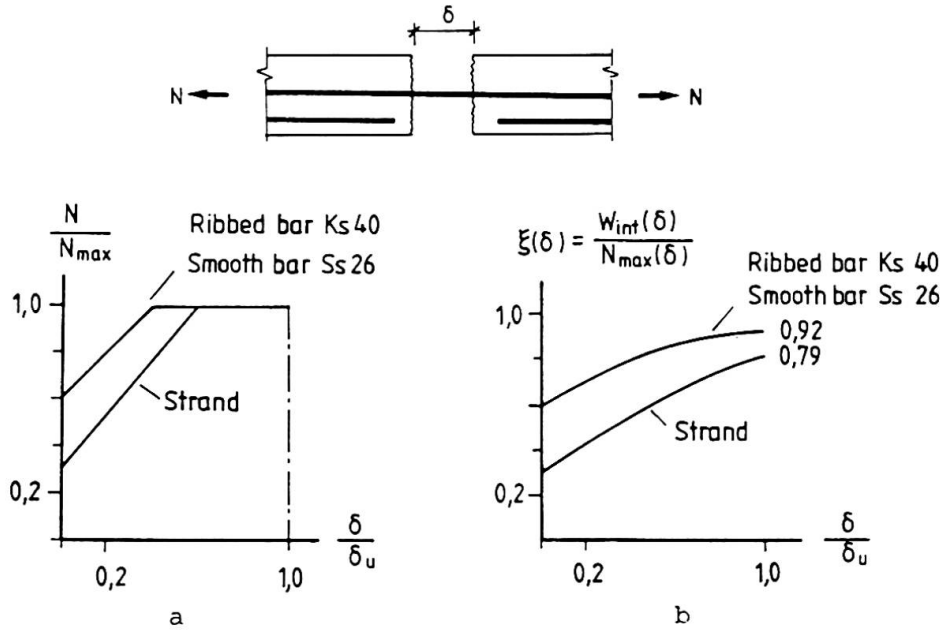

Fig. 2 Characteristic relationships for simple tie connections provided with wholly anchored tie bars from smooth bars (Ss26) or strands anchored by end-anchors or ribbed bars (Ks40) anchored by bond*
a) relationship between tensile force N and elongation δ
b) efficiency function

* The tie bars were made from ordinary reinforcement bars of type Ks40 or Ss26 according to Swedish Standards. Type Ks40 stands for a high bond, ribbed, hot-rolled bar with a minimum yield stress of 390 MPa. Type Ss26 stands for a smooth, hot-rolled bar of mild steel with a minimum yield stress of 260 MPa.

3. ANALYSIS OF ROTATION MECHANISMS

Consider a precast building with a partial damage of the structural system. A system of interacting precast elements forms a composed cantilever above the damaged area. A driving force Q is acting in the centre of gravity of the cantilevering system. The driving force is constituted by gravity forces, i.e. the weight of the elements and working loads.

Under the action of the driving force, the cantilevering system tends to rotate but the rotation is counteracted by tie connections when they are forced to elongate. Such a cantilever system is exemplified in Fig. 3. Full-scale tests on this type of alternative load-bearing systems were reported in [3].

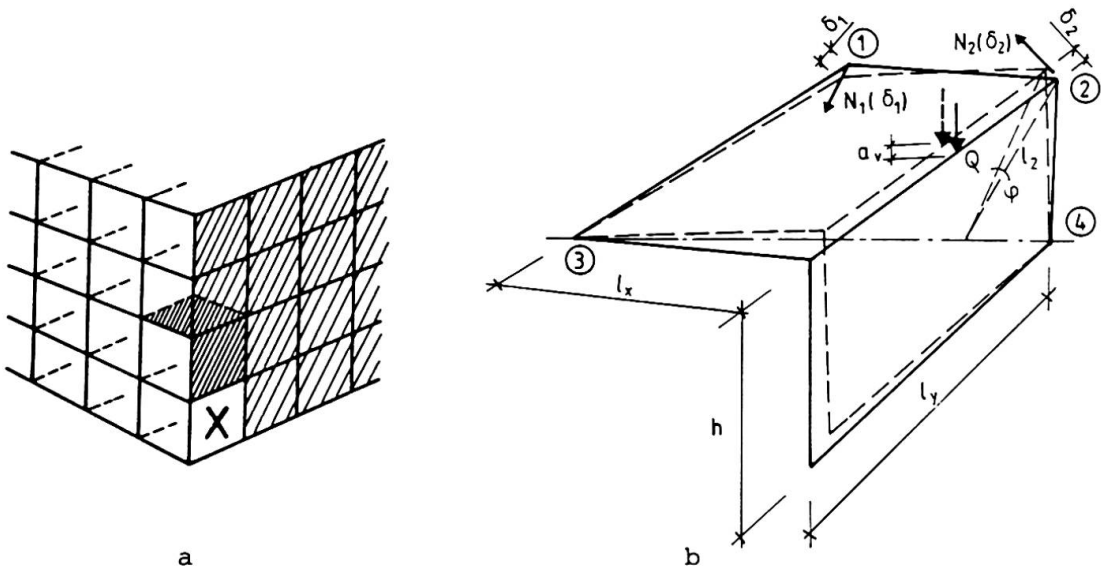

Fig. 3 Example of an alternative load-bearing system acting as a composed cantilever above the damaged area
a) assumed partial damage in a stabilizing gable wall
b) model for the alternative load-bearing system. Two interacting tie connections 1 and 2. Rotation axis 3-4

In the design approach, the elements are now assumed to be perfectly rigid. Hence, there will be a simple geometric relationship between the vertical displacement a_v of the driving force and the elongations δ_i of each tie connection i. For small rotations the following approximative expression can be adopted

$$\delta_i \cong \frac{l_i}{l_{q0}} a_v \qquad (2)$$

where l_i = radial distance between the rotation axis and tie connection i
l_{q0} = horizontal distance between the rotation axis and the driving force Q in the undeflected state

The bridging effect of the alternative load-bearing system can be regarded as a resistance $R(a_v)$, defined as the ability to withstand a driving force acting in the centre of gravity. For a certain rotation of the cantilever system and a corresponding vertical displacement a_v of the driving force, the static resistance will be

$$R_{stat}(a_v) = \frac{1}{l_q} \Sigma N_i(\delta_i) \cdot l_i \qquad (2)$$

where l_q = actual horizontal distance between the rotation axis and the driving force Q
δ_i is determined by (2)

For estimation of the dynamic resistance it is now favourable to introduce a formal value R_{max} of the maximum static resistance in the undeflected state

$$R_{max} = \frac{1}{l_{q0}} \Sigma N_{i,max} \cdot l_i = \Sigma R_{max,i} \qquad (3)$$

where $R_{max,i}$ = contribution to R_{max} from tie connection i

This value is formal as the tie connections are contributing with maximum capacities simultaneously and without any displacement of the cantilever system. In the real situation the tie connections may fracture one after the other depending on the locations and the mutually deformability.

The dynamic resistance must be related to a certain state of displacement. Hence, the designer has to choose a maximum displacement $a_{v,max}$, for which the deflected state of equilibrium should be obtained. The value of $a_{v,max}$, must be established with due regard to free space for displacements, elongation capacities of the respective tie connections and a desired safety level. The dynamic resistance $R_{dyn}(a_{v,max})$ states the maximum driving force Q_{dyn} which can be bridged in case of a sudden support removal, if the maximum displacement should be limited to $a_{v,max}$.

In order to analyse the dynamic effects during the deflection course, the collapse mechanism is regarded as an one-degree-freedom system. On the safe side the support is assumed to be lost suddenly. The system is exposed to the driving force Q, which acts with constant intensity during the deflection course. The motion of the rotating element is counteracted by the action of the tie connections. This action varies during the deflection course, and the composed effect of the interacting tie connections is represented by the resistance $R(a_v)$ according to (2).

A deflected state of equilibrium can only be possible if the velocity of the rotating system equals zero. This is the case when the internal energy of the system equals the external energy during the deflection course, i.e.

$$W_{int} = W_{ext} \tag{4}$$

The internal energy which is related to a certain displacement a_v of the driving force will be constituted by the strain energy of the tie connections under the corresponding imposed elongations δ_i. The external energy can be expressed as the driving force times its vertical displacement. By means of (1) the condition of energy equilibrium (4) can now be expressed as

$$Q_{dyn} \cdot a_{v,max} = \Sigma\, \xi(\delta_{i,max}) N_{i,max} \cdot \delta_{i,max} \tag{5}$$

where $\delta_{i,max}$ is determined by (2) for $a_v = a_{v,max}$.

By introducing the geometrical relationship (2), the dynamic resistance $R_{dyn}(a_{v,max})$ can be derived from (5)

$$R_{dyn}(a_{v,max}) = \Sigma\, \xi(\delta_{i,max}) \frac{l_i}{l_{q0}} N_{i,max} \tag{6}$$

or by means of (3)

$$R_{dyn}(a_{v,max}) = \Sigma\, \xi(\delta_{i,max}) R_{max,i} \tag{7}$$

Hence, the dynamic resistance can be regarded as a reduced value of the maximum static resistance according to (7), where the contributions from the respective tie connections have been reduced by efficiency factors $\xi(\delta_{i,max})$. The efficiency $\xi(\delta)$ will always, according to the definition (1), be less than or equal to 1. The actual value depends on to what extent the elongation capacity $\delta_{i,u}$ of the respective tie connections is utilized.

In addition to (7) the following condition of static equilibrium must be fulfilled in the deflected state. Otherwise, the system is under acceleration and will continue to deflect.

$$R_{stat}(a_{v,max}) \geq Q_{dyn} \qquad (8)$$

where $R_{stat}(a_{v,max})$ is determined by (2).

The formulas (7) and (8) are appropriate to use in the design of alternative load-bearing systems. Examples of application are presented in [2] and [4].

4. COMPARISON WITH TEST RESULTS

In order to check the applicability of the theoretical approach a series of tests concerning a simple well-defined collapse mechanism was carried out [5]. The test specimens were formed by strips of precast hollow core floors on three supports, see Fig. 4. A collapse situation was simulated by a sudden removal of an exterior support. Thus, one panel was transformed to a cantilever and the adjacent tie connection was loaded in negative bending. Normally, the yield strength was reached in the connection, resulting in large plastic rotations.

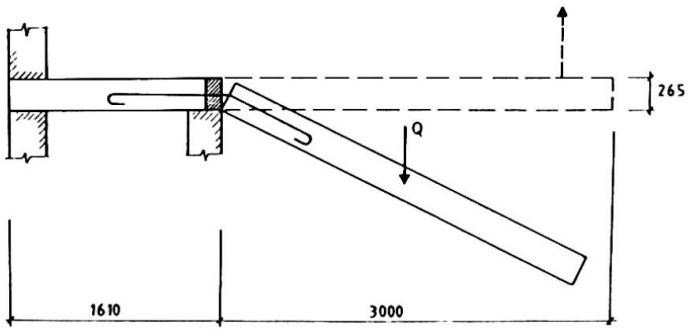

Fig. 4 Test arrangement

In most of the tests it was possible to take advantage of the ductility of the tie connection and receive a deflected state of equilibrium. The theoretical analysis was made in accordance with the principles presented above. The calculated values of the dynamic resistance were always in good agreement with the actual driving forces.

5. REFERENCES

1. ENGSTRÖM B., Ductility of tie connections for concrete components in precast structures. Technical report, Chalmers University of Technology, Divsion of Concrete Structures, Publication 83:1, Göteborg 1983.

2. ENGSTRÖM B., Resistance of locally damaged precast buildings - Influence of the structural connections, Connections between precast concrete elements. VTT Symposium 62, Technical Research Center of Finland, Espoo 1985, pp. 41-59.

3. LEWICKI B., CHOLEWICKI A., MAKULSKI W., Large-panel building: Behaviour in partial damage. Building Research and Practice, CIB, July 1983.

4. ENGSTRÖM B., Rassituationer i betongelementstommar, Inverkan av anslutningars seghet (Collapse situations in precast concrete structures, The effect of ductile tie connections). Chalmers University of Technology, Division of Concrete Structures, Publication 86:3, Göteborg, June 1986.

5. ENGSTRÖM B., Alternative load-bearing by cantilever action, Experimental study of the dynamic behaviour at sudden support removals. Chalmers University of Technology, Division of Concrete Structures, Report 87:1, Göteborg 1987.

Bending Tensile Strength of Steel Fibre Concrete under High Thermal Loads

Résistance à la traction-flexion de béton de fibres sous sollicitation thermique élevée

Biegezugfestigkeit von thermisch hochbeanspruchtem Stahlfaserbeton

Ulrich DIEDERICHS
Physicist
TU Braunschweig
Braunschweig, FRG

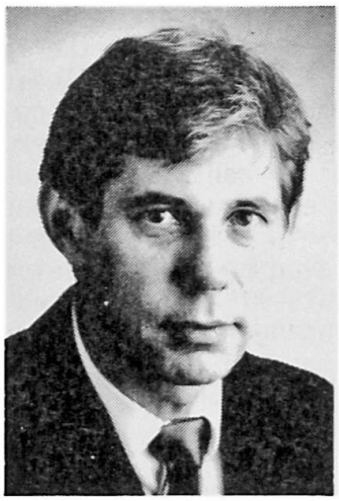

SUMMARY
The use of steel fibre concrete offers considerable advantages with elements and constructions which are exposed to high thermal loads during service or catastrophes (e.g. energy technology, shelters, fires in buildings, LNG-tanks during leakages etc.). To obtain the relevant material data for the design of such elements bending tensile tests have been conducted. Then investigations were mainly concentrated on high temperatures up to 800°C. The low temperature region down to –196°C was investigated to elucidate the fundamental effects of steel fibre reinforcement in microstructurally damaged concrete.

RÉSUMÉ
L'utilisation de béton de fibres d'acier présente des avantages pour les éléments de construction et les bâtiments soumis à des sollicitations thermiques élevées, soit en permanence lors de l'utilisation, soit en cas de catastrophe (p.ex. en technique de l'énergie, abris, coffres-forts, éléments de construction lors d'un incendie, réservoirs à gaz naturel liquéfié lors de fuite). Pour obtenir les données nécessaires sur les matériaux, des essais de traction-flexion ont été faits. Les recherches ont surtout porté pour des températures jusqu'à +800°C. Les basses températures allant jusqu'à –196°C ont aussi été incluses pour mettre en évidence l'influence des fibres d'acier dans un béton à microstructure détériorée.

ZUSAMMENFASSUNG
Die Anwendung von Stahlfaserbeton bietet erhebliche Vorteile bei Bauteilen und Bauwerken, die hohen thermischen Belastungen – entweder dauernd im Betrieb oder in Katastrophenfällen – ausgesetzt sind (z.B. in der Energietechnik, Schutzräume, Tresore, Bauteile bei Schadensfeuern, LNG-Tanks bei Leckagen). Um die für die Bemessung solcher Bauteile notwendigen Materialdaten zu gewinnen, wurden Biegezuguntersuchungen durchgeführt. Hauptsächlich wurde der Bereich bis +800°C erforscht. Die tiefen Temperaturen bis –196°C wurden mit einbezogen, um die grundsätzliche Wirkung von Stahlfasern in mikrostrukturgeschädigtem Beton zu erhellen.

1. INTRODUCTION

Since a number of years the effect of steel fibre reinforcement on the strength and deformation properties of concrete has been quite extensively studied. The results have shown that the incorporation of steel fibres in the relatively brittle concrete or mortar matrix improves the tensile strength properties and ductility of the unreinforced matrices. Because of these particular properties steel fibre reinforced concrete has already got a wide spread application in practice, although, it is a rather expensive material and requires more care in mix designing and concreting.

The results of various studies conducted at the Institute für Baustoffe, Massivbau and Brandschutz /1, 2, 3/ led to the conclusion that steel fibre reinforced concrete also indicates at high as well as at low temperatures, respectively after low temperature cycling a considerable higher ductility and an improved post maximum load behaviour than plain concrete. Obviously the response of constructions and elements exposed to extreme thermal loads under certain service conditions as well as during accidents (like fires in buildings or leakages in LNG-tanks) could be markedly improved by using steel fibre concrete. For instance, slender normal concrete elements like prestressed double-T-girders or beams with thin webbs are, in general, endangered by destructive spalling during a fire attack. On the other hand, composite elements possibly could be manufactured more economically with steel fibre concrete instead of stirrups and longitudinal reinforcement.

The objectives of the research program reported here /4/ were to study the mechanical behaviour, especially bending tensile properties, because they are decisive for ductility and crack formation. The main emphasis was laid on the experimental investigation of the high temperature region up to 800°C. Low temperature investigations down to -196°C were involved, too. It was anticipated that the results of such investigations gain the general understanding of the specific effect of steel fibre reinforcement in microstructurally deteriorated concrete.

2. EXPERIMENTAL

The test programme contained besides the testing temperature and loading conditions the following variables:

- concrete composition (mineralogical type of aggregates (gravel, limestone, diabase), cement content, type of binder (Portland cement, Portland cement + micro silica), W/C-ratio),
- steel fibre content, type of fibres (cut wires (WIREX); Ø = 0,4 mm, ℓ = 25 and 40 mm, resp. crimped cut wires (DRAMIX) ; Ø 0,5 mm, $\ell \approx$ 30 mm, machined fibres (HAREX, made of massive steel blocks by milling, with sickle-shaped cross-section)).

The test specimens were small concrete beams (64 mm x 72 mm x 280 mm) sawed out of small concrete slabs, which were stored after concreting for at least 28 days under water. After cutting, the small beams were again stored under water until testing. The basis mix proportions and some concrete data of the various batches are given in Tab. 1.

The test equipment is shown in Fig. 1. The specimen is simply supported. The load is applied by a steel frame which is connected with a steel rod and via a load-cell with a servohydraulic jack. The bending movements are transferred by two fused silica rods through the hot oven and measured by the aid of a magnetic transducer as the difference movement of both the silica rods. The obtained electrical signal is used for controlling the displacement of the hydraulic piston during the bending tensile test. The test procedure is shon in Fig. 2.

basis concrete mix	SF-Q	SF-D	Ko	Do	Quo	Qm0,55	Qm0,65	Mo
cement content [kg/m³]	340	340	340	340	340	340	340	500
silica fume [kg/m³]	60	60	-	-	-	-	-	-
aggregate content [kg/m³]	1824	1854	1884	1854	1847	1847	1847	1500
sand (crushed stone) 0/2 mm	-	35 %	20 %	30 %	-	-	-	-
crushed stone 2/8 mm	-	-	40 %	-	-	-	-	-
crushed stone 8/11 mm	-	25 %	15 %	30 %	-	-	-	-
crushed stone 11/16 mm	-	40 %	25 %	40 %	-	-	-	-
sand 0/2 mm	34 %	-	-	-	34 %	34 %	34 %	69 %
gravel 2/8 mm	26 %	-	-	-	26 %	26 %	26 %	31 %
gravel 8/16 mm	40 %	-	-	-	40 %	40 %	40 %	-
water [kg/m³]	191	200	153	153	165	221	221	250
w/c	0,57	0,59	0,45	0,45	0,485	0,55	0,65	0,5
plasticizer *)	2 %	3 %	1 %	1,5%	1 %	2 %	1 %	1 %
density [kg/dm³] **)	2,35	2,48	2,47	2,48	2,40	2,45	2,43	2,31
cube strength [N/mm²]								
28 d	51	54	51	52	54	54	42	55
when tested	59	59	53	59	65	59	46	64

*) related to cement weight; **) fresh concrete

Table 1 Mix proportions and data of the concrete basis mixtures

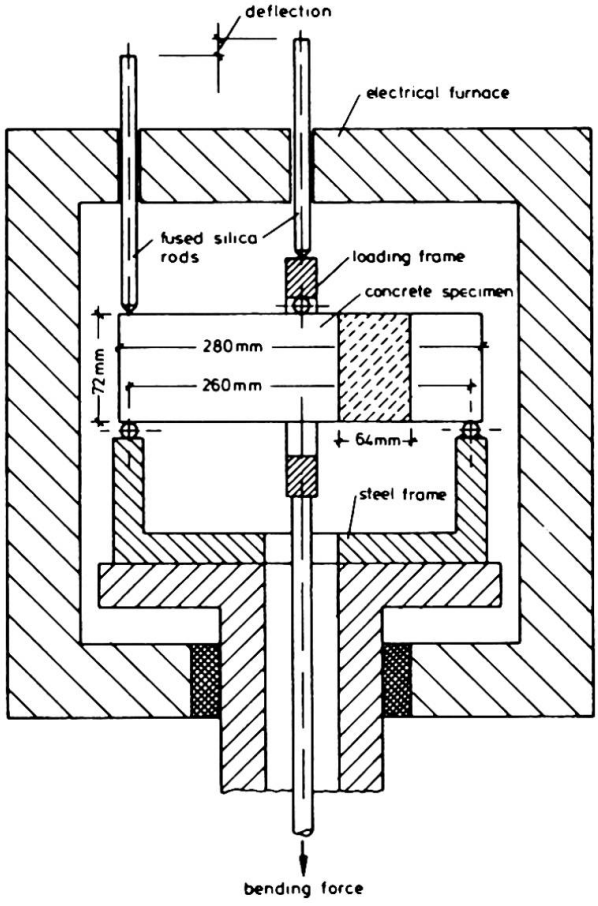

Fig.1 Schematic representation of the test equipment

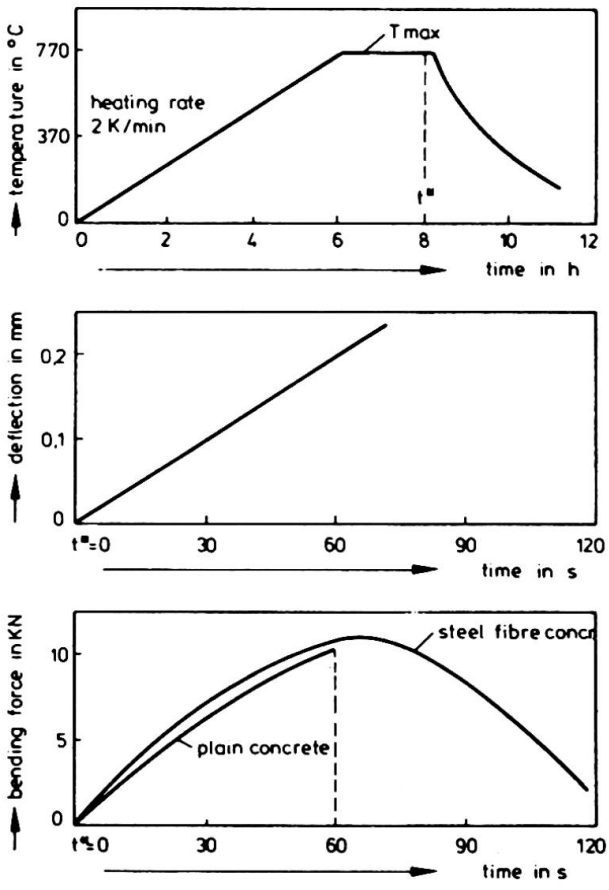

Fig.2 Testing procedure for high temperature investigations

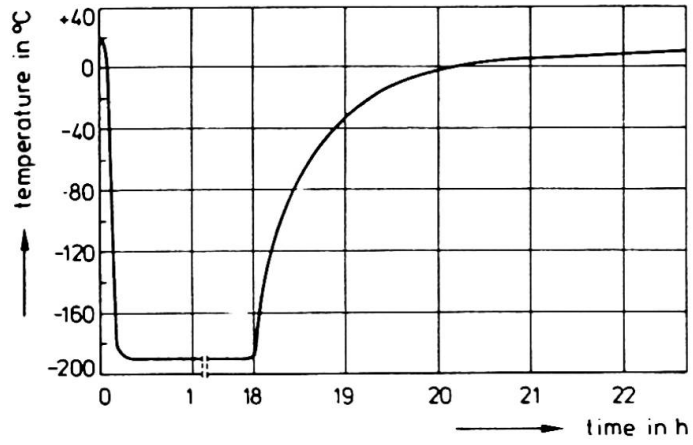

Fig.3 Temperature exposure of "low-temperature-specimens"

The specimens are heated in an electrical oven with a heating rate of 2 K/min to the desired maximum temperature (T_{max}). Then this temperature is kept constant for nearly 2 hours. At the time t* the specimens are loaded with a constant deflection rate of about 0.2 mm/min. Simultaneously the resulting load response is measured. The "low-temperature-specimens" were rapidly cooled down to -196°C by spraying liquid nitrogen into the sample container (Dewar vessel), held for 18 h at -196°C and subsequently slowly warmed up to room temperature (Fig.3), tested in the same way like the 20°C-reference specimens.

3. RESULTS AND DISCUSSION

From the deflection-load response measurements bending force-deflection relationships are obtained as shown in Figs.4 and 5 for Portland cement concrete made with siliceous aggregates tested at high temperature and after low temperature cycling. The y-axis indicates the measured bending forces; the x-axis the deflection in mm, noteworthy, after the onset of matrix cracking the crack mouth opening is nearly half of the measured deflection. The dotted lines in Fig.4 belong to the plain concrete and the full lines represent the response of steel fibre concrete. In this case the fibre content was 3-weight-% of smooth cylindrical fibres with a diameter of 0.4 mm and a length of 25 mm. With other mixtures comparable deflection-bending force characteristics have been obtained. The maximum bending forces - in terms of "bending tensile strength" β_{ts} (defined by the equation $\beta_{ts} = 1.5 \cdot F \cdot l/b \cdot h^2$, F = maximum bending force, l,b,h = length, width and height of the specimens) - of the various mixtures are compiled in Figs.6-9.

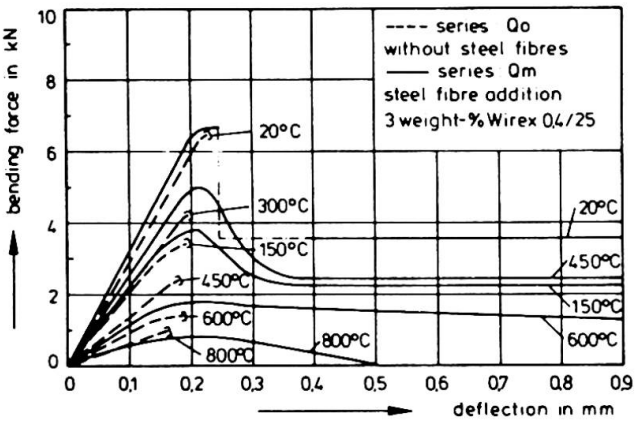

Fig.4 Bending force-deflection relationships of steel fibre reinforced gravel concrete at high temperature

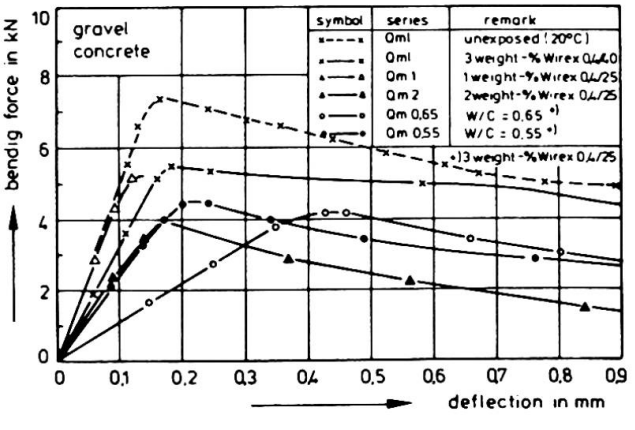

Fig.5 Bending force-deflection relationships of various steel fibre reinforced gravel concretes after low temperature cycling

In the initial parts of the curves obtained at ambient temperature (20°C) hardly any difference between plain and fibre concrete occurs. Both curves run nearly linear up to deflections of about 0.2 mm, then follows a plateau indicating the onset of cracking. A further small increase of the deflection leads to collapse of the plain concrete due to unstable crack propagation.

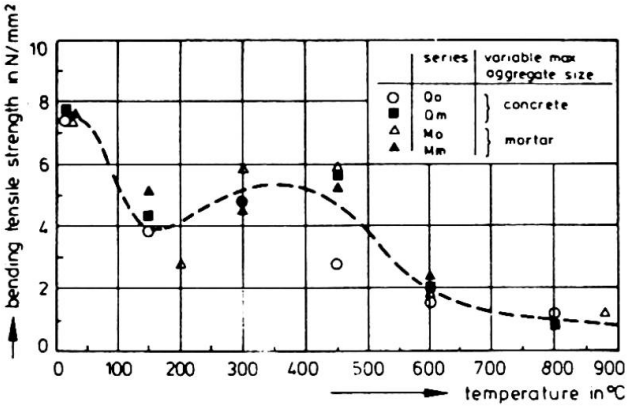

Fig.6 Effect of aggregate size on the bending tensile strength of steel fibre concrete

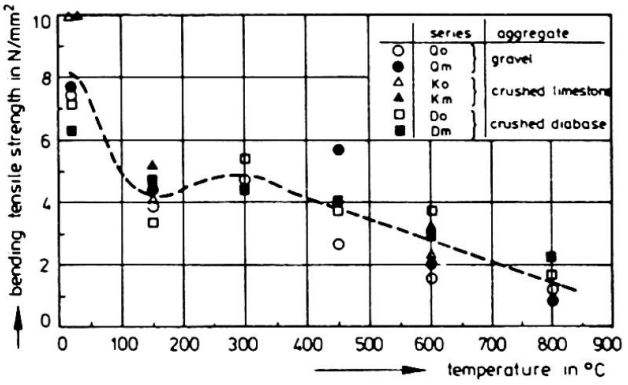

Fig.7 Effect of mineralogical type of aggregate on the bending tensile strength of steel fibre concrete

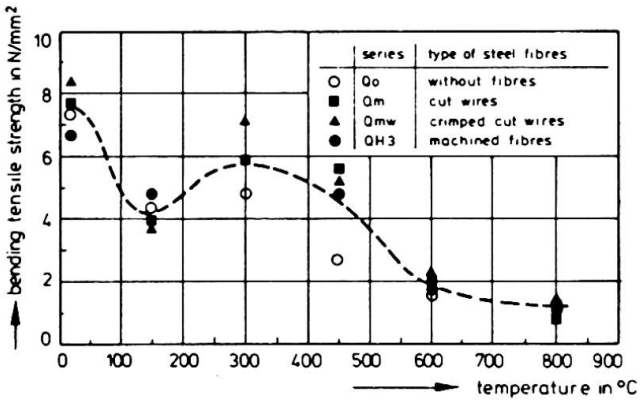

Fig.8 Effect of type of steel fibres on the bending tensile strength of concrete

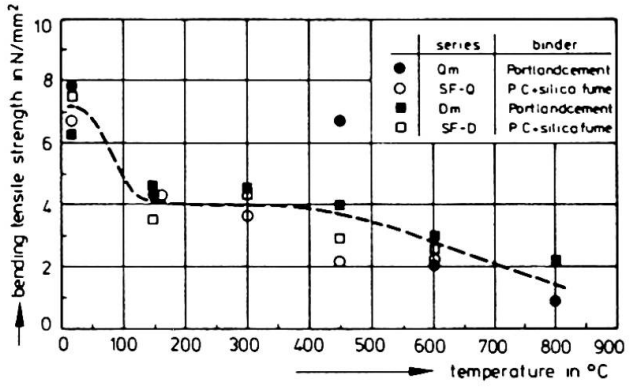

Fig.9 Effect of binder on the bending tensile strength of steel fibre concrete

The steel fibre specimens show a slightly more extended plateau. However, with a deflection of nearly 0.25 mm unstable matrix cracking occurs. This causes simultaneously debonding of fibres and their activation to bridge the gross crack and to transfer tensile loads by frictional forces. The related unstable transition (onset of matrix cracking → continuously cracked matrix) runs too rapidly to be reliably controlled and recorded by the testing equipment, therefore the transient response is indicated by the dashed line in Fig.4.

After deflections of nearly 0.35 mm the deflection-load response is again stable and the load - now significantly lower compared to the maximum level - hardly decreases in course of a further increase of the deflection up to 1 mm.

In the temperature region from 150°C to 450°C the peak stresses of both the plain and the steel fibre concrete are already significantly reduced, although, the peaks are shifted only to a small extent towards lower deflections. As expected, the plain concrete specimens show the same behaviour as the 20°C-specimens. They collapse after the onset of gross cracking. A very similar behaviour is observed after low-temperature-cycling.

The steel fibre specimens indicate a quite different post-maximum-load behaviour than the respective 20 °C-specimens: After exceeding the maximum stress, with increasing deflection the load is decreasing in a stable manner to a certain lower level. This lower and more stable crack propagation originates from the more ductile behaviour of the heated concrete. Since the heated concrete contains a great number of critical cracks, satellite and multiple cracking occurs. This enables a stepwise, respectively continuous activation of steel fibres to bridge the gross crack.

That means both the matrix and the fibres are transferring the tensile stress during the transient phase.

After reaching deflections of nearly 0.35 mm the load, respectively the stress level, hardly decreases up to deflections of 1.0 mm. This behaviour could be explained in terms of steel fibre bridging and stress transfer from the concrete matrix to the fibres by friction.

At 600 °C and 800 °C the matrix contains a lot of cracks. Already low bending tensile forces lead to a collapse of the plain concrete. In the fibre concrete, the steel fibres are partially activated in a very early phase and fully activated after deflections of nearly 0.2 mm. For the 600 °C-specimens the stress from the fibres to the matrix is transferred by friction. - The fibres are pulled-out of the matrix at very high deflections, respectively crack mouth opening displacements. The 800 °C-specimens show a somewhat different behaviour. At 800 °C the steel fibres are already very soft and the friction forces are higher than the tensile strength of the fibres, so they fail in tension, if crack mouth opening of 0.25 mm is exceeded.

4. CONCLUSIONS

From the results obtained it can be concluded: High temperature as well as low temperature exposure leads to a significant reduction of the bending tensile strength of both plain concrete and fibre reinforced concrete. This is caused mainly by formation of cracks especially in the contact zone between the coarse aggregates and the fine grained mortar matrix due to thermal incompatibilities of cement paste and aggregates. Steel fibre reinforcement imparts a well defined post-cracking behaviour to the composite and increases the post maximum ductility. At high temperatures the stress transfer from the fibres to the matrix is caused mainly by frictional forces, this holds for low temperature damaged concrete, too. At ambient temperature the main stress transfer mechanism is friction. Adhesion is relevant only up to the onset of matrix failure.

REFERENCES

1. ROSTASY, F.S.; WIEDEMANN, G.: Festigkeit und Verformung von Beton bei sehr tiefer Temperatur. Beton 2/80.

2. ROSTASY, F.S.; SPRENGER, K.H.: Strength and Deformation of steel fibre reinforced concrete at very low temperature. The International Journal of Cement Composites and Lightweight Concrete, Volume 6, No. 1, February 1984.

3. DIEDERICHS, U.; SCHNEIDER, U.: Pilotstudie zum Spannungs-Dehnungs- und Warmkriechverhalten von Stahlfaserbeton. Bericht aus dem Teilprojekt B 3 des Sonderforschungsbereichs 148 "Brandverhalten von Bauteilen" der Technischen Universität Braunschweig. Braunschweig, 1979 (unveröffentlicht).

4. KORDINA, K.; WYDRA, W.; DIEDERICHS, U.: Untersuchungen zur Biegezugfestigkeit von thermisch hochbeanspruchtem Stahlfaserbeton. Bericht des Instituts für Baustoffe, Massivbau und Brandschutz, Technische Universität Braunschweig, August 1986.

Material Properties of High Strength Concrete at Elevated Temperatures

Propriétés d'un béton à haute résistance sous des températures élevées

Materialeigenschaften von hochfestem Beton bei hohen Temperaturen

Ulrich DIEDERICHS
Physicist
TU Braunschweig
Braunschweig, FRG

Ulla-Maija JUMPPANEN
Civil Eng.
Techn. Res. Centre
Espoo, Finland

Vesa PENTTALA
Prof. Dr.
Helsinki Univ. of Technol.
Espoo, Finland

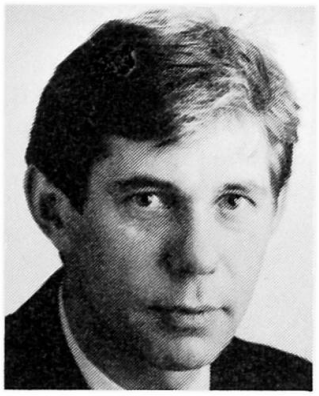

SUMMARY
By the use of high strength concretes the economy and safety of the structures in energy technology as well as in conventional house-building can be enhanced considerably. This involves a knowledge of high temperature behaviour of these concretes because the structures may – either in normal service or under catastrophic conditions – be subjected to high temperatures, and they must be correspondingly designed. This paper reports results of experimental investigations of high temperature behaviour of three high strength concretes.

RÉSUMÉ
De par l'installation d'un béton à haute résistance comme matériau de construction, il est possible d'améliorer la rentabilité et la sécurité de constructions et d'éléments de construction dans le domaine de la technique de l'énergie et celui du bâtiment. Ceci suppose une bonne connaissance des propriétés à hautes températures, puisque les éléments de construction sont exposés à des températures élevées, soit en service normal, soit lors de catastrophes, et qu'ils doivent être dimensionnés en conséquence. Les résultats des essais de matériaux sont présentés.

ZUSAMMENFASSUNG
Durch Einsatz von hochfestem Beton als Konstruktionswerkstoff kann die Wirtschaftlichkeit und Sicherheit von Bauwerken und Bauteilen der Energietechnik und des normalen Hochbaus erheblich verbessert werden. Dies setzt die Kenntnis der Hochtemperatureigenschaften voraus, weil die Bauteile entweder im Normalbetrieb oder bei Katastrophen (z. B. Feuer) hohen Temperaturen ausgesetzt sind und entsprechend dimensioniert werden müssen. Ergebnisse von umfangreichen Materialuntersuchungen werden vorgestellt.

1. INTRODUCTION

The application of high strength concretes in off-shore-platforms and prestressed reactor pressure vessels arouses special interest because of the increased economy and safety of the structures. Besides, the use of high-strength concretes can be increased also in normal structures, cast in situ as well as in prefabricated elements - like hollow core slabs and composite columns. In all the cases the high temperature properties of the concrete in question must be known as the structures may be subjected to high thermal loads either in their service or catastrophic conditions (reactor accident, fire etc.) and must be correspondingly designed.

Up to now our knowledge of the high temperature behaviour of concrete is restricted to normal strength concretes (K15...K50). Extending the known data by linear extrapolation to cover also high strength concretes is not necessarily relevant, because due to their special composition and microstructure high strength concretes may be subjected to high temperature phenomena up to now not perceived (destructive spalling, exceptionally strong destruction of cement matrix due to thermal exposure etc.).

This paper presents the results of the experimental investigations carried out on three high strength concretes based on different combinations of binder and superplasticizers (compressive strengths - 100 mm cubes - at the age of 90 d: 101...112 MPa).

2. EXPERIMENTAL

2.1 Materials

Three different high strength concretes (HSC) were investigated experimentally. The concretes differed in the composition of the binder (blast furnace slag cement, series Tr; Portland cement with silica fume, series Si; Portland cement with class F fly ash, series Lt). The type of aggregates was same in all three concretes and the grading of the aggregates was similar in Si and Lt concretes and slightly different in Tr concrete. The mix proportions and some concrete data are given in Table 1, where also the respective data for a normal strength concrete (OPC /3/) are given. The aggregate of the high strength concretes comprised granite-based sand and crushed diabase, whereas the OPC concrete contained mainly greywacke, sandstone, quartz and quartzite as coarse aggregates. The preparation and conditioning of the specimens (cubes 100x100x100 mm^3 for strength tests and cylinders 80 mm in diameter and 300 mm in length for high temperature tests) until testing are thoroughly reported in /4, 5 and 6/.

2.2 Test methods

To determine the strength and deformation behaviour at high temperatures stress-strain, transient creep and restraint tests were performed.

For the σ-ε-experiments the specimens were heated without external load in a special testing machine with a furnace using a heating rate of 2 K/min up to the desired temperatures. After homogenizing for 2 hours at the maximum temperature σ-ε-tests were performed with a constant strain rate of about 0.5 ‰/min.

To get information about the transient creep the specimens were loaded with a certain load level α ($\alpha = \sigma / \sigma_{ult}$, where σ_{ult} is the compressive strength at 20 °C) at ambient temperature and heated under constant load with constant heating rate (2 K/min) until failure. Simultaneously the total deformation and the surface temperature were measured. Total deformation with α = 0 represents thermal expansion.

Concrete series	Si	Lt	Tr	OPC
Cement type	P40/91	P40/7	M40/91	P40/91
- content (kg/m^3)	530	472	530	418
Additional binder	Silica	Fly ash	-	-
- content (kg/m^3)	53	157	-	-
Water content	129.2	147.0	145.0	188.0
Superplasticizer	Scancem	Scancem	Conflow	-
- dosage (kg/m^3)	14.6	15.7	15.0	-
Aggregate content (kg/m^3)	1876	1729	2002	1754
Water/binder ratio	0.26	0.27	0.30	0.45
Density (kg/m^3)	2648	2594	2654	2390
Cube strength (MPa)				
- 28 d	114.4	87.3	91.4	48.0
- 90 d	100.8	106.9	111.9	36.0
Cylinder strength (MPa)				
- > 90 d	106.6	91.8	84.5	32.9

Table 1 Mix proportions and concrete data.

To measure the development of restraint forces the specimens were loaded at ambient temperature, the initial load levels applied were 15, 30 and 45 % of σ_{ult}(20 °C). The measured strain was kept constant during heating (heating rate 2 K/min) and the imposed force as well as the temperature of the specimen were measured.

2.3 Test results

Fig. 1 shows the measured σ-ε-relationships of the high strength Lt concrete at elevated temperatures. Quite similar curves were obtained also for the other HS-concretes. They differ distinctly from those of normal strength concrete (OS-concrete) (Fig. 2). In general, the failure of HS-concrete is more brittle than that of OS-concrete. HS-concretes show already at 150 °C a very distinct loss of strength, about 30 %, whereas OS-concrete up to a temperature of 350 °C indicates even slight increase of strength (Fig. 3). Although the modulus of elasticity of OS-concrete at 20 °C is much lower than those of the HS-concretes, its relative decrease is stronger in the whole temperature range (Fig. 4).

Fig. 5 shows the total deformation of Si- and OPC-concrete measured during heating. Because of the smaller binder content and the higher thermal expansion of the coarse aggregate in OS-concrete also the thermal expansion of the OS-concrete is distinctly higher than that of the HS-concrete. If the specimens are heated under load the thermal expansion is much lower. With a load level of 20 % of σ_{ult}(20 °C) the HS-concretes show nearly no expansion. With load level of 60 % of σ_{ult}(20 °C) heated specimens of Si and Lt concretes failed already soon after exceeding 100 °C, whereas the specimens of series Tr maintained their load bearing capacity still with a load level of 70 % up to 110 °C and the specimens of series OPC with load level of 60 % even up to 450 °C.

The thermal expansions of the high strength concretes differ only slightly; also the total deformations are almost similar. This was to be expected as the binder content of the HS-concretes differed only marginally. The OS-concrete (OPC)

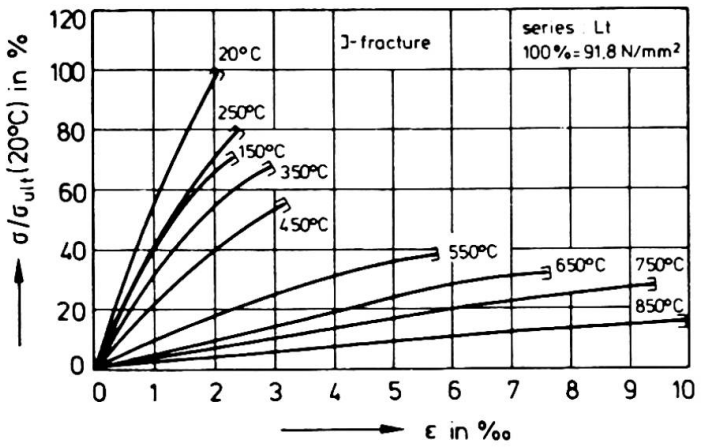

Fig. 1. Stress-strain relationships of high-strength concrete made with fly ash and Portland cement.

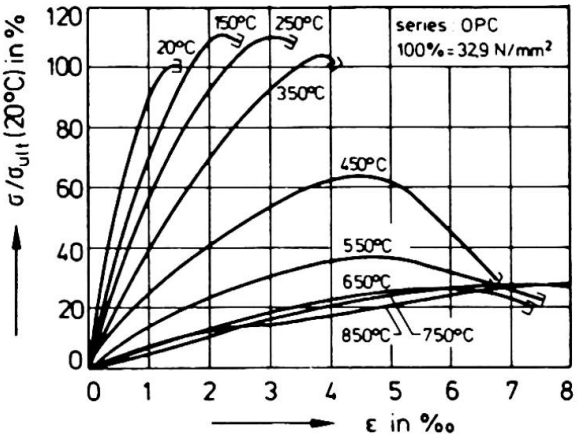

Fig. 2. Stress-strain relationships of Ordinary Portland cement concrete.

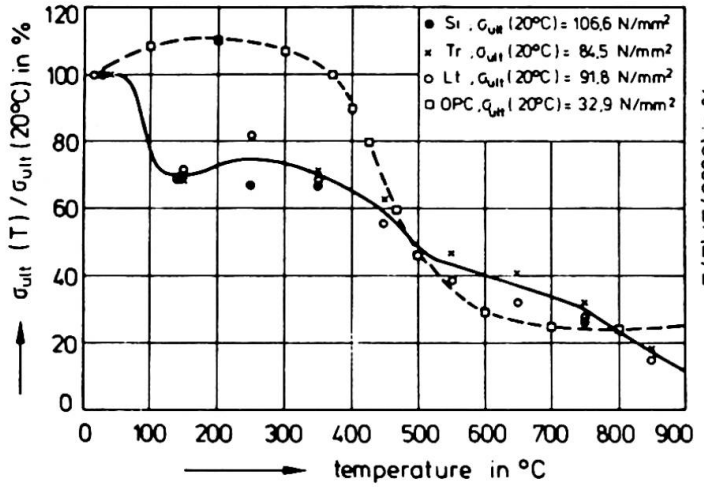

Fig. 3. Compressive strength of various high-strength and a normal strength concretes.

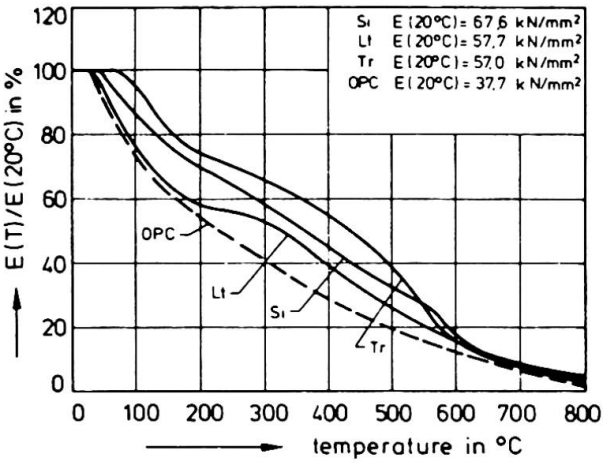

Fig.4. Modulus of elasticity of various high-strength and a normal concretes concrete.

contains considerably less binder and shows also correspondingly lower transient creep.

The development of restraint forces (Fig. 6) is mainly determined by the temperature dependence of the modulus of elasticity, thermal expansion and creep. Because of the likeness of the corresponding data for the series Si, Lt and Tr also the developing restraint forces are of the same magnitude. The slightly lower creep of Tr concrete at temperatures above 200 °C results in higher restraint forces especially in that temperature region. As expected, the OS-concrete shows higher restraint forces than the HS-concretes.

Destructive spalling occurred in no specimen heated with a heating rate of 2 K/min, like reported by Hertz /2/. Some cylindrical specimens under load were heated with a maximum heating rate within reach of the furnace (max. 32 K/min measured on the surface of the specimen). In some cases, however independent of the load level, slight spalling occurred. With bigger specimens (prisms 100x100x400 mm^3) also loaded and heated with the maximum heating rate spalling occurred in all specimens (Si, Lt and Tr); in the especially dense concretes (Si and Lt) it caused failure of the specimen. It can be concluded that besides the

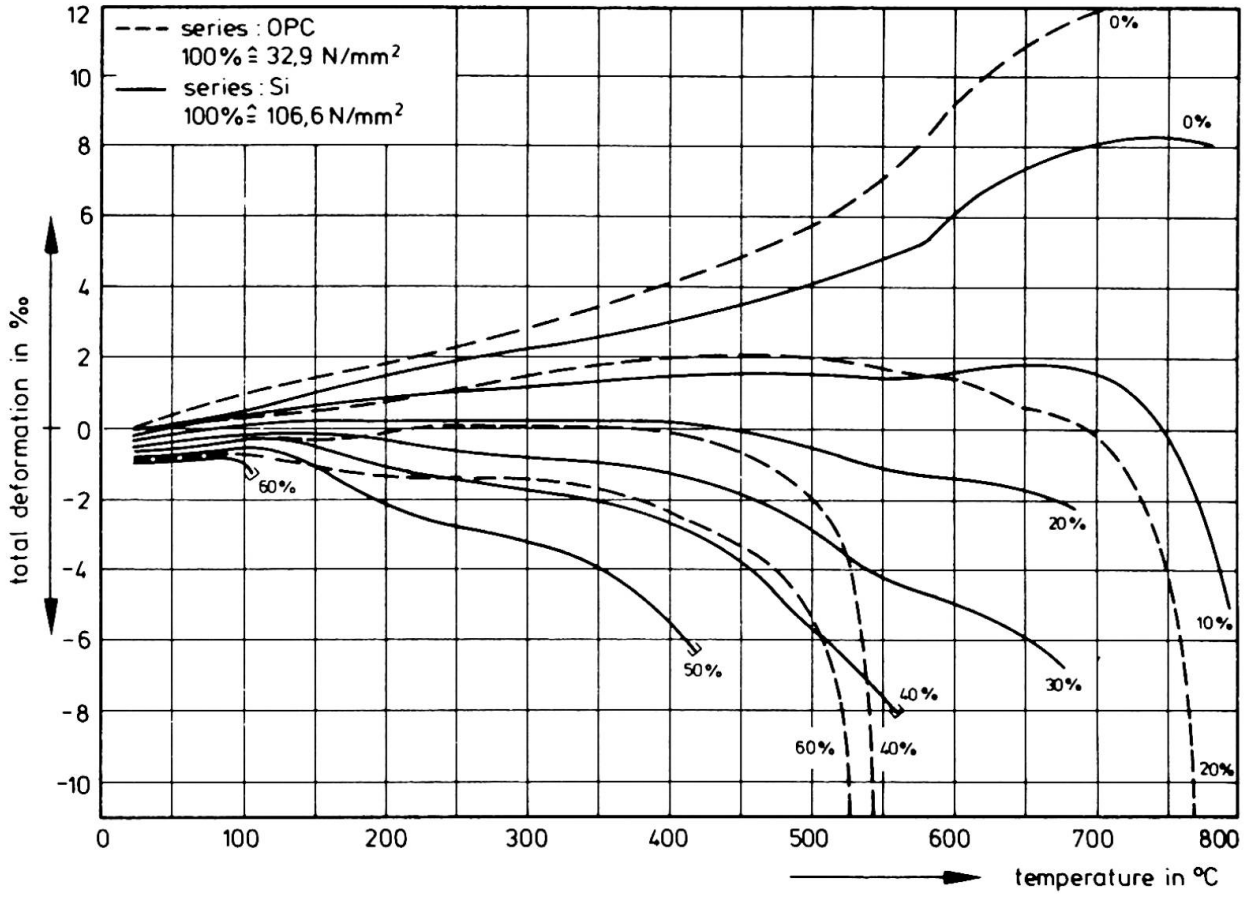

Fig. 5. Total deformation of loaded high-strength and normal strength concrete during heating.

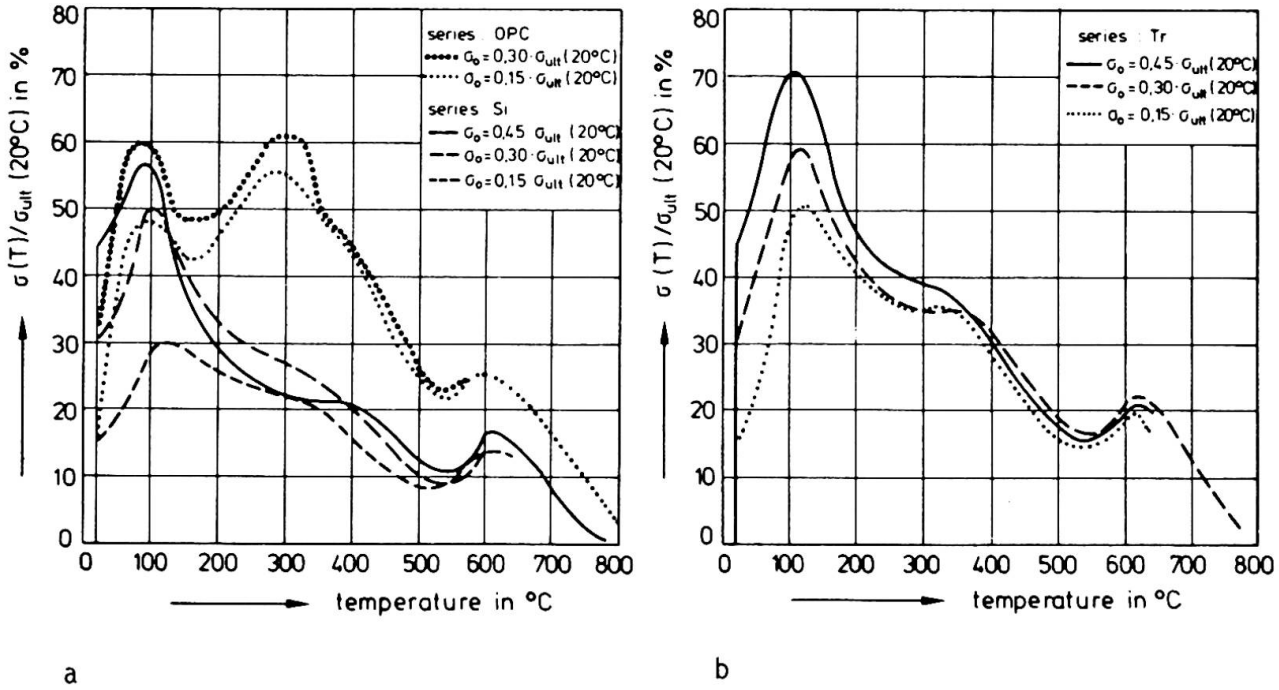

a b

Fig. 6. Restraint forces of high-strength Si- (a) and Tr- (b) concretes and a normal strength concrete (a).

heating rate and the density of the concrete also the dimensions and the shape of the member are decisive with regard to destructive spalling.

3. CONCLUSIONS

To summarize, the high strength concrete, especially in the temperature region from 100 °C to 350 °C, show a stronger loss of strength than normal strength concrete. This is caused by temperature dependent destruction of cement paste. Its influence on the strength of high strength concretes is bigger than on that of normal strength concrete, because the cement paste matrix of high strength concrete must carry higher loads than in normal strength concrete (more homogeneous stress distribution between the aggregate and cement paste). Because the cement paste of high strength concrete is essentially denser compared with that of normal strength concrete it dries also at elevated temperatures relatively slow and the so called drying hardening causing mainly the increase of strength in normal strength concrete between 150 and 350 °C does not happen in high strength concrete. Besides, considering the structures exposed to high thermal loads (e.g. fire) higher risk of spalling must be taken into account.

REFERENCES

1. DIEDERICHS, U. et al. Hochtemperaturverhalten von Festbeton. In Sonderforschungsbereich 148 "Brandverhalten von Bauteilen", Arbeitsbericht 1983-1986, Teil II, TU Braunschweig, 1987.

2. HERTZ, K. Heat-induced explosion of dense concretes. Technical University of Denmark, Report no. 166. Lyngby 1984. 20 p.

3. JUMPPANEN, U-M. et al. Material properties of F-concrete at high temperatures, Technical Research Centre of Finland, Research Report 452, Espoo, November 1986. 60 p.

4. PENTTALA, V. et al. Production methods of high-strength concrete. Helsinki University of Technology, Department of Civil Engineering, Publication 77. Espoo 1986. 128 p. (In Finnish).

5. PENTTALA, V. Mechanical properties of high strength concretes based on different binder combinations. Proceedings of the symposium on "Utilization of high-strength concrete", Stavanger, Norway, June 1987.

6. PENTTALA, V. et al. Mechanical properties of high-strength concretes. Helsinki University of Technology, Department of Civil Engineering, Publication 91. Espoo 1987. 109 p. (In Finnish).

Effects of Ice Formations in Cylindrical Water Tanks

Effet de la formation de glace dans des réservoirs à eau cylindriques

Auswirkungen der Eisbildung in zylindrischen Wassertanks

T. I. CAMPBELL
Prof. of Civil Eng.,
Queen's University
Kingston, ON, Canada

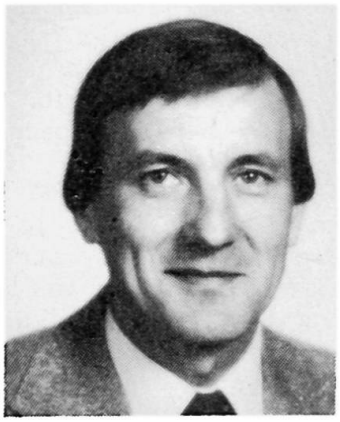

Ivan Campbell received his engineering degrees from the Queen's University of Belfast, Northern Ireland. For the past seventeen years he has been involved with research into concrete structures with particular emphasis on prestressed concrete transportation structures.

W. L. KONG
Res. Assoc.
Queen's University
Kingston, ON, Canada

Wei-ling Kong obtained his M.Sc and Ph.D degrees from Queen's University, Kingston, Canada. During the past six years he has been involved with research projects on railway ties, concrete water tanks and bridge bearings.

SUMMARY
A mathematical model for simulation of ice under stress is discussed and a method of determining the hoop stress induced in the wall of a cylindrical tank by an internal ice cap subjected to increasing temperature is developed. These predictions are validated by comparison with test data and it is concluded that hoop stresses capable of cracking the wall of a non-prestressed concrete tank may be induced by an expanding ice cap. A number of other defects observed during inspections of water tanks in Ontario, and attributed to the effects of a freezing environment, are discussed.

RÉSUMÉ
Un modèle de simulation du comportement de la glace sous l'effet de contraintes est présenté. Une méthode de détermination des contraintes latérales, provoquées sur la paroi d'un réservoir cylindrique par un bouchon de glace soumis à une température croissante, est développée. Ces calculs sont comparés avec des résultats d'essais et font apparaître que les contraintes latérales sont capables de provoquer des fissures dans la paroi d'un réservoir en béton non précontraint, par l'augmentation du volume du bouchon de glace. Certains autres dégâts – résultant d'effets de la température – ont été observés lors de contrôles de réservoirs en Ontario.

ZUSAMMENFASSUNG
Ein mathematisches Modell für Eis unter Spannung und eine Methode zur Bestimmung der Ringspannung in einem zylindrischen Behälter infolge Temperaturerhöhung der Eisdecke im Behälter werden vorgestellt. Die Berechnungen werden mit Versuchsdaten verglichen. Die auftretenden Ringzugkräfte können zur Rissbildung in schlaff bewehrten Stahlbetontanks führen. Verschiedene, bei Inspektionen von Wassertanks in Ontario, als Folge von Frostwirkung beobachtete Defekte, werden besprochen.

1. INTRODUCTION

A study [1] of 53 concrete cylindrical water tanks in the Province of Ontario, Canada, indicated performances ranging from two failed tanks through tanks exhibiting distress of varying degrees to tanks which were performing adequately. The major problems observed could be related to faults in construction methodology and to inadequate design criteria in view of the freezing environment during winter in Ontario. Ice formations consisting of a horizontal ice cap at the top water level and/or a vertical ice tube on the inside of the wall of the tank were observed during the inspections. Similar ice formations in water tanks in Finland have been described by Pitkanen [2].

Pressure exerted on the wall of a cylindrical water tank, as a result of warming and related expansion of an ice cap, is addressed in this paper. A mathematical model for simulation of ice under stress is discussed and a method of determining the hoop stress induced in the wall of a cylindrical tank by an ice cap subjected to increasing temperature is developed. These predictions are validated by comparison with test data from a model water tank. It is concluded that hoop stresses capable of cracking the wall of a non-prestressed concrete tank may be induced by an ice cap. A number of other defects observed during the inspections of the tanks in Ontario, and attributed to the effects of a freezing environment, are discussed. It is recommended that ice formations be prevented from forming in a tank by some appropriate means.

2. MECHANICAL PROPERTIES OF ICE

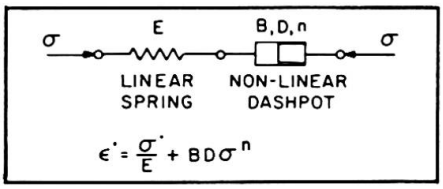

Fig. 1 Model for ice

The mechanical properties of ice depend on many factors. The properties of different types of ice have been discussed by Michel [3] and Tuomioja et al [4]. Bergdahl [5] has proposed the following model, illustrated in Fig. 1, to describe the behavior of ice under pressure:

$$\dot{\varepsilon} = \dot{\sigma}/E + BD\sigma^n \qquad (1)$$

where $\dot{\varepsilon}$ is the strain rate, $\dot{\sigma}$ is the stress rate, E is the modulus of elasticity, D is the self-diffusion coefficient and B and n are coefficients of viscous deformation. Suitable values of E, D, B and n have been suggested [5].

An ice cap in a concrete or steel tank subjected to an increase in temperature will be subjected to biaxial in-plane compressive stress since the coefficient of thermal expansion of ice is 4 to 5 times that of concrete or steel. The relationship between stress and strain, given in Eqn. (1), is nonlinear and the effect of combined stresses may be considered using a procedure [6] which defines the creep strain rate in the form

$$\dot{\varepsilon}_{cr}^{*} = G\sigma^{*n} \qquad (2)$$

where G is a constant and σ^* is the octahedral stress defined by

$$\sigma^* = \frac{1}{\sqrt{2}}[(\sigma_1 - \sigma_2)^2 + (\sigma_2 - \sigma_3)^2 + (\sigma_3 - \sigma_1)^2]^{1/2} \qquad (3)$$

where σ_1, σ_2 and σ_3 are principal stresses. Thus, from Eqn. (1), the creep strain rate may be expressed as

$$\dot{\varepsilon}_{cr} = BD\sigma^{*n} \qquad (4)$$

The in-plane stress condition at any level in an expanding ice cap within a cylindrical tank is analogous to a disc subjected to a uniform radial pressure, p, around its circumference. For this case, the in-plane principal stresses have a magnitude equal to p throughout the disc and consequently, from Eqn. (3) with $\sigma_1 = \sigma_2 = p$ and $\sigma_3 = 0$, the octahedral stress in the ice cap is given by $\sigma^* = p$.

A creep strain rate of the form given in Eqn. (2) is adopted for the analysis of creep under combined stress in the ABAQUS computer program [7]. Figure 2 shows the variation, with time and related temperature, of the pressure in the ice as predicted by ABAQUS for a test reported by Lindgren [8]. The good agreement observed between the test data and the prediction of ABAQUS demonstrates the validity of Eqns. (1) and (2).

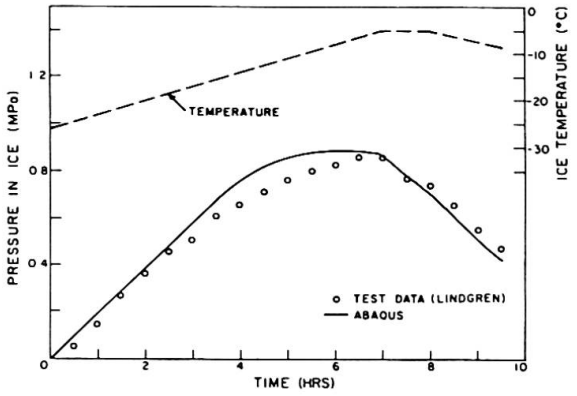

Fig. 2 Simulation of Lindgren test [8]

3. ANALYSIS OF CYLINDER WITH ICE CAP

Figure 3(a) shows an ice cap contained within a long cylinder. Assuming that a linear pressure distribution develops (creep of the ice neglected) when the ice cap is subjected to an increase in temperature, which varies linearly over its thickness (Fig. 3(b)), the problem reduces to that of a long cylinder subjected to a band of linearly varying pressure around its circumference (Fig. 3(c)). This condition may be analyzed using an approach suggested by Timoshenko and Woinowsky-Krieger [9]. It can be shown [10, 11] that, within the loaded area at a location defined by the parameters b and c in Fig. 3, the hoop stress, σ_h, in the wall of the cylinder is given by

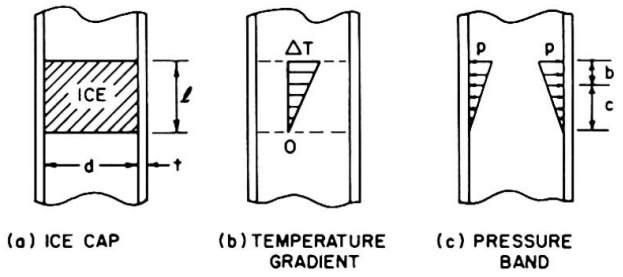

Fig. 3 Cylinder with ice cap

$$\sigma_h = Kpd/2t \qquad (5)$$

where the parameter, K, is given by

$$K = -\{c(e^{-\beta c}\cos \beta c + e^{-\beta b} \cos \beta b - 2)/2\ell + [e^{-\beta c}(\sin \beta c - \cos \beta c - 2\beta c \cos \beta c) - e^{-\beta b} (\sin \beta b - \cos \beta b - 2\beta b \cos \beta b)]/4\beta\ell\}, \qquad (6)$$

p is the maximum pressure, ℓ is the thickness of the ice cap, d is the diameter of the cylinder, t is the thickness of the cylinder wall and $\beta^4 = 12(1-\nu_T^2)/d^2t^2$ where ν_T is the Poisson's ratio of the cylinder material. Similar expressions can be developed [10] for hoop stresses in the portions of the cylinder wall outside the loaded area. Flexural stresses in the wall of the cylinder can be determined in a similar manner [10].

The pressure, p, at the top of the ice cap may be found by considering compatibility of deformations at the location of maximum deformation in the cylinder wall [10] and is given by

$$p = \frac{c}{\ell} \Delta T \, E_I(\alpha_I - \alpha_T)/[K \frac{\eta}{2} + (1 - \nu_I) \frac{c}{\ell}] \quad (7)$$

where the location of maximum deformation, is defined by

$$\frac{c}{\ell} \approx 0.667 + 0.01\beta\ell \quad (8)$$

and α_I is coefficient of thermal expansion of ice, α_T is coefficient of thermal expansion of cylinder material, E_I is modulus of elasticity of ice, ΔT is temperature increment at the top of the ice cap and $\eta = E_I d/E_T t$ where E_T is the modulus of elasticity of the cylinder material.

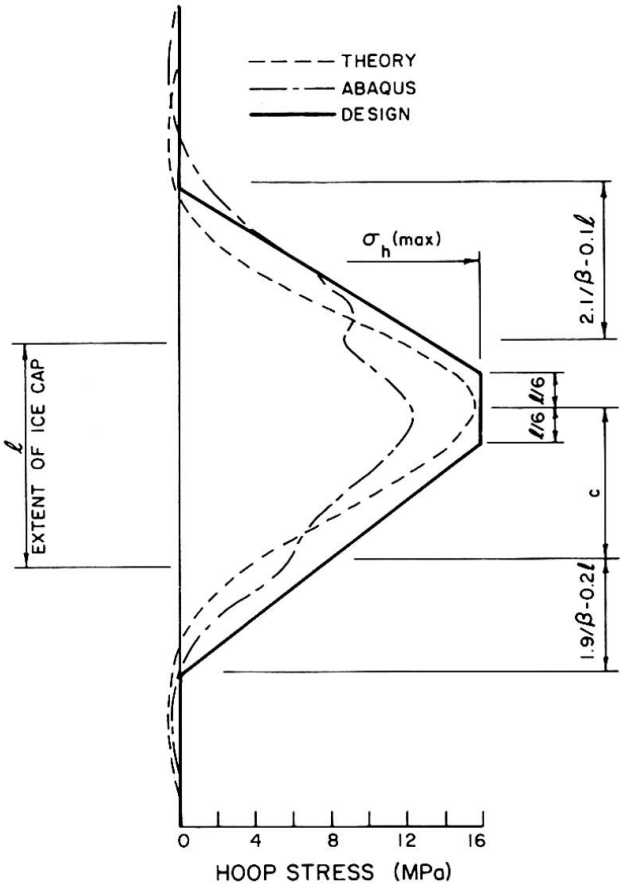

Fig. 4 Variation of hoop stress

A typical variation of hoop stress in the wall of a tank, as predicted by the above theory, is shown in Fig. 4, which also shows for comparison corresponding variations obtained using ABAQUS [7] to model the ice cap in the tank but neglecting creep in the ice. It can be seen that the hoop stress variations obtained by both approaches are similar. An idealized variation of the hoop stress proposed for design purposes is also indicated in Fig. 4. The locations of peak hoop stress and zero hoop stress in the wall of a tank are indicated. The zero stress locations are a function of β and ℓ. The magnitude of the peak hoop stress may be determined using Eqns. (5), (6) and (7). Charts to aid these computations, as well as those for flexural stresses, have been developed by Kong and Campbell [11].

4. EFFECT OF CREEP OF ICE

Creep of the ice will reduce the pressure exerted by an ice cap subjected to a rise in temperature over a finite time. The maximum static values of pressure and related hoop stress, determined as described previously, can be adjusted for creep using charts similar to that in Fig. 5. These charts have been developed from a study [11] of restrained ice discs under different values of initial temperature, heating rate and parameter η, which is a measure of the degree of confinement. The peak pressure developed in the ice has been expressed as a percentage of the

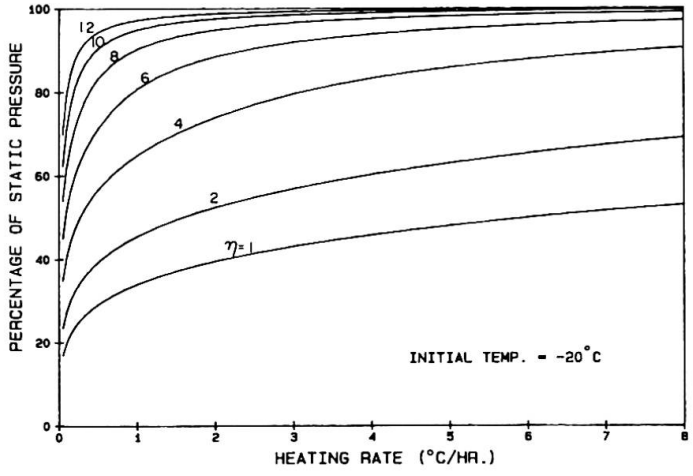

Fig. 5 Effect of creep of ice

corresponding maximum static pressure which would occur if creep were neglected. Figure 5 shows that, for a particular initial temperature, the effect of creep diminishes with increasing values of η, and heating rate. These reduced values of static pressure may be used in conjunction with Fig. 4 to determine the variations of hoop stress in the wall of a cylindrical tank.

A maximum tensile hoop stress of 6.5 MPa has been computed [11] for a concrete tank having a mean diameter of 7140 mm, a wall thickness of 400 mm and containing an ice cap 1000 mm thick. The initial temperatures in the ice cap were -20°C and 0°C at the top and bottom surfaces, respectively, and the heating rate was 2°C per hour at the top surface.

5. TESTING OF MODEL TANK

Tests [10], similar to those reported by Bergdahl [5], were carried out on a model steel tank to examine the ability of ABAQUS with Eqn. (1) incorporated to model the behavior of an ice cap in a water tank. The tank had an internal diameter of 886 mm, a wall thickness of 14 mm and a height of 1310 mm. Biaxial electrical resistance strain gauges (aligned circumferentially and axially) were attached to the wall of the tank. Thermocouples were placed at various levels within the tank, as well as on the wall. The tank was wrapped with 400 mm of fibreglass insulation over its entire height, and 100 mm of insulation was used underneath the tank.

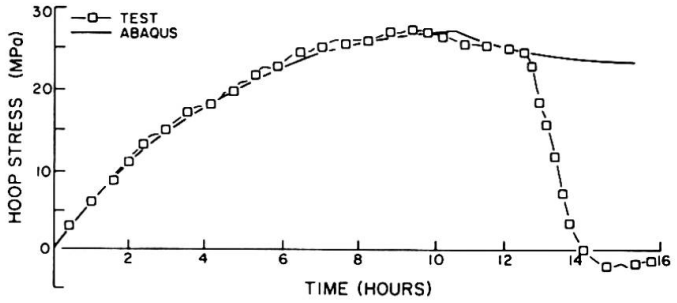

Fig. 6 Hoop stress vs. time

The tank was filled with tap water to the desired level and the temperature in the cold room facility, in which the tank was located, was lowered gradually to around -25°C. Ice formed initially on the top surface of the water and the ice cap gradually grew in thickness downwards. After the ice cap reached the desired thickness, the temperature in the room was raised gradually to 0°C. The test was concluded when melting of the ice cap occurred adjacent to the wall of the tank.

Type	Description
1	Wall delamination
2	Vertical cracks in wall
3	Wall/floor joint deterioration
4	Vertical voids in shotcrete
5	Jack-rod spalls
6	Shotcrete cover coat delamination
7	Waterproof coating failure
8	Cover coat cracking
9	Cold joints and horizontal cracks
10	Corrosion of prestressing steel

Table 1 Types of defects in tanks

Three tests were carried out. The thicknesses of the ice cap were 240, 300 and 308 mm and the heating periods were 14, 16 and 11 hours, respectively. Typical test data, showing the variation of the hoop stress in the tank wall with time at a depth of 46 mm below the top surface of the ice cap, are given in Fig. 6. Good agreement is obtained with a simulation of the test using ABAQUS.

6. DEFECTS OBSERVED IN CONCRETE TANKS

Ten of the main defects observed during surveys of concrete water tanks in Ontario are listed in Table 1. Most of the defects may be attributed to the influence of a freezing environment and possible mechanisms causing these defects are discussed in Ref. [1]. Delamination of the wall was prevalent and has been attributed to radial tensile stresses in the wall. Such stressses may be induced by either freezing and thawing with related dilation of saturated concrete in the outer portion of the wall exposed to solar radiation, or by trapping a lens of unfrozen water between an inward moving freezing front and the impermeable frozen zone in the interior of the wall section. Vertical cracking in the wall was attributed to pressure and induced hoop stress from internal ice formations which have been addressed in this paper.

7. CONCLUSIONS

A mathematical model for ice has been validated by data from tests on a model steel water tank containing an ice cap and has been used to develop a method for prediction of the hoop stress in the wall of a tank containing an ice cap. Hoop stresses large enough to crack the wall of a non-prestressed reinforced concrete tank may be induced by internal ice formations. It is recommended that internal ice formations be eliminated by suitable means such as providing insulation to the tank.

REFERENCES

1. GRIEVE, R., SLATER, W.M. AND ROTHENBURG, L., "Deterioration and Repair of Above-Ground Concrete Water Tanks in Ontario, Canada", Report to Ministry of Environment of Ontario, 1987.
2. PITKANEN, A., "Roihuvuori Water Tower", Prestressed Concrete in Finland 1974-78, Concrete Association of Finland, Helsinki, 1978. pp. 24-25.
3. MICHEL, B., "Ice Mechanics", Les Presses de L'Universite Laval, Quebec, 1978.
4. TUOMIOJA, M., JUMPPANEN P. and RECHARDT, T., "JaanLujuudesta ja Muodonmuutoksista" (The Strength and Deformation of Ice), Rakennustekniikka, March 1973, pp. 233 - 236.
5. BERGDAHL, L., "Thermal Ice Pressure in Lake Ice Cover". Report A2, Department of Hydraulics, Chalmers University of Technology, Sweden, 1978.
6. FINNIE, I. and HELLER, W.R., "Creep of Engineering Materials", McGraw-Hill, 1959.
7. ABAQUS User's Manual, Hibbitt, Karlson and Sorensen Inc., Providence, USA, 1984.
8. LINDGREN, S., "Thermal Ice Pressure", IAHR Ice Symposium, Reykjavik, 1970.
9. TIMOSHENKO, S. AND WOINOWSKY-KRIEGER, S., "Theory of Plates and Shells", McGraw-Hill, 1959.
10. KONG, W.L., "Thermal Ice Pressure in Cylindrical Water Tanks", Ph.D. Thesis, Queen's University, Kingston, Canada, 1986.
11. KONG, W.L. AND CAMPBELL, T.I., "Thermal Pressure due to an Ice Cap in an Elevated Water Tank", Can. J. Civ. Eng., Vol. 14, No. 4, 1987.

Behälterkonstruktion unter extremen Bergbaueinwirkungen

Drain tank construction under extreme mining influences

Construction de citernes sous des influences minières extrêmes

Klaus SCHÄFERS
Oberingenieur
Bauges Hanebeck
Dortmund, Bundesrep. Deutschland

Klaus Schäfers, geboren 1925, arbeitete nach Abschluß des Bauingenieurstudiums 1947 im Brückenbüro der Straßenbauverwaltung Westfalen an der Projektierung von Brückenbauwerken. Seit 1952 in der Baugesellschaft Hanebeck, Statiker für Brückenkonstruktionen in Spannbetonbauweise. 1962 Ernennung zum Oberingenieur und Leiter des techn. Büros, zuständig für den Gesamtbereich konstruktiver Ingenieurbau.

ZUSAMMENFASSUNG
Der Beitrag zeigt, wie bei extrem hohen Pressungen aus Bergbaueinwirkungen Erdbehälter wasserdicht hergestellt werden können, wenn man auf klar erfaßbare Grundsysteme zurückgreift und die Verträglichkeit untereinander durch konstruktive Maßnahmen löst.

SUMMARY
The exposition shows that in spite of the extremely heavy rock pressures, the underground tanks can be made watertight provided one relies on clearly conceived basic systems and brings about mutual compatibility by constructive measures.

RÉSUMÉ
L'exposé démontre comment des citernes souterraines étanches peuvent être construites en dépit de pressions extrêment élevées dues à des influences minières. Il recourt à des systèmes de base facilement compréhensibles et résout la compatibilité entre les citernes par des mesures constructives.

1. EINLEITUNG

1.1 Bergbaueinwirkungen auf Bauwerke

In Gebieten, in denen unter Tage Kohle oder Erze abgebaut werden, treten durch Nachsackungen in die entstandenen Hohlräume Verformungen im Deckgebirge ein, die sich bis zur Geländeoberfläche fortsetzen. In den Steinkohleabbaugebieten an der Ruhr und Lippe, wo der Abbau bereits Tiefen von über 1000 m erreicht, addieren sich aus den übereinanderliegenden abgebauten Flözen Senkungen an der Geländeoberkante in Größenordnungen von über 10m. Diese Senkungen sind nicht eben. Sie bewegen sich zwischen null und dem Maximalwert. Es kommt zu einer Trogbildung (Fig.1). Bezogen auf Bauwerke in diesen Bereichen bewegen sich diese zwischen einer Wannen- und einer Sattellage. Bedingt durch die Bodenbewegungen treten Dehnungen und Verkürzungen auf. Bauwerke, eingebettet in diese Böden erfahren aus diesen Längenänderungen Pressungen (Wannenlage) oder Zerrungen (Sattellage) (Fig.1). Bewegungen von 2-4 ‰ sind im Bereich des Kohleabbaues an der Tagesordnung, d.h. auf 1,00m Länge treten Bewegungen von 2-4 mm auf. Bei Zerrungen von 8‰ führt dies zu Bodenrissen selbst. Durch die Relativverschiebung zwischen Boden und Bauwerk werden bei Zerrungen auf alle vom Bauwerksschwerpunkt weggerichtete Flächen Zugkräfte, und bei Pressungen auf alle zum Bauwerksschwerpunkt hingerichteten Flächen Druckkräfte erzeugt (Fig.1).

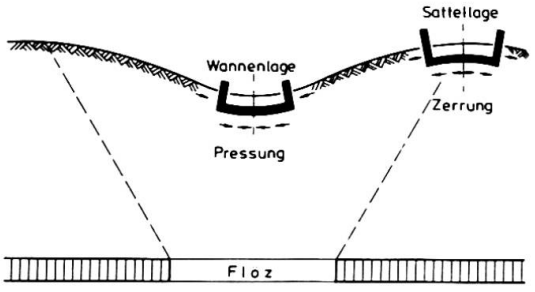

Fig.1 Prinzip der Bergbaueinwirkung

1.2 Beispiel: Bergbaueinwirkung auf einen Tiefbehälter

Die Bedeutung der zuvor dargestellten Bergbaueinflüsse werden nachfolgend am Beispiel eines Regenrückhaltebeckens gezeigt, welches die Bergbau AG Westfalen nach den, die Bergbaueinwirkung erfassenden Berechnungen des Büros Prof.Zerna, Schulz + Partner, in Hamm ausführen ließ, als Auffangbehälter bei starken Niederschlägen, um die Kapazität der vorhandenen Kanalleitungen nicht zu überanspruchen. Am Standort werden Pressungen von 7,7‰ erwartet, also einem extrem hohen Wert.
Der Behälter mußte angelegt werden für ein Fassungvermögen von 4000m³. Wegen der begrenzten örtlichen Verhältnisse mußte in die Tiefe gebaut werden, was zu einem Durchmesser von 20m und einer Bauwerkstiefe von 22m führte. Dabei bindet das Bauwerk 18m in den Felsboden ein. Wegen der knappen Grundstücksverhältnisse mußte eine Pumpstation von 12·5 m bis zur halben Bauwerkstiefe unmittelbar an den Behälter angebaut werden.
Bei dem erforderlichen Durchmesser von 20m und der zu erwartenden Pressung von 7,7‰ ergibt sich eine Zusammendrückung von 15cm, die von der Betonkonstruktion nicht ohne besondere Maßnahmen aufgenommen werden kann, zumal die angehängte Rechteckkammer das sonst rotationssymmetrische statische Grundsystem stört. Die Forderung nach absoluter Wasserdichtigkeit konnte nur durch besondere statische Annahmen und konstruktive Maßnahmen erfüllt werden.

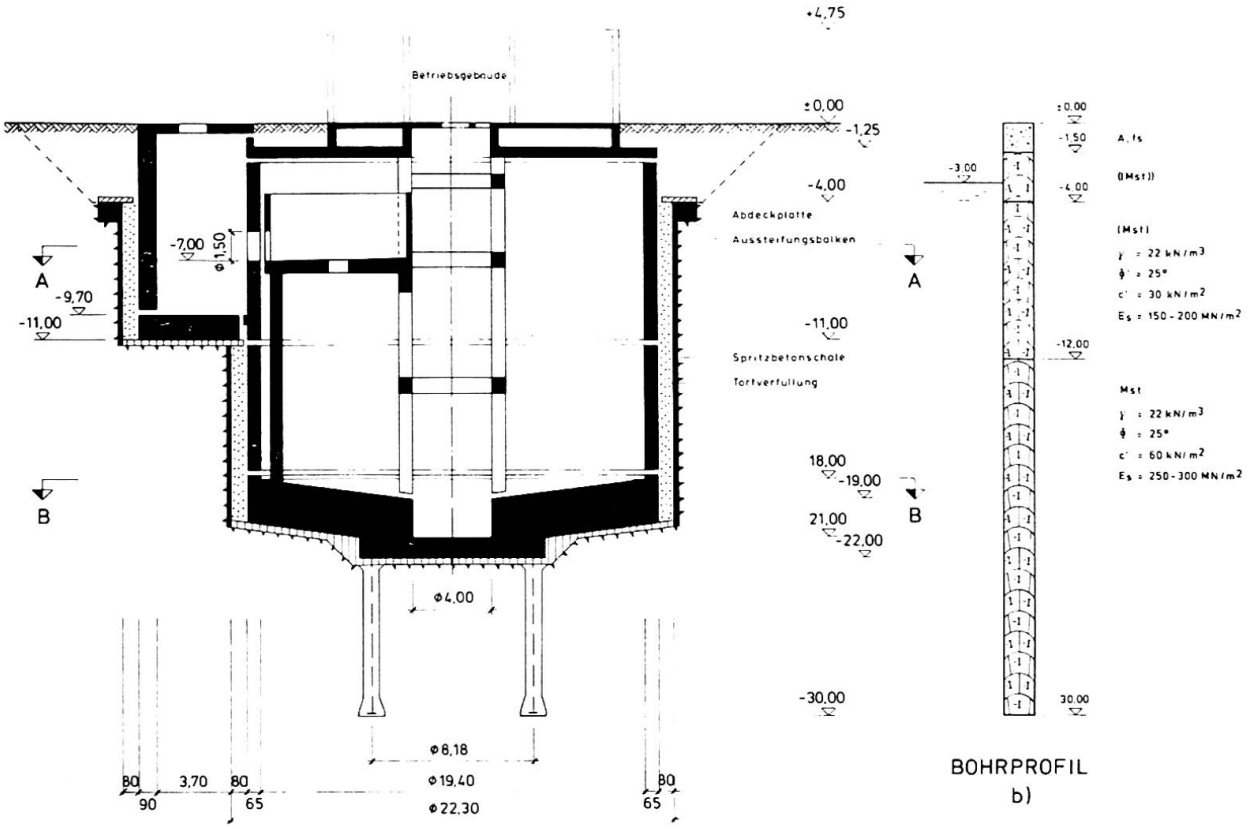

SCHNITT C-C
a)

BOHRPROFIL
b)

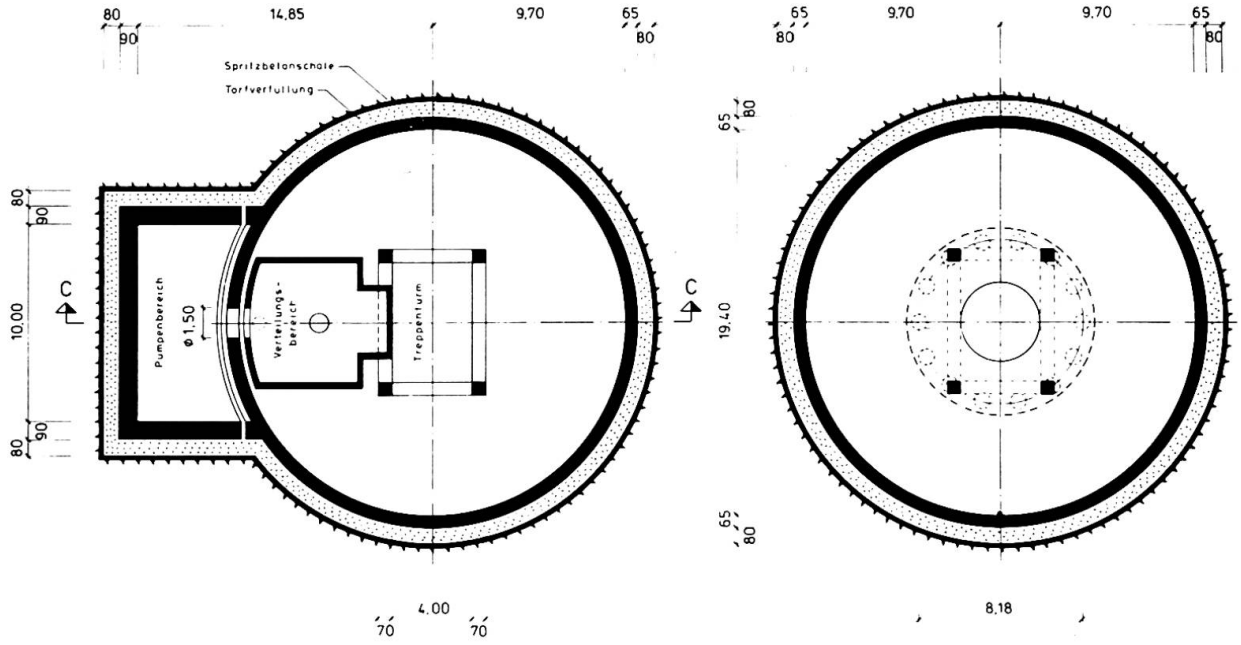

SCHNITT A-A
c)

SCHNITT B-B
d)

Fig.2 Übersicht

2. STATIK UND KONSTRUKTION

2.1 Geologische Verhältnisse

Fig.2b zeigt das Bodenprofil. Nach 4,00m feinsandigem Überlagerungsboden folgt der Felsboden in Form eines Kreidemergels. Die Festigkeit, ausgedrückt durch die Steifezahl E_s, schwankt zwischen 150-300 MN/m² . Für die Berechnung wurde einheitlich der Wert E =200 MN/m² festgelegt. Fig.3 zeigt den Ansatz des Felsdruckes, sowie den Wasserdruck, bei einem Grundwasserstand auf der Höhe -3,00m unter der Geländeoberkante.

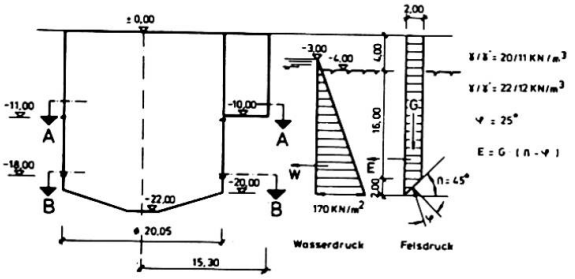

Fig.3 Fels- und Wasserdruck

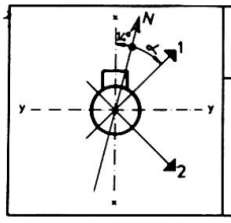

α °	Zerrung (+) Pressung (-) Richtung 1	Richtung 2
22,5	-6,0 mm/m	-1,1 mm/m
45,0	-7,7 "	+0,4 "
67,5	-7,0 "	±0,0 "
90,0	-4,3 "	-2,8 "

Tabelle 1 Bergbaueinwirkungen

2.2 Bergbaueinflüsse

Die Gebirgsverformungen werden seitens des Bergbaubetreibers für den Endausbauzustand angegeben, gemäß der Tabelle 1. Wie die Zahlenwerte erkennen lassen, treten im wesentlichen nur Pressungen auf. Auch in den Zwischenphasen sind keine größeren Zerrungen zu erwarten. Die Pressungskräfte haben in den verschiedenen Kraftrichtungen, ausgedrückt durch den Winkel α bezogen auf die Nordrichtung unterschiedliche Größen.

2.3 Statisch-konstruktives Grundprinzip

Die Behälterzusammendrückung von 15cm gestattet keine wasserdichte Stahlbetonkonstruktion, die aber wegen der besseren Unterhaltungsaufwendung gewünscht wurde. Die Lösung der Aufgabe wurde durch mehrere konstruktive Eingriffe ermöglicht.
Zur Reduzierung der Verformungen aus den Bergbaueinflüssen wurde eine verformbare Schicht zwischen Behälterwand und Gebirge angeordnet. Zur Diskussion standen zunächst Einlagen aus Styropor oder Porenschlacke (Perlite). Bei näheren Untersuchungen stellte sich heraus, daß diese Stoffe unter Wasseraufnahme bei schwankenden Belastungseinflüssen einen Großteil ihrer Federwirkung verlieren. Als geeignet stellte sich die Verwendung von faserigem Torf heraus. Fig.4 zeigt das Last-Setzungs-Diagramm des verwendeten Materials. Der in die Berechnung einzusetzende Steifemodul wurde zu E_s =0,5 MN/m² ermittelt.
Im Hinblick auf den für die Baudurchführung erforderlichen Arbeitsraum und eine entsprechende Kostenoptimierung ergab sich eine Stärke der einzubauenden Torfschicht von 80cm zwischen Behälterwand und Gebirge. Diese Schicht wurde in der statischen Berechnung des Behälters durch einzelne Federn diskretisiert (Fig.5), wobei sich die Federsteifigkeit ergibt aus der Beziehung $c = \frac{P}{v} = \frac{\sigma \cdot a \cdot b}{\varepsilon \cdot d} = \frac{E \cdot a \cdot b}{d}$ Der in die Berechnung einzuführende Elastizitätsmodul ergibt sich aus den eingangs angegebenen Steigemoduli E_s für den Fels und den Torf nach der Beziehung $E = E_s \left[1 - \frac{2 \cdot \nu^2}{1-\nu}\right]$, $\nu = 0.3$

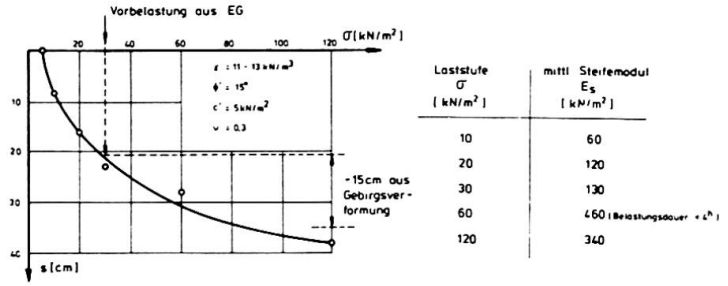

Laststufe σ [kN/m²]	mittl. Steifemodul E_s [kN/m²]
10	60
20	120
30	130
60	460 (Belastungsdauer < 4h)
120	340

Fig.4 Lastsetzungslinie Torf

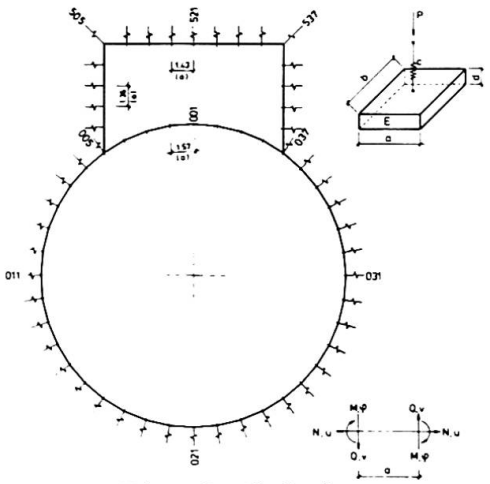

Fig.5 Abfederung der Grundkonstruktion

Die Lasteinwirkungen wurden an den in Fig.6 dargestellten Einzelsystemen untersucht. Die Berechnung als geschlossenes Behältersystem hätte zu schwer kontrollierbaren Spannungszuständen geführt, die auch durch Bewehrungen nicht klar abgedeckt werden konnten.
Die Wechselwirkung zwischen Gebirge, Torfpolster und Bauwerk wurde an einem Gedankenmodell von 76,2/76,2m mit Hilfe Finiter Elemente errechnet. Als Auszug aus dieser Berechnung zeigt Fig.7 den Momentenverlauf an beiden Systemen unter dem ungünstigen Lastfall "Bergbaueinwirkung unter 45°" und "Wasserdruck". Die Verformungen, die diesen Momentenbildern analog verlaufen, lassen die unterschiedlichen Bewegungen an den Systemrändern erkennen. Sie betragen bis zu ± 4cm.

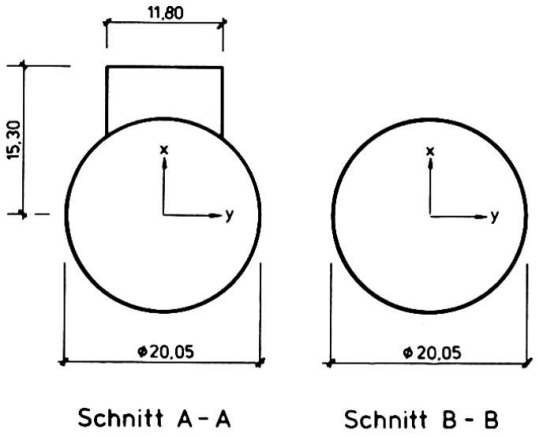

Fig.6 Grundsysteme

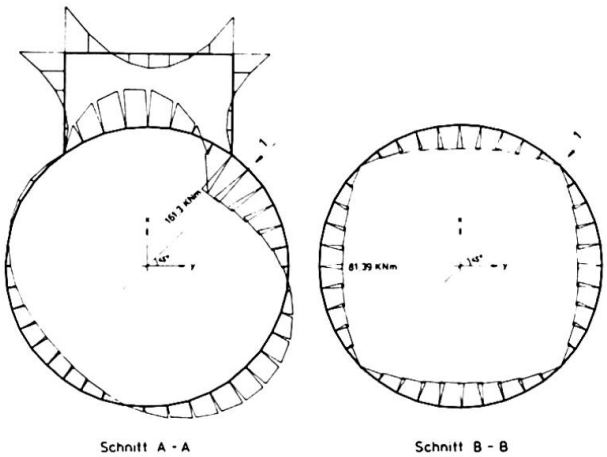

Fig.7 Momentenverlauf

2.4 Konstruktive Besonderheiten

Um diese Bewegungen aufnehmen zu können, mußte der Fugenausbildung besondere Aufmerksamkeit gewidmet werden. Nach der Abb.1a sind die systembezogenen Bewegungsübergänge zunächst vorhanden oberhalb der Sohlplatte, auf der Höhe -11,0 und unterhalb der Deckenkonstruktion. In diesen genannten Schnittebenen müssen die Vertikallasten V, die Horizontallasten H und die damit einhergehenden Verformungen aufgenommen werden. Darüber hinaus müssen sie

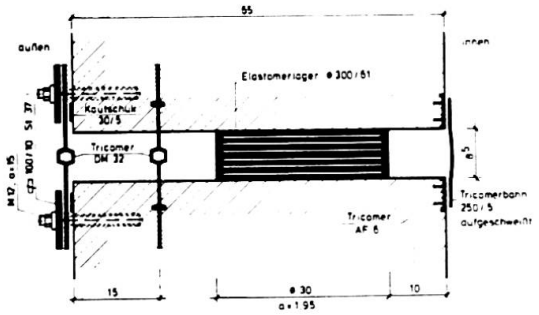

Fig.8 Fugenausbildung

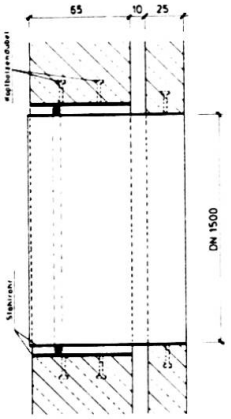

Fig.9 Rohreinlauf

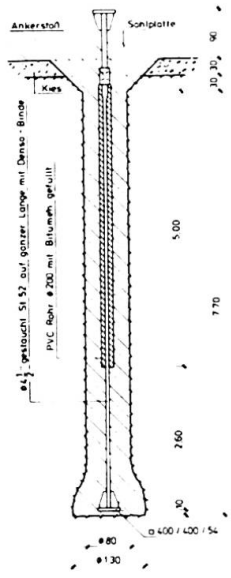

Fig.10 Ankerpfahl

der Forderung nach Wasserdichtigkeit genügen. Fig.8 zeigt die Lösung. Die V und H-Lasten werden durch bewehrte Neoprenlager mit Abmessungen Ø 300/61 im Abstand von 1,95m aufgenommen. Diese Lagerkörper haben ein Verschiebungsvermögen von 42,5mm. Die eigentliche Behälterdichtigkeit wird erreicht durch ein hinter den Lagern angeordnetes Kunststoff-Fugenband mit Mittelschlauch auf Polymerbasis, ausgelegt auf einen Bewegungsspielraum von 40mm. Da ein auswechseln dieser Teile nicht mehr möglich ist, wurde die Bewegungsfuge zusätzlich an den Außenkanten durch bewegliche Fugenbänder verschlossen, um einem Korrosionsverfall vorzubeugen. Für die betriebliche Funktion der Behälteranlage waren Einbauten vorzunehmen (Fig.1a), die bewegungsfrei von der Wandkonstruktion zu halten waren. Für den Wassereinlauf von der Pumpenkammer in die Verteilungskammer war dabei eine verschiebliche Rohrkonstruktion vorzusehen, die die Bewegung von ±40mm mitmacht (Fig.9).

2.5 Auftriebssicherung

Der Behälter taucht im Endausbau 19,0m in das Grundwasser ein. Er erfährt damit eine Auftriebskraft von 64 MN. Dieser Kraft konnte kein entsprechendes Eigengewicht gegenübergestellt werden. Die Wandstärken konnten zur Gewichtserhöhung nicht verstärkt werden, da sie im Hinblick auf die Verformungen elastisch gehalten werden mußten. Eine Aktivierung der Wandreibung war wegen der erforderlichen Torfpolsterschicht nicht möglich. Die Restauftriebskraft $\Delta A = A-G$ mußte daher über Erdanker von der Sohle aus auf den Felsuntergrund übertragen werden. Dies erfolgte über 14 Stahlanker Ø 90/115mm in St 52, die bis in die Tiefe von -30,0 in Bohrlöcher Ø 80cm eingesetzt wurden mit anschließender Ausbetonierung. Der Fuß der so angelegten Großbohrpfähle erhielt zur Aktivierung des Bodengewichtes eine Verbreiterung auf 1,30m (Fig.10) Die Pfähle sind ringförmig mit einem Durchmesser von 8,18m in der Sohlplatte angeordnet. Bei der zu erwartenden bergbaubedingten Verschiebung von 7,7‰ erfährt der Ankerkopf eine Bewegung von 32mm. Bei starrer Einspannung würde das zum Bruch des Stahlankers führen. Wie Fig.10 zeigt, wurde der Ankerstab auf 5,0m Länge mit einem mit Bitumen gefüllten Plastikrohr ummantelt, um so eine Verformungsmöglichkeit zu gewährleisten.

Energy Absorption Capability of Slabs with Different Reinforcement Steel

Capacité d'absorption d'énergie de dalles en béton avec différentes armatures

Energieaufnahmefähigkeit von Betonplatten mit verschiedener Bewehrung

Lars ANDERSSON
Tekn lic
Royal Inst. of Technology
Stockholm, Sweden

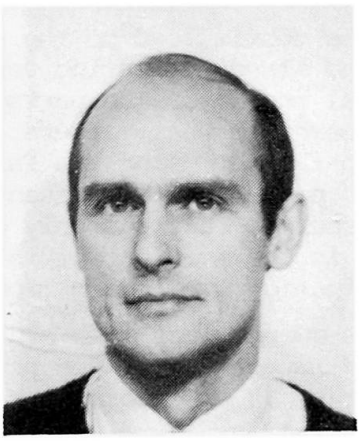

Lars Andersson, born 1947, received his civil engineering and licentiate degree at the Royal Inst. of Technology. Since 1969 he has been working in the field of building construction. In 1983 he started research work with the aim of determining debris loads on shelters.

SUMMARY
One-way reinforced concrete slabs with different types of reinforcement steel have been loaded in impact by a free falling drop weight of steel. The aim was to study how different reinforcement steel influence the capability of the slabs to absorb energy. The dissipated energy was estimated by comparing the sum of potential and kinetic energy before and after impact. Positions and velocities of the slab and drop weight were determined with a high speed camera in order to calculate the energy after impact.

RÉSUMÉ
Des dalles en béton armé renforcées dans une seule direction mais avec différentes armatures ont subi les chocs d'une masse d'acier en chute libre. L'objectif de l'étude était de voir l'influence des différentes armatures sur la capacité d'absorption d'énergie de ces dalles. L'énergie dissipée a été calculée en comparant la somme des énergies potentielle et cinétique avant et après le choc. La position et la vitesse de la masse métallique et de la dalle ont été déterminées avec un appareil photo à haute vitesse, afin de calculer l'énergie après le choc.

ZUSAMMENFASSUNG
In einer Richtung gespannte Betonplatten mit verschiedener Bewehrung wurden mit einer fallenden Masse aus Stahl stossbelastet. Das Ziel war es, den Einfluss verschiedener Bewehrungsstähle auf die Energieaufnahmefähigkeit der Platten zu bestimmen. Die kinetische und potentielle Energie vor und nach dem Stoss wurden mit einer Hochgeschwindigkeitskamera bestimmt. Der Unterschied der Energie vor und nach dem Stoss ist gleich der Energieaufnahme der Betonplatte.

1. INTRODUCTION

To protect civil people from damages in war, shelters are built. The shelters are often placed in the basement of a building. To design the shelters one first have to decide what kind of loads the shelter shall be designed for. The Swedish formula code says that two loads as a result of war actions are to be considered: first, the shock wave from an exploding bomb and second, the debris load from the collapsing buildings.

The author has since 1983 studied how to calculate the debris load. The aim was to divide buildings into different types depending on their capability to reduce the debris load.

Briefly one can say that the debris load on the shelter will be a function of the mass of the building and its distribution vertically above the shelter-roof. In other words the potential energy of the parts of the building that can be transformed into kinetic energy is what matters. The collapse of the building is assumed to start at the top floor. During the fall energy losses will occur when the building is broken into parts. In the present Swedish code formula used to calculate the load on the shelter-roof the only energy loss during the collapse that is taken into account is the energy that is needed to fail the floor slabs in flexure and energy dissipation at plastic impact.

To estimate and compare the energy loss when slabs are loaded to ultimate failure, several static and impact tests were performed and reported in [1] and [2]. In the tests different types of slab strips and loadings were used.

It was found that in slabs with the reinforcement arranged so that membrane effect could occur the energy dissipation to exhaust the bearing capacity was very high compared with slabs with only bending moment.

The consequence of this for calculating the debris load on shelters is that buildings could be separated into two parts. One with only flexure moments in the slabs and one where the reinforcement is arranged so that membrane effect more or less can occur. In buildings with membrane effect the debris load will be smaller.

Different kinds of reinforcement are used in practice. It would therefore be of great interest to compare how the choice of different reinforcement steel influence on the energy dissipation when a slab with membrane effect is loaded to ultimate failure. Impact tests on slabs with different reinforcement steel were carried out and are reported in [3] and [4]. A summary of this research work is given here.

2. TEST SPECIMEN

Mainly four kinds of reinforcement steel were used. They had the notations Ss26S, Ks40, Ks60 and NPs50 and are frequent in Sweden. S stands for plain bars, K stands for deformed bars, sxx stands for nominal yield strength in kp/mm^2, S in the end stands for weldable.

The slabs had the dimensions: length 1,96 m, width 1,20 m and depth 0,1 m. (An example can be seen in fig 1). The number of reinforcement bars was chosen so that the same total tensile force in the slabs was attained independent of the type of reinforcement steel. The calculation of how many bars each slab should have was based on the yield force of a single bar. The total force in the slab was 210-220 kN. Totally 34 slabs were tested.

3. PERFORMANCE OF THE TESTS

The load was a free falling drop weight of steel. The mass of the drop weight was one ton which was twice as much as the mass of the slab. The drop weight

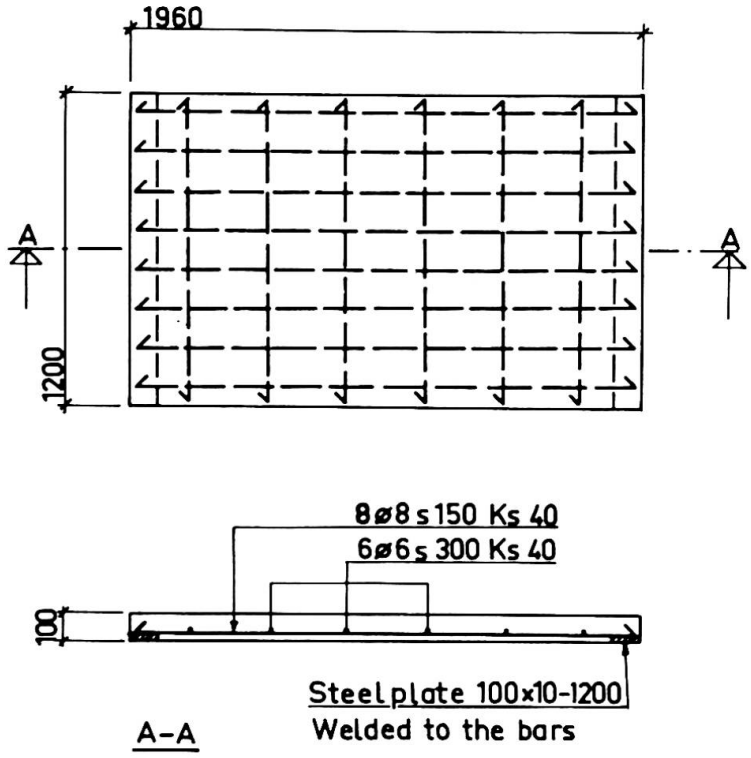

Fig.1 Test specimen.

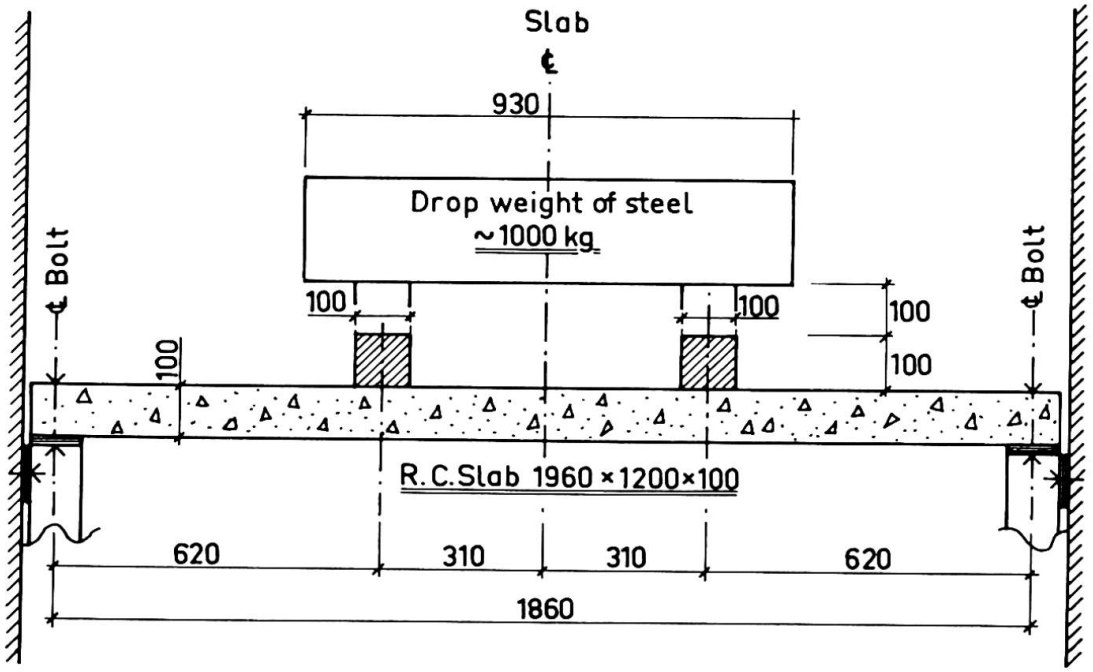

Fig.2 The drop weight standing on the test specimen.

standing on the plate is shown in fig 2.

The drop heights were mainly 4, 8 and 11 meters. In the case of 4 m the drop weight was stopped or nearly stopped if the reinforcement was Ss26S, Ks40 or Ks60.

4. ANALYSIS OF THE TESTS

The tests were filmed with a high speed camera (~500 pictures/sec). On the films the course of events could be followed. With help of the films, the kinetic and potential energy was calculated when positions, velocities and masses of the drop weight and plate were known. These energies were compared with the initial total energy for the drop weight slab system to get the energy dissipation during the time it took to exhaust the bearing capacity of the plate. See one example in fig. 3.

The remaining strain of the bars after the impact tests was measured. This strain was about 15 to 40 % of the limit strain. The limit strain is the strain at maximum force in tensile tests on reinforcement bars.

The theoretical modelling of the test was done by replacing the real drop weight/slab system with an equivalent mass-spring system. The equivalent system has the same characteristics concerning energies and work done under the deformation as the real system. Data from the tests were used to verify the calculation model.

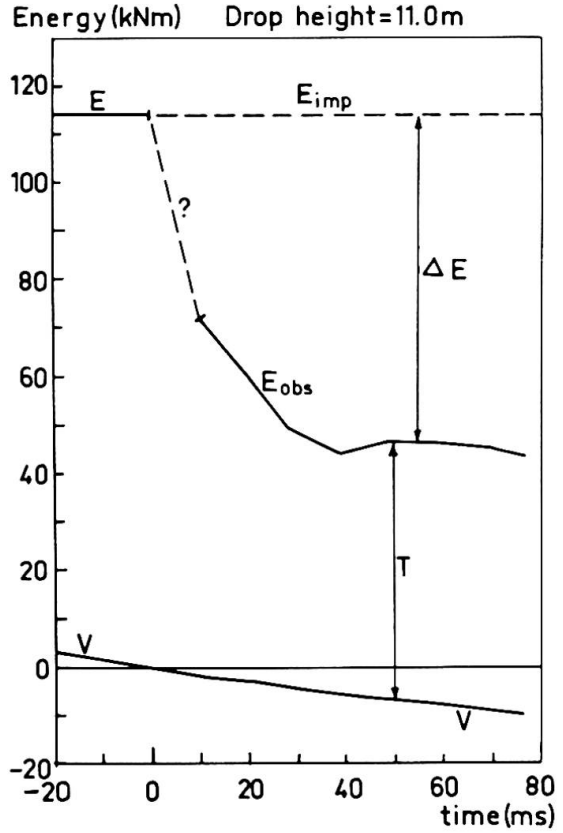

Reinforcement: $\frac{Ks40}{8\phi 8 s150}$

Fig.3 Comparison between the sum of potential and kinetic energy before and after impact.
Time at impact = 0.
V = Potential energy. Zero at impact.
T = kinetic energy.
E_{imp}=V+T at the moment of impact.
E_{obs}=Observed sum of V and T after impact.
ΔE = Energy dissipation. (= $E_{imp} - E_{obs}$)

5. RESULTS

The relation between energy absorbed in the whole plate (with different kinds of reinforcement) was, if the energy absorbed in plates reinforced with Ks60 is set to 1,0:

Drop height (m)	Ss26S Φ8	Ks40 Φ8	Ks60 Φ8	NPs50 Φ6
11 m	1,9	1,2	1,0	0,65
8 m	2,6	1,4	1,0	>0,45

An estimation of the relation between energy absorbed in the reinforcement bars was, if the energy absorbed in Ks60 is set to 1,0:

Drop height (m)	Ss26S Φ8	Ks40 Φ8	Ks60 Φ8	NPs50 Φ6
11	2,7-2,5	1,7-1,4	1,0	0,6-0,5
8	3,0-2,8	1,7-1,5	1,0	-
4	(2,3-2,1)[1]	2,0-1,7	1,0	0,5-0,4

[1] Should be higher because the ultimate strain was not reached.

It is seen from the first table that it is possible to rank the reinforcement after its capability to absorb energy. The plain bar Ss26 is best. The ranking is the same as if you would have compared the limit strain of the bars. You could also see from the two tables that an increased drop height makes the difference in energy absorption capability smaller.

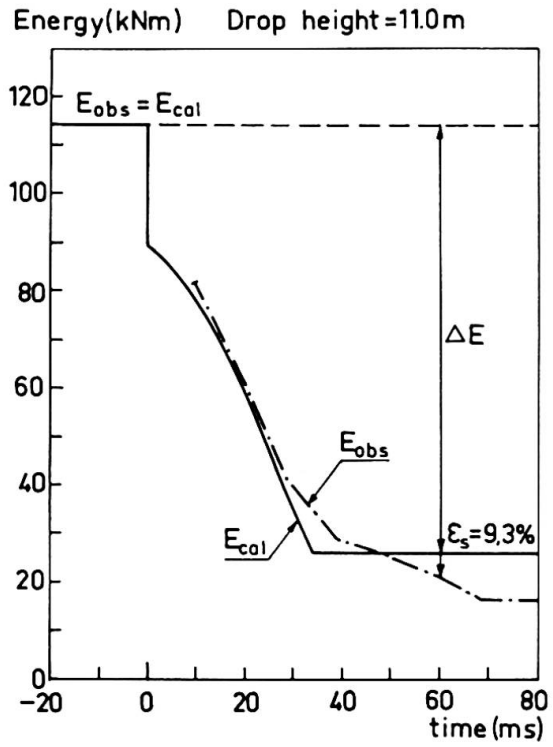

Reinforcement: $\frac{\text{Ss26S}}{13\phi\ 8\ s92}$

Fig.4 Comparison between observed (E_{obs}) and calculated (E_{cal}) sum of potential and kinetic energy. Time at impact = 0.

ΔE = Energy dissipation.
ε_s = Measured ultimate strain in the reinforcement bars.

The extended drop height also gave an increased energy dissipation. The reason for this is that the plates are broken into smaller parts and therefore the reinforcement loses the surrounding concrete. Free reinforcement bars have higher strain capability than bars embedded in concrete.

The theoretical estimation of the sum of kinetic and potential energy shows good agreement with the energy from the tests. See one example in fig.4. The calcula tion of the energy dissipation is stopped when the calculated remaining strain in the bars is equal to the observed remaining strain in the plates. A high value of the tensile force of the bars is presumed.

6. ACKNOWLEDGEMENT

This work has been done under the guidance of my teacher Professor Sven Sahlin.

The tests reported here were carried out in the laboratory of the Department of Structural Mechanics and Engineering at the Royal Institute of Technology, Stockholm, under the direction of Kent Lindgren.

This study is a part of a larger research program sponsored by the Swedish National Rescue Service Board with the aim to study debris loads of buildings on shelters.

REFERENCES

All references are published by the Department of Structural Mechanics and Engineering, Royal Institute of Technology, S-100 44 Stockholm, Sweden.

1. ANDERSSON L., Influence of Debris Loads on Shelters. Static and Impact Loads on Slab Strips of Concrete. A study of the Energy Dissipation. Bulletin No. 141, 1985.
2. ANDERSSON L., Loads on Shelters from Collapsing Buildings. Energy Dissipation in Impact tests on One-Way R.C. Slab Strips. Bulletin No. 145, 1987.
3. ANDERSSON L., Impact Tests on One-Way R.C. Slabs, part 1. Influence of Different Reinforcement Steel on the Energy Absorption Capability of the Slabs. Bulletin No. 148, 1987.
4. ANDERSSON L., Impact Tests on One-Way R.C. Slabs, part 2. Influence of different Reinforcement Steel on the Energy Absorption Capability of the Slabs. Bulletin No. 150, 1987.

Structural Design of Blast Resisting Chambers

Calcul de chambres résistantes à l'explosion

Bemessung einer Explosionskammer

Boris BALJKAS
Lecturer
University of Zagreb
Zagreb, Yugoslavia

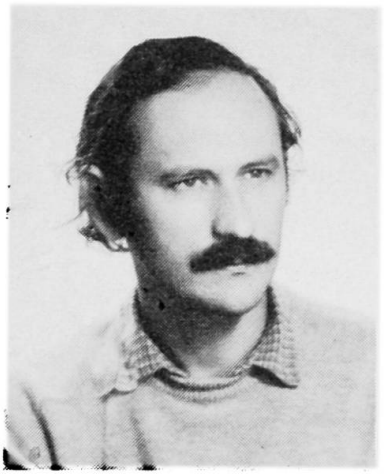

Boris Baljkas, born 1949, graduated at the Civ. Eng. Fac. at the University of Zagreb. Since 1976 lecturer and since 1981 senior consultant at the Civil Eng. Fac. He has published a large number of scientific and professional papers from the field of computer design, static and dynamic analysis and theory of structures. Practical works includes design of r.c., steel, aluminium and wood structures.

Zvonimir ZAGAR
Professor
University of Zagreb
Zagreb, Yugoslavia

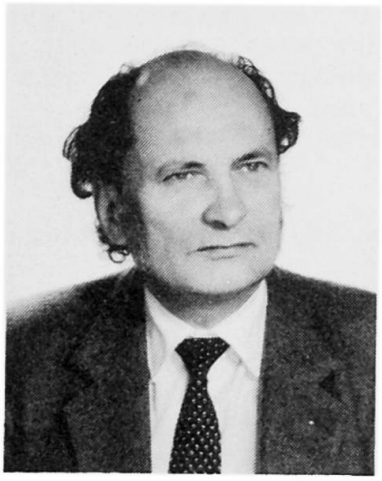

Zvonimir Zagar, born, 1931, graduated at the Civil Eng. Fac. in Zagreb. Professor at the Fac. of Arch., Kumasi University from 1965–1971, from 1971 to 1976, at the Interfaculty Transport and Traffic Study, Univ. of Zagreb. Since 1982 professor and Head of the Dept. for Wooden Struc. at the Civil Eng. Fac. Practical works includes design of r.c., steel, wood structures, ultra light and NU shelter structures. Published several books and large number (over 150) scientific papers.

SUMMARY
Structural design, static and dynamic analysis of a 'Protective Centre' is described. Special, in building, explosion-resistance chambers for explosion detection and initiation are designed. The results of dynamic analysis of a chamber due to a fixed explosive TNT charge is described in detail. The finite element method was applied using computer programs.

RÉSUMÉ
L'article explique les méthodes de calcul statique et dynamique d'une structure d'un centre de protection comportant des chambres de detection et de mise à feu de colis explosifs. Les résultats de l'analyse dynamique des chambres sont décrits en détail. La méthode des éléments finis ainsi que des programmes de calcul ont été appliqués.

ZUSAMMENFASSUNG
In diesem Artikel ist die statische und dynamische Berechnung von Explosionskammern für ein Schutzzentrum dargestellt. Im Gebäude sind spezielle Kammern für die Entdeckung und eventuelle Vernichtung von Explosivsendungen vorgesehen. Die Methode der finiten Elemente sowie Berechnungsprogramme wurden angewendet.

1. THE STRUCTURE

The 'Protective Center' is a 5-storey reinforced concrete building, consisting of three dimensional frame type of structure with slabs and shear-walls. Position of the shear-walls is determinated exclusively by functional reasons and less by some structural demands. In this way a very stiff system was created with relatively regular grids without greater differences in the positions of the center of stiffness and the center of mass. On the top floor there are very great masses in a joint block-the three rc chambers, for the control of eventual explosive packages. The chambers are covered with a protective vaulted structure with some openings in order to protect the surrounding population and neighboring buildings in the event of an explosion. Above the roof openings a suspesion chain net is fixed to protect the surrounding area. Some parts are disposable. The floors are rc slabs and beams where there are greater spans. The foundation is a rc slab, on a gravel layer.

2. STATIC AND DYNAMIC ANALYSIS OF STRUCTURE

2.1. The whole building

At the first step the whole structure was analysed as a 3D structure using the SD2A program. In the static and dynamic analysis all load-bearing structural elements were included in the mathematical model: columns, beams, girders, shear-walls, with certain restrictions of the calculation model. The masses are concentrated at the height of the floor slabs. The great masses of the Blast Resisting Chambers were included in the analysis.

The modal analysis method and response spectra analysis were applied to the dynamic analysis according to the YU Seismic Code. This was done using the SD2A computer program.

Maximum member and element forces are obtained for the influence of the earthquake applied in three independent directions, two in orthogonal directions and one in a direction at 45 degrees to the building axes, according to the estimate of the possible greatest effect of torsional mode. Special program for proportioning of rc members according to the ultimate strength method, were used on the PC SC328.

2.2. The foundation

The STRUDL program and TOPOLOGY subsystem, generator of data, were used for the analysis of the foundatin slab. Finite elements were used to simulate the slab on Winkler base. The elastic spring constants of the base are assumed according to the geomechanical report. The cellar walls and the cores were included in the FEM model.

3. ANALYSIS OF THE TNT EXPLOSION IN BLAST RESISTING (BR) CHAMBERS

The BR chambers and floor slabs on the third floor where a TNT blast could possibly take place have been analysed for both, static and dynamic loading as follows:

- the floor slab for uniform and ckeck distributed load,
- the floor slab for control static load 60 KN/mm,
- the floor slab, walls and roof core of the chamber for explosion impact load,
- the floor slab and walls for equivalent static load.

The postulated impact wave is shown in the Fig. 1. The values are obtained from (13) and factorized with the factor

f = p /p * F where:

p - pressure at a distance of from the center of the explosion,
p - pressure at a distance of 1.5 meters from the center of the blast and comes to 400 KN/mm,
F - a surface that belongs to a specific node.

The same method was used for designing the vaulted roof structure and heavy moving parts (doors etc) as parts of the whole structure.

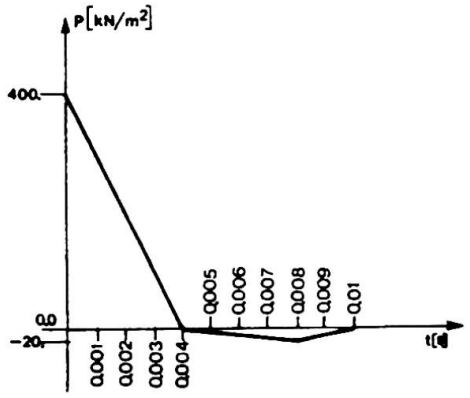

Fig. 1. Assumed impact wave explosion.

For the needs of dynamic analysis in real time the impact wave is described as 'Time History' in the data storage of the program STRUDL. It was obtainted in a separate research study.

From (1) and (6) we can conclude that analysis of the blast impulse effect on the entire system is conducted up to the substructures of the system. For this reason special consideration is given to the effect of shocks to possible walls, slabs and a sector frame of the whole building from the roof to foundation, with possible blasts in the inner and outer chambers. In this analysis the plate bending FE of the slabs and walls were used.

Independent of this, the whole system of the chamber, shown in Fig. 2, is modeled as the FE members model in order to provide a global insight into effect of a blast on the whole. The impact wave in this case is divided into three directional components (x, y, z) and placed to act at the crosspoints of members which represents the slabs and walls with corresponding stiffness.

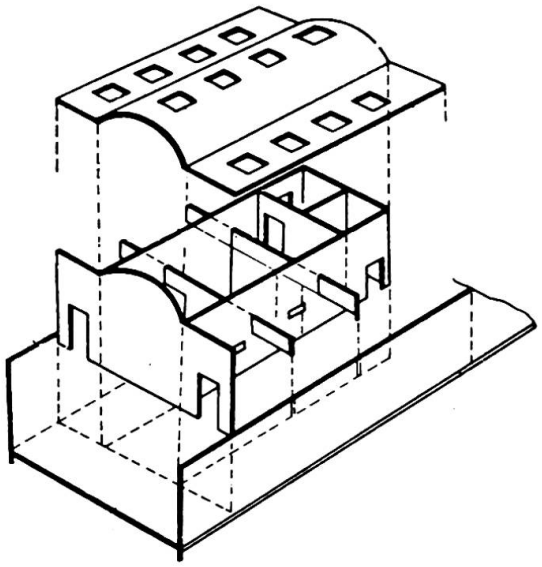

Fig. 2. The chambers divided into substructures.

Characteristic results obtained using dynamic modal analysis are shown in Fig. 3. The deformation time history of the point on the wall is visible during the time of the blast effect.

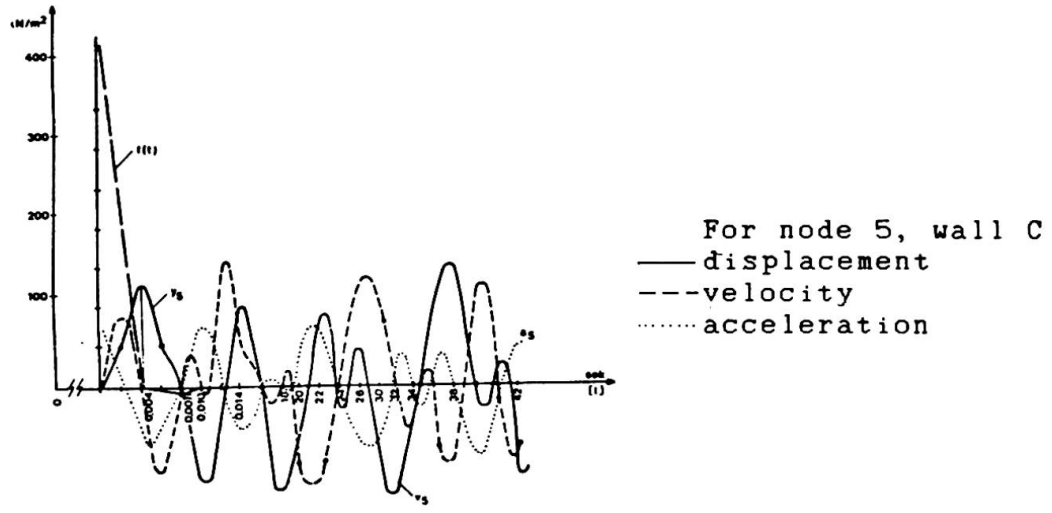

Fig. 3. Result of dynamic analysis. The finite element method and real-time response.

4. CONCLUSION

All these analyses have shown a relatively small effect of certain possible amounts of TNT explosive charge to the building and its structural elements. The cause of this is the large mass at the top of building that provides resistance to the dynamic shock wave. Dynamic shock of the blast is relatively great in intensity but very brief in duration. The forces that erupt in such a short interval are relativly small and it is not necessary practically to provide much additional reinforcement above the normal reinforcing, constructive reinforcments. Dynamic analysis of this type shows the lack of reality in today's analysis of NU shelters that do not take the sites into consideration, the speed with which the nuclear impact wave spreads and its intensity. An obligatory application of real-time dynamic analysis is proposed when designing explosion resistant or blast protective shelters because it can provide considerable savings in the amount of building material.

REFERENCES

1. ABRAHAMSON G. R., LINDBERG H. E., Peak Load Impuls characterization response of Structures. Pergamon Press, N. Y.

2. BIGS M. J., Introduction to Structural Dynamics. McGraw-Hill, N. Y.

3. MOSQUERA J. M., KOLSKY P., SYMONDS S., Impact Tests on Frames and Elastic-Plastic Solution. J. of Eng. Mech., Vol III, No. 11/85, 1380-1401.

4. GHABOUSSI J., W. A. MILLAVEC, J. ISONOBERG, R/C Structures Under Impulsive Loading. J. of Str. Eng., 1985, 505-522.

5. ZUKAS A. J., T. NICHOLS, H. F. SWIFT, D. R. CURRAN, Impact Dynamics, Moskva, MIR, 1985.

6. ZAGAR Z., Javna sklonista kao visenamjenski objekti, disertacija, FGZ Zagreb, 1984.

7. ZAGAR Z., Kompjutersko proracunavanje konstrukcija sa ICES-STRUDL sustavom, FGZ Zagreb, 1986.

8. xxxxx Users Manual ICES-STRUDL, MIT.

9. MARTIN J. B., LEE L. S., Approximate Solution for Impulsively Loaded Elastic-Plastic Beams. J. of Appl. Mech., Vol 35, 803-809, 1968.

10. PERRONE N., Response of Rate-Sensitive Frames to Impulsive Load. J. of the Eng. Mech. Div., ASCE, Vol 97, 49-62, 1971.

11. SYMONDS P. S., MOSQUERA J. M., A Simplified Approach to Elastic-Plastic response to General Pulse Loading, J. of Appl. Mech., Vol. 52, 115-121, 1985.

12. SYMONDS P. S., Elastic-Plastic Deflections Due to Pulse Loading. Procced. of the Sec. Spec. Conf. on Dynamic Response of Structures.

Leere Seite
Blank page
Page vide

Fire under a Long Span Bridge

Incendie sous un pont à grande portée

Brand unter einer Brücke grosser Spannweite

Shunsuke BABA
Associate Professor
Nagoya University
Nagoya, Japan

Shunsuke Bana, born 1949, received his degree of Dr.Eng. in 1977 at Nagoya University. He has worked at Nagoya University as associate professor for 9 years.

Tateo KAJITA
Associate Professor
Nagoya University
Nagoya, Japan

Tateo Kajita, born 1942, received his degree of Dr.Eng.. in 1971 at Nagoya University. He has worked at Nagoya University as associate professor for 14 years.

Kohki NINOMIYA
Research Associate
Nagoya University
Nagoya, Japan

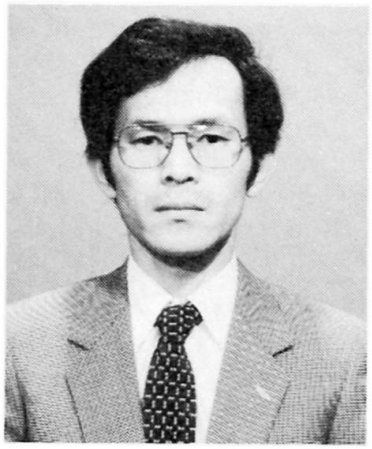

Kohki Ninomiya, born 1951, received his degree of Dr.Eng. in 1986 at Tokai University. He has worked at Nagoya University as research associate for 8 years.

SUMMARY
Structural behavior of cable-stayed and box girder bridges in fire environments is estimated numerically on the assumption that the ship runs against the bridge pier, or the ship collides with another ship under the bridge. Heat radiation from the fire to the surfaces of the girder is calculated by the finite element method. Thermal deformation of the bridge is evaluated by thermo-elasto-plastic finite element analysis, in which various combinations of bridge type and location of fire are compared.

RÉSUMÉ
Le comportement d'un pont à haubans et d'un pont en poutre-caisson dans un incendie est étudié dans les cas d'une collision d'un navire avec une pile du pont ou avec un autre navire sous le pont. L'échange de chaleur par radiation entre la source de chaleur et les surfaces de poutre est calculé par la méthode des éléments finis. La déformation thermique du pont est évaluée sur la base de l'analyse thermo-élasto-plastique des éléments finis, dans laquelle combinaisons du type du pont et la location du feu varient.

ZUSAMMENFASSUNG
Unter der Voraussetzung, daß ein Schiff an einen Brückenpfeiler prallt, oder daß zwei Schiffe unter der Brücke zusammenstoßen, wurde das Tragverhalten von Schragseilbrücken (Zx) und der Kastenträgerbrücken numerisch untersucht. Die Wärmestrahlung vom Feuer an den Brückenträger wurde mit der Methode der finiten Elementen berechnet. Die thermische Formänderung der Brücke ist in der thermo-elasto-plastischen Analyse erfaßt, wobei die verschiedenen Kombinationen von Brückentypen und Lage des Brandes verglichen werden.

1. INTRODUCTION

Due to an increased construction of long span bridges across a channel, the possibility of ship-fire under bridges cannot be ignored. The ship carrying combustibles such as petroleum and liquefied petroleum gas may run against a bridge pier, or collide with another ship under the bridge. Bridge deformation under such circumstances are numerically evaluated here. Object of numerical calculation are cable-stayed and box girder bridges with central span of 160 meters. Heat radiation from fire to the surfaces of the girder is calculated by FEM. Thermal deformation of the bridge is calculated also by thermo-elasto-plastic FE analysis, in which various combination of bridge type and location of fire are taken into account.

2. TYPE OF BRIDGES

Cable-stayed and box girder bridges as shown Fig.1 are considered in the article. In order to show the difference of stress state and deformation, we assume that both bridge sections be continuous girder, having span of 60m+160m+60m, with variable cross-section. These bridges are roughly designed according to allowable stress design considering dead and traffic loads. Cross-section at the span center is indicated in Fig.2 as a representative. In the case of cable-stayed bridges, the effect of cable sag is approximately evaluated by modified Young's modulus provided by Ernst, and towers are assumed to be stiff.

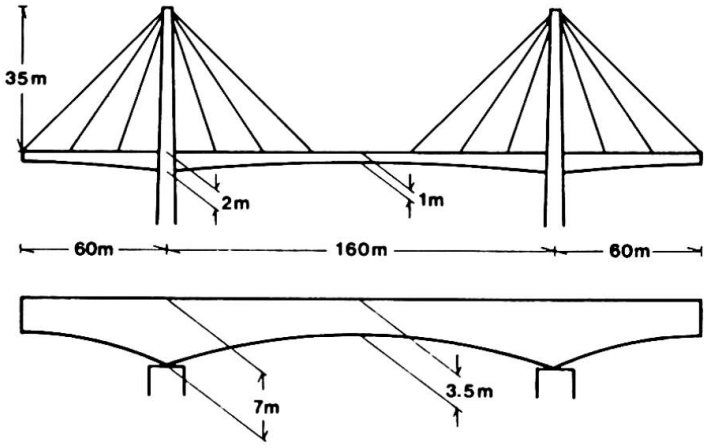

Fig.1 Bridge types.

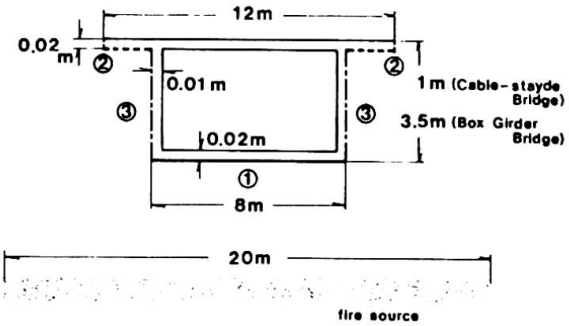

Fig.2 Cross-section at the span center of bridges.

3. HEAT TRANSFER ANALYSIS

3.1 Heat Transfer from Fire to Bridge

Heat transfer from fire source to the structural members in the building fire is conducted by heat radiation and convection [1-6]. For such cases, heat capacity can be put into members by "heated air to surface" transition, because the room is filled with heated air and flame as in a furnace. However, the bridge fire, inflow of heat is conducted through surfaces of the girder by "surface (heat-source) to surface" transition, because the bridge is no more than a strip of plate placed on an open space. Thus, heat capacity is not constant along the bridge, and should be determined by the horizontal and vertical distance between different parts of girder and fire source.

In this work, heat transfer between different parts of girder (called girder segments) and fire source is conducted only by heat radiation. The phenomenon can be defined analytically by heat radiation between girder segment and fire source as

gray bodies; and spatial relation between the two is represented by a geometrical factor. On the contrary, in recent years, radiation-convection interaction has been formulated based on the continuum mechanics by limiting to the enclosed space problem [7]. However the procedure has not yet been so developed to be applied to the open space problem, even if we ignore the effect of wind.

Let the size of fire source be 20mx20m. Since the width of lower flange member (8m) is less than the width of fire (20m) as shown in Fig.2, inflow of heat is conducted by radiation through three surfaces, that is, ① bottom surface of lower flange, ② bottom surface of upper flange which is not screened by webs and lower flange, and ③ side walls of webs.

Let the fire source be placed directly beneath the bridge. Conserning the location of fire source, two cases are considered as shown in Fig.3, that is, (a) left end of central span on the supposition that the ship runs against bridge pier, and (b) center of central span on the supposition that the ship collides with another ship under the bridge. Also for the distance between bridge and fire source, two cases are considered as shown in Fig.3, that is, (a) 10m (river) and (b) 30m (channel).

3.2 Heat Radiation between Two Surfaces

Fig.4 shows a spatial relation between girder segment and fire source for the inflow of heat through bottom surface of lower flange. Inflow of heat for the n-th girder segment Q_n is represented by

$$Q_n = C_{1f}(\sigma_0 \varepsilon_s \varepsilon_f / \pi)(T_f^4 - T_{sn}^4) \tag{1}$$

in which geometrical factor C_{1f} is as follows:

$$C_{1f} = \iiiint (Z_n - x_2 \sin\phi_n)\{Z_n + \tan\phi_n (X_n - x_1)\}\cos\phi_n / R^4 \cdot dx_1 dx_2 dy_1 dy_2$$

In Eq.(1), $\sigma_0 = 4.88 \times 10^{-8}$kcal/m^{2}h°K^4 is coefficient of Stefan-Boltzmann, $\varepsilon_s = 0.5$ and $\varepsilon_f = 0.7$ are emissivities of heated air and steel, respectively. X_n, Z_n are horizontal and vertical distance between center of girder segment and fire source, respectively, ϕ_n is inclination of girder segment, T_{sn} and T_f are temperature of the n-th girder and fire source, which is substituted by the standard fire time-temperature curve. x_1, x_2, y_1, y_2 are local co-ordinates, R is expressed as under:

$$R^4 = \{(X_n + x_2 \cos\phi_n - x_1)^2 + (y_2 - y_1)^2 + (Z_n - x_2 \sin\phi_n)^2\}^2$$

Longitudinal and cross-sectional distribution of geometrical factor of lower flange (C_{1f}) are calculated by Eq.(1). The rest of geometrical factors corresponding the upper flange and webs (C_{uf} and C_w) are also evaluated in the same manner as Eq.(1).

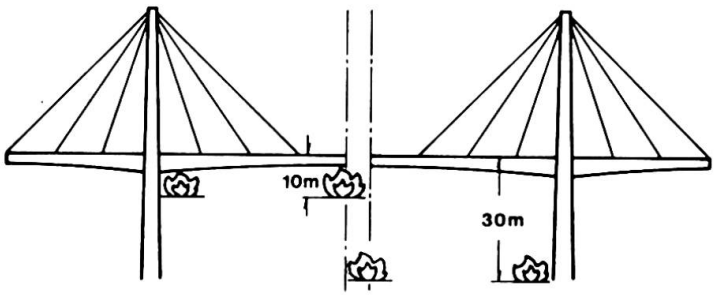

Fig.3 Locations of fire.

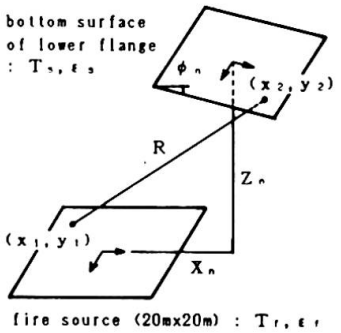

Fig.4 Heat radiation between two surfaces.

3.3 FE Analysis

Prior to a series of calculations, heat conduction in the longtitudinal direction is compared with that in the cross-sectional direction. The result shows that the former is negligibly small compared with the latter. It implies that the thermal distribution inside the girder cross-section can be calculated with good accuracy by using two-dimensional FE analysis.

Central span of the bridge is cut into 32 girder segments, and the typical cross-section of each segment is discretized by using three node three degrees-of-freedom triangular elements. Inflow of heat for each segment is evaluated by using geometrical factors according to the spatial relation between girder segment and fire source. Coefficient of heat conductivity and specific heat of steel follow the CTICM's recommendations. Integration by time is carried by the Crank-Nicholson method, and the temperature distributions of cross-sections are calculated at intervals of 0.05 hours (3 minutes).

Thermal deformations are calculated numerically in the combined cases of the following three parameters. Table of short signs representing the combination of (1), (2) and (3) are indicated in the Table 1.

(1) Bridge type : cable-stayed bridge / box girder bridge
(2) Location of fire source : bridge center / pier side
(3) Distance between bridge and fire : 10 meters / 30 meters

Maximum temparature for all cross-sections in the longitudinal direction are indicated in Fig.5. Temperature distribution at the span center in every hour after a break of fire is shown in Fig.5 for the case of (1) cable-stayed bridge, (2) bridge center and (3) 10 meters.

4. THERMO-ELASTO-PLASTIC ANALYSIS

4.1 Material Properties

Let the material be SS41 steel whose nominal strength is 41kg/mm^2 (402MN/m^2). Due to the previous studies including material tests [3-6], the writers have presented material properties as function of temperature, which is distinct from CTICM's recommendations. That is, modulus of elasticity (E), yield strength (σ^Y), work-hardening parameter ($H=d\sigma^H/d\varepsilon^{ip}$; slope of tangent of instantaneous stress-strain curve) and coefficient of thermal expansion (α) are expressed as follows:

$$E(\theta)=E_0 \quad (\theta \leqq 350℃), \qquad E_0(-0.26\theta+271)/180 \quad (\theta>350℃)$$

$$\sigma^Y(\theta)=\sigma^Y{}_0 \quad (\theta \leqq 200℃), \qquad \sigma^Y{}_0(0.0002\theta^2-0.33\theta+142)/84 \quad (\theta>200℃)$$

$$H(\theta,\varepsilon^{ip})=H_1(\theta)/[\varepsilon^{ip}+\exp\{-H_2(\theta)/H_1(\theta)\}]$$

$$H_1(\theta)=800/(\theta-250)-0.5, \qquad H_2(\theta)=10000/(\theta-164)-7.3$$

$$\alpha(\theta)=1.45\times10^{-9}\theta+1.32\times10^{-5}-3{,}85\times10^{-4}/\theta$$

where E_0(=198 GN/m^3) and $\sigma^Y{}_0$(=281 MPa) are those at room temperature ($\theta=20℃$), and ε^{ip} is instantaneous plastic strain. By using these properties, and ignoring the effect of creep, good approximation in deformation analysis using FEM has been obtained [5].

4.2 FE Analysis and Numerical Results

A three node seven degrees-of-freedom beam-column element is used here under the Bernoulli-Euler's assumption and the additional assumptions such as in-plane and small deformation. Thermal and creep (ignored here) deformations are treated as initial deformation, and the modified incremental method is employed in the non-linear iterative calculation. Stress increment due to work-hardening is decided by assuming von Mises-type yield criterion with isotropic work-hardening [4-6].

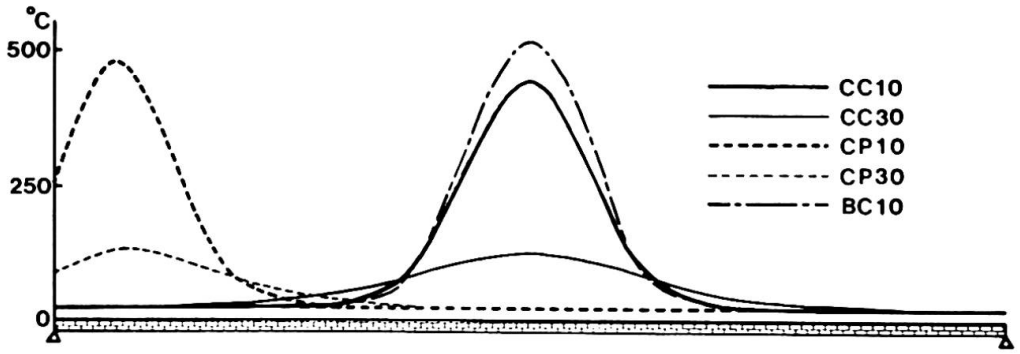

Fig.5 Temparature distribution of central span at two hours after fire breaks out.

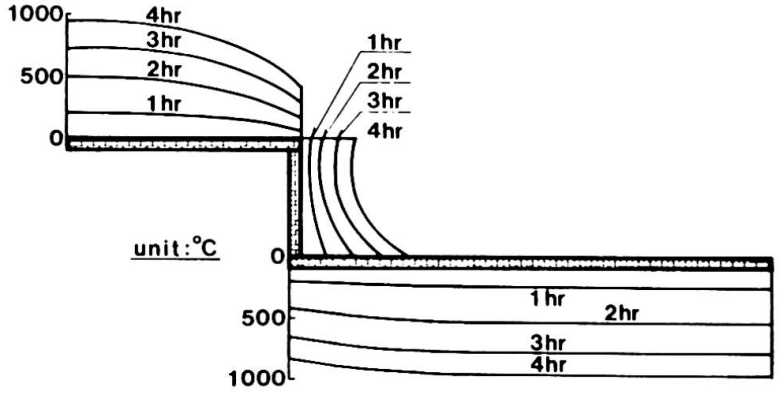

Fig.6 Temperature distribution of cross-section at every one hour (CC10).

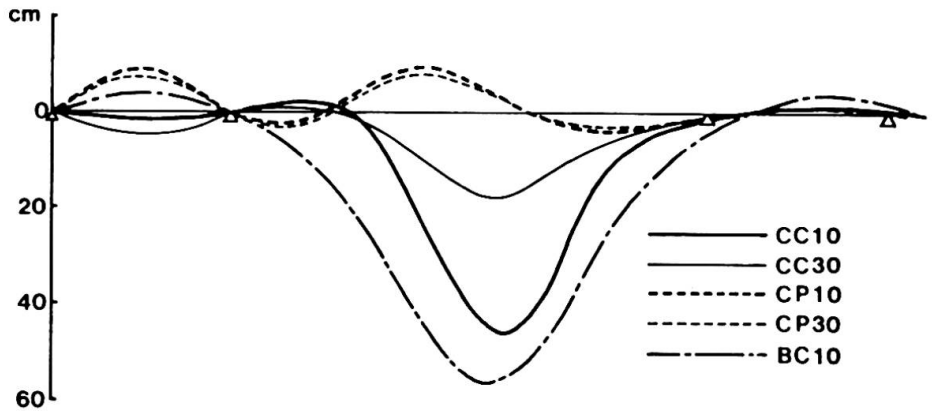

Fig.7 Deformation of bridges at two hours after fire breaks out.

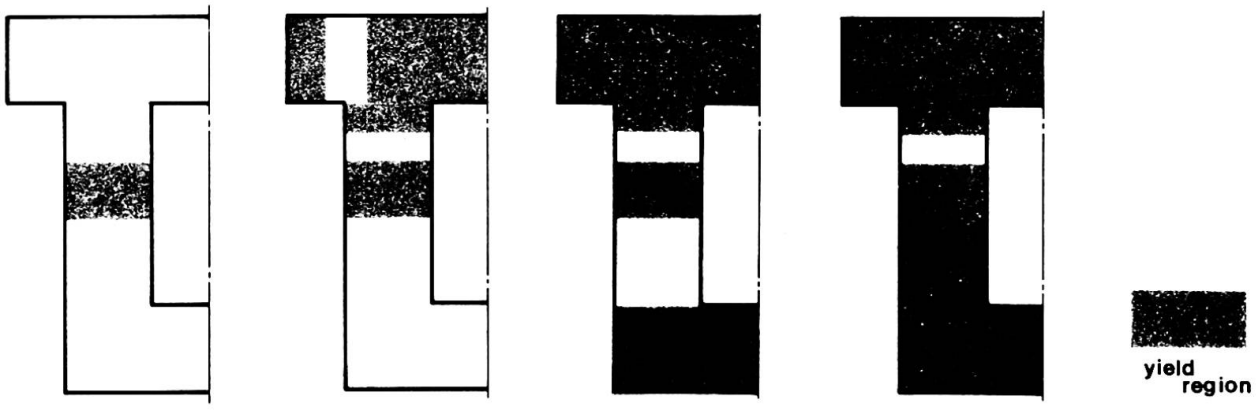

Fig.8 Progress of yield region in cross-section at every one hour (CC10).

Table 1 Endurance time of the bridge.

combination	short sign	endurance time (min.)
box girder center,10m	BC10	165
cable-stay center,10m	CC10	189
cable-stay pier, 10m	CP10	222
cable-stay center,30m	CC30	>240
cable-stay pier, 30m	CP30	>240

Concerning the external load during the fire, the live load is excluded from analysis, because no traffic will across the bridge during the fire.

Distributions of vertical deformation in the longitudinal direction are indicated in Fig.7. Progress of yield region after a start of fire is also shown in Fig.8 in the same case as the cross-sectional temparature. Endurance time of the bridge during fire is provided in Table 1.

5. CONCLUSIONS

The following conclusions have been obtained:

(1) Concerning the effect of bridge type on the structural behavior in fire, the "cable-stayed" type is stronger than the "box girder" type. However, the result may not be due to the difference of bridge type directly. It is due to the difference of temperature caused by the difference of vertical distance between fire and lower surface of the girder;

(2) Concerning the effect of longitudinal location of fire on the structural behavior, "center fire" causes serious effects on the bridge compared with "side fire";

(3) Concerning the effect of vertical distance between bridge and fire on the structural behavior in fire, there is a serious effect on the bridge only in the case of "height=10 meters". These results are only valid for a four hour fire.

REFERENCES

1.BABA S., KAJITA T., Out-of-Plane Deformation of Steel Frame in Fire, Proc.of Int.Conf.on Computing in Civil Engng., New York, May 1981, pp.343-358.
2.BABA S., YAMAMOTO T., Strength of Steel Frame Structures in Fire, Final Rep.of IABSE Symp., Venezia, Sept.1983, pp.243-250.
3.BABA S., NAGURA H., Effect of Material Properties on the Deformation of Steel Frame in Fire, Proc.of JSCE, April 1985, pp.47-57.
4.BABA S., NAKADA N., Time Dependent Deformation of Steel Structure in Fire, Proc. of Int.Conf.on Numer.Meth.for Non-Linear Problems, Dubrovnik, Sept.1986, pp.536-549.
5.BABA S., NAKADA N., Steel Frame Structures in Fire — Effect of Creep and Work-hardening, Proc.of Int.Conf.on Steel Structures, Budva, Sept.1986, pp.89-97.
6.BABA S., NAKADA N., SEGI K., Deformation and Strength of Steel Frame Structure in Fire Environments (in Japanese), Proc.of JSCE, April 1987, pp.303-310.
7.CHANG L.C., YANG K.T., LLOYD J.R., Radiation-Natural Convection Interactions in Two-Dimensional Complex Enclosures, Trans.of ASME, J.of Heat Transfer, February 1983, pp.89-95.

Stability of a Stone Arch Bridge against Flood Pressure and its Preservation

Stabilité de ponts arcs en pierre sous la pression des flots lors d'innondations et leur préservation

Stabilität von Steinernen Bogenbrücken bei Hochwasser und deren Instandhaltung

Yasunori KONISHI
Prof. Dr.-Eng.
Nagasaki Univ.
Nagasaki, Japan

Yukio MAEDA
Prof. Dr.-Eng.
Kinki Univ.
Higashi-Osaka, Japan

Akira MUROTA
Prof. Dr.-Eng.
Osaka Univ.
Suita, Osaka, Japan

Yasunori Konishi, born in 1926, received his B.E. and Dr.-Eng. from Osaka University. Since 1977 he has been Professor of Structural Engineering. Nagasaki University.

Yukio Maeda received his B.E. at Hokkaido Univ. and Dr.-Eng. at Univ. of Tokyo. In 1985 he retired from Osaka Univ., awarded Professor Emeritus of Osaka Univ. Since 1985 he is Prof. of Structural Eng. at Kinki Univ. At Present he is serving IABSE as Chairman of Technical Committee.

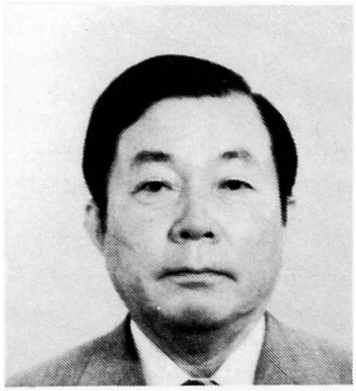

Akira Murota, born in 1927, received his B.E. and Dr.-Eng. from Osaka University. Since 1964 he has been Professor of hydraulics. Osaka University.

SUMMARY

Dynamic water pressure caused by the rapid flood water which hit Nagasaki, Japan, in 1982, took away the spandrels and railings of the Momotani, Megane and Fukuro Bridges of stone arch, but their arch stones remained. Six other bridges of a similar type were completely destroyed. To measure the hydrodynamic pressure which caused great damage to the stone arch bridges, two stone arch models of the Fukuro Bridge were tested in a testing channel. Based on the test results, the stability of a stone arch bridge against flood pressure and its preservation are discussed in this paper.

RÉSUMÉ

La pression hydrodynamique, engendrée par le débit de flots rapides, qui frappa Nagasaki au Japon, en 1982, emporta les voûtes et les garde-corps de plusieurs ponts arcs massifs mais leurs pierres d' arche demeurèrent intactes. Six autres ponts du même type furent complètement détruits. Pour mesurer la pression hydrodynamique ayant endommagé les ponts arcs en pierres, deux modèles réduits d' arcs en pierre du pont de Fukuro ont été testes dans un canal d' essai. Sur la base des résultats des tests, la résistance des ponts en arcs pierre contre la pression des flots et sa préservation sont discutés dans ce document.

ZUSAMMENFASSUNG

Die dynamischen Drücke schnell-strömender Hochwasserfluten, von denen Nagasaki, Japan 1982, betroffen wurde, rissen die Bogenfüllungen und die Fahrbahn der Momotani-, Megane- und Fukuro-Brücken weg, liessen aber Steinbögen stehen. Sechs weitere Brücken ähnlichen Typs wurden völlig zerstört. Um die für die Zerstörung der steinernen Bogenbrücken verantwortlichen dynamischen Wasserdrücke zu messen, wurden zwei Modell-Steinbögen der Fukuro Brücke in einem Testkanal getestet. Basierend auf diesen Testergebnissen wird in diesem Beitrag die Stabilität einer Steinbogenbrücke gegen Hochwasserdruck und ihre Instandhaltung diskutiert.

1. OUTLINE

The present paper is related with exceptional conditions due to extreme flood flow, and discusses experimentally the stability of a stone arch bridge against flood pressure and its preservation. A heavy local downpour hit the Nagasaki area of Kyushu Island in Japan on July 23, 1982, causing a sudden increase of water flow in many rivers, so that the flow reached the superstructures of bridges crossing the Uragami, Nakajima, Hachiro and other rivers. [1)]

In Kyushu, including Nagasaki, Kumamoto and Kagosima prefectures, there still remain many rivers spanned by stone arch bridges. The stone arch bridges were constructed by a traditional method which was one of the most reliable methods of bridge construction, as well proven by many ancient Roman Bridges still stoutly remaining after some two thousand years.

While such stone bridges are a valuable property in the history of building techniques, they were appointed important cultural assets in Japan. In addition, along the River Nakajima, Nagasaki, there are many other stone bridges like Momotani, Oide, Amigasa, Furumachi, Ichiran, Susukihara, Higashi-shin and Fukuro bridges, which were rated as the important cultural properties by the City and have formed the sights of the city.

This Nakajima River, running through the center of Nagasaki City, was struck by the aforementioned local downpour and the flooding occurred which submerged the road surfaces of these stone bridges. Dynamic water pressure generated by the fast flood flow (3.5 m/sec to 4.0 m/sec) took away the arch spandrels and upper railings of the Momotani, Megane and Fukuro bridges, but left the arch stones. Six other bridges were completely destroyed and only some of the bridge foundations were left.

Since these bridges provide the City's road network with arteries, they have been playing an important role in the city transportation, especially as escape ways for emergency or as access for the reconstruction works after a disaster.

The combined forces and moments working on the arch stones, caused by drag, lift, yawing moment, pitching moment and rolling moment were measured through an experimentation of the model stone arch bridge. As a result of calculation of the resistance of the stone arch bridge against flood flow, we confirmed that as far as the Fukuro bridge is concerned the arch stones were stable.

Collapse tests of the flood flow pressure on a stone arch bridge model of the same construction as the actual bridge were also carried out.[2)]

2. EXPERIMENT ON STONE ARCH BRIDGE MODEL

2.1 Model Dimensions and Experimental Facilities

The experiment was carried out by putting a 1/38.5 scale model of the existing Fukuro bridge into the test water channel with the width of 40 cm and the slop of 1/94.14 to reproduce the flood condition. Fig.1 shows a beam instrument used for measuring the loads and Fig.2 shows the construction of the model stone arch.

Load magnitudes on each arch stone ②, ③ . . . . ⑫ were measured by detecting strains with a strain meter on load converters tied by piano wires of 0.5mm to the lift measurement points ①, ②, ③ and ④ and the drag measurement points ⑤, ⑥, ⑦, and ⑧. An alienating paper is inserted in 2mm gap between arch stones illustrated in Fig.1 in order to plug water flow to avoid hydraulic stress and to lower frictional coefficient between stones. The magnitudes and application points of resultant flow forces working on each

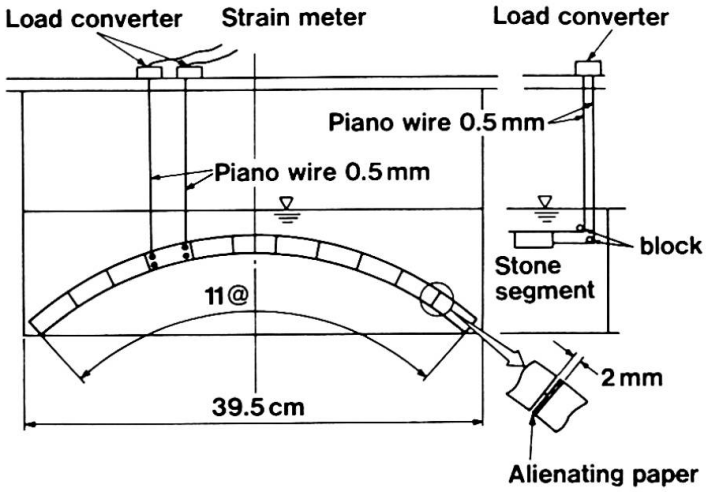

Fig. 1 Illustration of model experimental facilities

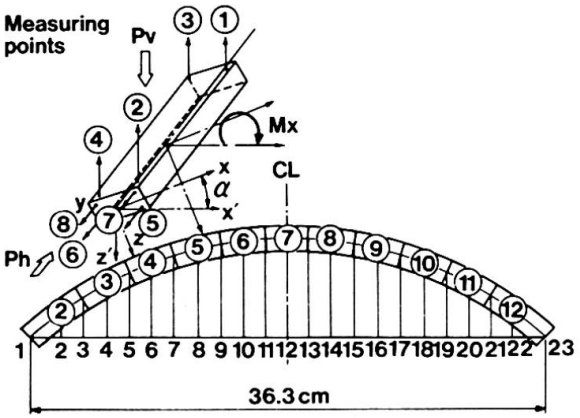

Fig. 2 Fukuro bridge model

arch stone were thus measured, and such external forces determining the limiting hydrodynamic fracture stress on the stone arch bridge as flow pressure, drag, lift (static water pressure + lift), horizontal pressure, yawing moment, rolling moment and pitching moment were computed from the measured values.

Table 1. shows the averge values Fm of the resultant forces measured about fifty times at the measuring points ①~⑧ for the eleven arch stones ② to ⑫. In Table 2, the drag Ph(g), the lift + static water pressure Pv(g), the pitching moment Mx(g-cm), the drag coefficient Cd, the lift coefficient Cl and the static water pressure Ps(g), and the average flow velocity at 90cm of the upper stream U(cm/sec), are given as the values calculated by the three kinds of stresses and the three kinds of moments mentioned above. Although the actual measurement values in Table 1 and Table 2 were in fact not necessarily symmetrical, these were averaged for the convenience of the calculation.

Table 1. Values of Fm

Stone number \ Measuring point	1	2	3	4	5	6	7	8
2	7.38	43.7	2.4	7.0	4.98	6.06	3.97	6.17
3	9.03	33.4	3.0	15.8	8.50	3.22	6.02	7.76
4	16.27	24.7	7.5	16.2	5.53	4.12	7.17	7.05
5	15.21	16.3	11.5	13.0	5.80	3.85	7.57	5.34
6	8.29	9.4	5.3	12.1	3.71	3.84	6.12	6.69
7	7.21	15.7	6.4	12.9	4.15	4.50	2.44	4.35
7A	4.58	13.3	6.0	13.8	1.16	1.29	1.49	2.79
8	4.89	18.2	9.3	16.2	3.54	3.11	4.32	4.35
9	9.84	11.5	14.3	17.0	5.44	8.60	4.62	6.62
10	6.50	17.4	21.0	22.5	4.22	8.16	4.86	8.10
11	0.80	9.1	13.7	37.2	2.42	4.10	11.54	8.64
12	4.59	9.1	8.9	40.2	6.32	4.58	6.00	5.33

3. STABILITY OF STONE ARCH BRIDGES AGAINST FLOOD FLOW

3.1 Experimental Results and Structural Analysis

A three-dimensional construction illustrated in Fig.2 was analyzed by F.E.M. using the measurement values of the drag Ph(g), the lift + static water

Table 2. P_h, P_v and other parameters (symmetrically rearranged)

Stone number	Ph (g)	Pv (g)	Mx (g-cm)	Cd	Cl	Static water pressure (g)	U (cm/s)
2	21.7	61.6	180.6	1.14	2.01	214.2	85.8
3	26.1	61.0	160.4	1.21	1.15	166.9	90.9
4	24.6	66.0	69.2	1.12	0.59	124.4	87.7
5	23.9	54.4	16.4	0.73	0.23	88.6	106.5
6	17.8	41.9	62.8	0.51	0.16	66.4	111.1
7	11.0	40.0	76.6	0.25	0.13	61.0	111.7

pressure Pv(g) and the pitching moment Mx (g-cm).

Elastic coefficients of the arch stones used for the model arch bridge were measured as follows:

$E=5.76\times10^{4}$ kg/cm^2, Poisson's ratio $\nu=0.18$, $G=2.43\times10^{4}$ kg/cm^2.

The weight of each stone segment was 2.23 g/cm^3 and the underwater coefficient of friction between the arch stones was 0.67. Through the structural analysis it was observed that the axial force Fx(g), the shearing stress Fz(g) and the flexural moment My(g-cm) due to the in-plane arch action, and the shearing stress Fy(g), the torque T(g-cm) and the flexural moment Mz(g-cm) due to the out-of-plane arch action, occurred as indicated in Table 3.

Table 3. Three-dimensional stresses and moments on arch bridge

Number of panel point	Axial load Fx (g)	Shearing stress (out-of-plane) Fy (g)	Shearing stress (In-plane) Fz (g)	Torque T (g-cm)	Flexure in-plane My (g-cm)	Flexure out-of-plane Mz (g-cm)
1	-897.3	119.7	4.2	-163.7	-102.7	-218.2
3	-832.8	98.0	40.5	-25.4	-130.3	115.1
5	-778.1	71.9	50.3	74.0	-54.1	366.7
7	-735.2	47.3	37.6	73.2	23.1	564.4
9	-710.2	23.4	27.4	7.9	61.2	686.4
11	-699.3	5.5	23.5	-16.4	76.7	728.4
13	-699.4	-5.5	18.3	-27.0	76.7	728.4

3.2 Calculation of Stability of Stone Arch Bridges against Hydrodynamic Pressures

Bridge stability against shearing stress τ_1 generated by torque τ_2 due to the in-plane arch action and the shearing stress τ_3 due to the out-of-plane arch action, can be maintained by frictional stress due to the arch thrust. The allowable shearing stress due to the friction is denoted by τ_a.

When the resultant stress of τ_1, τ_2, and τ_3 becomes larger than τ_a the stability of sealing material between arch stones is lost so that they may start rotating or slipping, and finally the bridge will collapse. Fig.3 shows the calculated results, proving that the stability was maintained in the model arch.

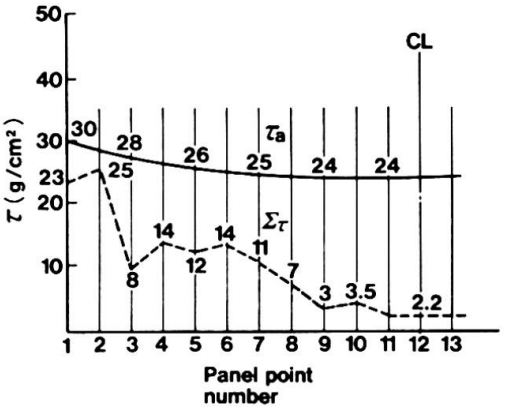

Fig. 3 Results of stability calculation with experimental values

4. COLLAPSE TEST OF MODEL STONE ARCH BRIDGE

For the collapse test under flood flow a model stone arch bridge using the same number of stones as the existing bridge and scaled down to 1/38.5, was installed in the experimental water channel with the 1/94.14 flow slope. The process of collapse was filmed on a video camera.

The road surface and spandrel of the arch bridge were washed away soon after the bridge was submerged, but the arch stones did not collapse. However, after being flooded for a long time, the seal started gradually to slip out and the arch stones to move. Finally, the sealant gap became larger and then the bridge collapsed. The details are shown in Photos 1-3.

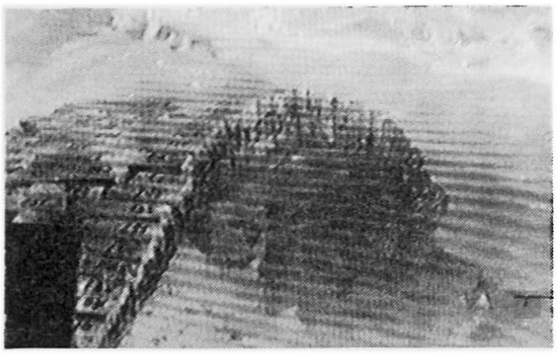

Photo 1 Collase of arch stones

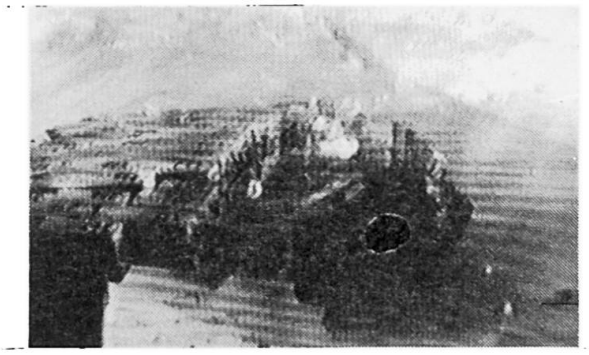

Photo 2 Collase of arch stones

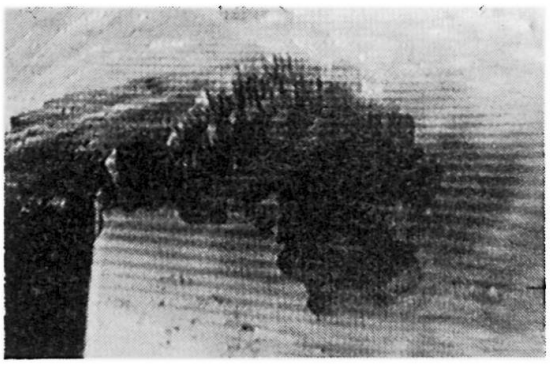

Photo 3 Collase of arch stones

Then, providing with an adhesive between arch stone segments, and making a continuous structure the arch stones may not collapse, and these stone arch bridge as the cultural properties will be able to be preserved against flood pressure.

The Fukuro bridge, only using an epoxy adhesive at the joint of the stones of arch spandrel and of pavemant of the road surface, could maintain the stability of the stone arch bridge against flood pressure. Photos. 4 and 5 show the appearance of Fukuro bridge.

5. CONCLUSIONS

The following conclusions were obtained.

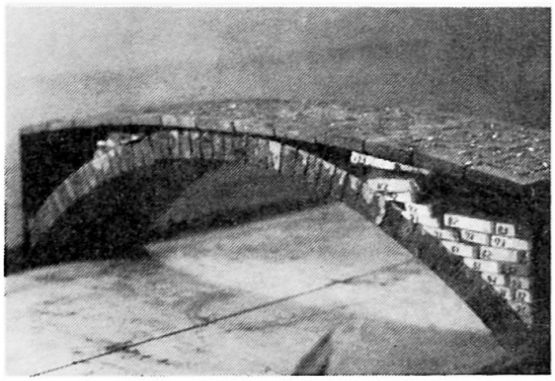

Photo 4 Collapse of arch spandrel of downstream side.

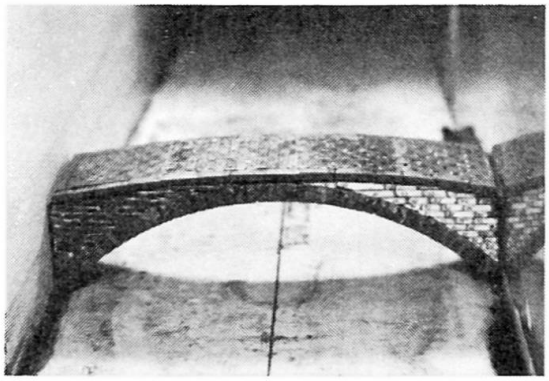

Photo 5 Non collapse of arch spandrel

(1) The experimental flow volume was calculated to be 216 m^3/sec for the actual bridge and this corresponds to 68 % of the flow of 320 m^3/ sec estimated for the flood.
(2) In the test to measure the resultant hydrodynamic forces acting on the arch stones by putting a model stone arch bridge in a reproduced flood flow, a substantial amount of standard deviation was recorded due to the jet stream and due to the existence of cavitation down-stream from the arch stones.
(3) Due to the hydrodynamic forces mentioned above, when the shearing stress caused by torque due to the out-of-plane arch action, the shearing stress due to the in-plane arch action and the shearing stress due to the out-of-plane arch action, exceed the frictional resistance produced by the axial torque of the arch sealing, the sealing between the arch stones will lose the stability, so that they start rotating or slipping and finally the collapse will take place. In the experiment, however, such a collapse did not occur and the arch stones stayed safe.
(4) The arch spandrel of the model stone arch bridge using the same number of stones as the actual bridge was immediately carried away in the collapse test, though the arch stones were not destroyed. However, when left in the flow for a long time, the sealant slipped away, the stone segments also dropped off and the bridge collapsed.
(5) By providing with an adhesive at the joint of the arch stone segments, stone arch bridges will be preserved against flood flow.

REFERENCES

1) konishi, Y. : "A Report on Flood Disaster in July 1982--- Damage to Bridges", A Study Report on National Disasters subsidized by the Scientific Research Fund of the ministry of Education, Japan, pp.109- 116. 1983.
2) Konishi, Y. : "Experimental Study on Effect of Stone Arch Bridge on Flood Flow and its Stability against Flood Pressure," Japan Society of Civil Engineers, Structural Eng./Earthquake Eng. Vol.4. No.1, pp61s-71s.1987.

Brückenschäden durch Anprall von hohen Fahrzeugen

Damage to bridges caused by collision with tall vehicles

Ponts endommagés par la collision de hauts véhicules

Herbert TRÄGER
Dipl.-Ing.
Minist. für Verkehr,
Budapest, Ungarn

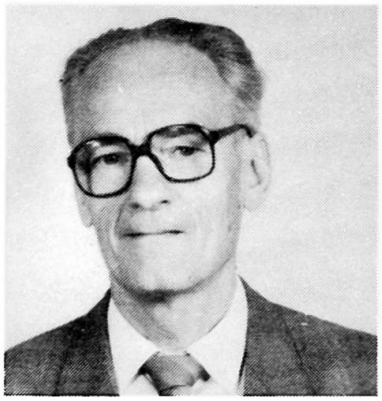

Herbert Träger, geboren 1927, Dipl.-Ing. seit 1949 / TU, Budapest /. Mitarbeiter des Ministeriums für Verkehr, später Leiter der Brückenabteilung, Oberrat. Tätig beim Entwurf, Genehmigung und Ausführung mehrerer grossen Brücken. Verantwortlich für die Angelegenheiten der Strassenbrücken in Ungarn. Dr. techn. seit 1970.

ZUSAMMENFASSUNG
Der Beitrag zeigt einige interessante Schadenfälle, die an Brücken und verschiedenen anderen Konstruktionen durch Anprall hoher Fahrzeuge entstanden sind. Er beschäftigt sich mit dem Verhalten der beschädigten Brücken, mit den Ausbesserungsmethoden und mit Vorbeugungsmethoden solcher Schäden, z. B. Schutzbalken, verschiedene Portale, elektrische Einrichtungen, usw.

SUMMARY
The report shows some interesting cases of damage caused to bridges and other constructions by collision with tall vehicles. It deals with the behaviour of the damaged bridges, with the methods of repair and with prophylactic methods against such damage e.g. protective girders, different types of portals, electric devices.

RÉSUMÉ
L'article présente quelques cas de dégâts dûs à la collision de hauts véhicules sur les ponts et d'autres constructions. Il traite du comportement des ponts endommagés, des techniques de réparation et des systèmes avec lequels on peut prévenir les dommages de ce genre par exemple les poutres de bordure, différents portails, appareillages électriques.

1. EINFÜHRUNG

Auf den Strassen fahren oft Fahrzeuge, deren Höhe die zugelassene Höhe von 4,0 m übertrifft. Es gibt auch Brücken und andere Konstruktionen, wo die lichte Höhe weniger ist, als 4,5 m. Die hohen Fahrzeuge bedürfen einer Sonderbewilligung, die niedrigen Konstruktionen müssen entsprechend beschildert werden. Die zuständigen Behörden bemühen sich einwandfreie Fahrtrouten vorzuschreiben, die laufende Kontrolle der hohen Fahrzeuge auf den Strassen ist aber nicht befriedigend. Im Prinzip ist die Kollision ausgeschlossen, in der Wirklichkeit kommen aber Zusammenstösse sehr oft vor. Die Fahrzeugbesitzer holen die Sonderbewilligung nicht ein, die Fahrer sind oft über die tatsächliche Höhe des Fahrzeuges bzw. der Ladung nicht informiert, oder sie fahren mit zu grosser Geschwindigkeit, ohne auf die Warnschilder zu achten. Es kam auch vor, dass Kipplader mit hoch stehendem Plateau gefahren sind.

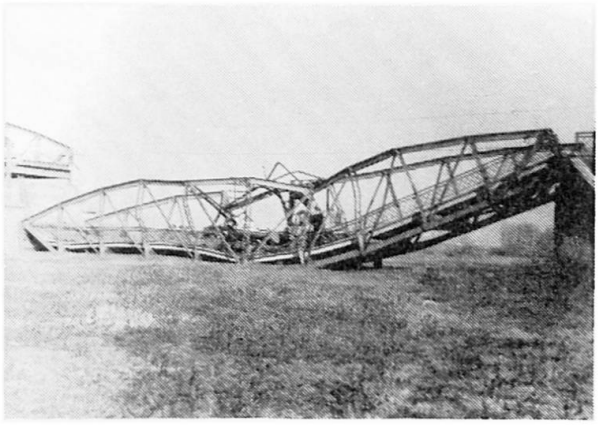

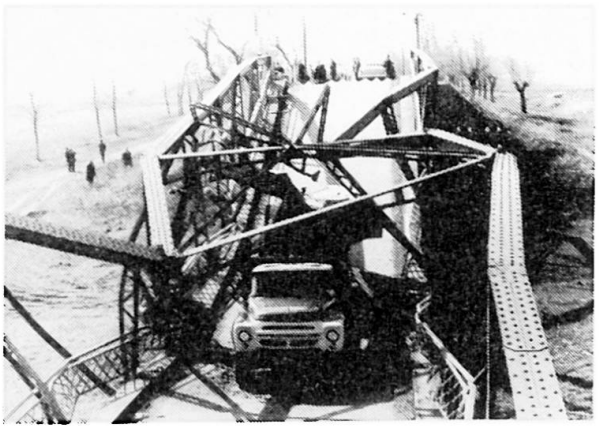

Bild 1.u.2.Eingestürzte Brücke

Die hohen Fahrzeuge gefährden die Windverbände oder Querverbände der Strassenbrücken mit unten liegender Fahrbahn, sowie leichte Brücken, wie kleine Eisenbahnbrücken, Fussgängerbrücken, Gerüste, Förderbandkonstruktionen usw.

In extremen Fällen kann der Anprall katastrophale Folgen gaben. In Ungarn kam es zweimal vor, dass eine Fachwerkbrücke mit unten liegender Fahrbahn sofort einstürzte, eine Fussgängerbrücke wurde weggerissen, und etliche Eisenbahnbrücken wurden in der Querrichtung verschoben. Bei den ersten beiden Fällen stürzten auch die hohen Fahrzeuge in die Tiefe /Bild 1. und 2./ und man muss es als grosses Glück ansehen, dass bisher keine Todesfälle oder schwere Verletzungen zu beklagen waren. Der Sachschaden ist natürlich meistens beträchtlich.

2. BESCHREIBUNG DER SCHÄDEN

2.1 Stahlbrücken

Wenn ein Fahrzeug an den Windverband einer stählernen Brücke stösst, wird der erste Querstab /oft auch mehrere/ stark gekrümmt. Dadurch werden die Hauptträger zueinander gezogen. Sie verlieren ihre Stablität, obwohl die Belastung der Brücke nicht

kritisch ist. Die Formänderung der Hauptträger ist manchmal gering. In einem solchen Fall kann die Brücke durch Richten der Hauptträger und den Einbau neuer Windverbandstäbe wieder instandgesetzt werden. In den erwähnten zwei Fällen war natürlich der Bau neuer Brücken nötig. In einem dritten Fall blieb zwar die Brücke stehen, die Verformung der schon wiederholt beschädigten Konstruktion war aber so gross, dass ein Richten nicht möglich war und die Brücke nach der sorgfältigen Untersuchung abgerissen werden musste. Solche Fälle verursachen natürlich grosse Störungen im Strassenverkehr, weil allgemein langzeitige und weite Umleitungen nötig sind.

2.2 Stahlbetonbrücken

Die Querverbände der Stahlbetonbogenbrücken werden durch nicht sehr hohe Fahrzeuge nur an der Unterkante beschädigt, wo meistens der Beton abgeschlagen wird, manchmal aber auch die Bewehrungsstäbe herausgerissen werden. In den zwei bisher schlimmsten Fällen brach der Stab infolge eines höheren und schnell fahrenden Fahrzeuges an der Stelle der Kollision und neben den Bögen. Im ersten Fall wurde die Stabilität der Bögen provisorisch - mit Holzbalken - gesichert und ein neuer Querverband eingebaut. Im zweiten Fall - wo die Brücke schon knapp vor dem Umbau stand - begnügten wir uns mit dem Zusammenspannen der Bögen durch Einbau von zwei Spannstäben neben dem gebrochenen Querverband.

2.3 Brücken über Strassen

Wenn die Unterkante einer Strassenbrücke durch Anprall angegriffen wird, kann diese meistens nicht weggeschoben werden, sondern die unteren Teile werden stärker oder weniger beschädigt. Zum Beispiel werden die Stahlträger deformiert, deren Reparatur meist möglich ist. Vorgefertigte Spannbetonträger erleiden oft sehr schwere Schäden. Bei einem Anprall rissen z. B. alle Spanndrähte des Randträgers. Hier mussten drei Träger der glücklicherweise ziemlich breiten Autobahnbrücke ausgewechselt werden. In einem ähnlichen Fall, wo die unteren Ebenen der nebeneinander liegenden beiden Brücken in einem Quergefälle angeordnet sind, erlitt der erste und letzte Fertigteilträger Schäden. Am ersten Träger entstanden lange waagerechte Risse im Steg, am letzten wurden nur Abplatzungen an den Kanten bemerkt. Über die Methode der Reparatur wurde hier noch nicht entschieden. /Bild 3./

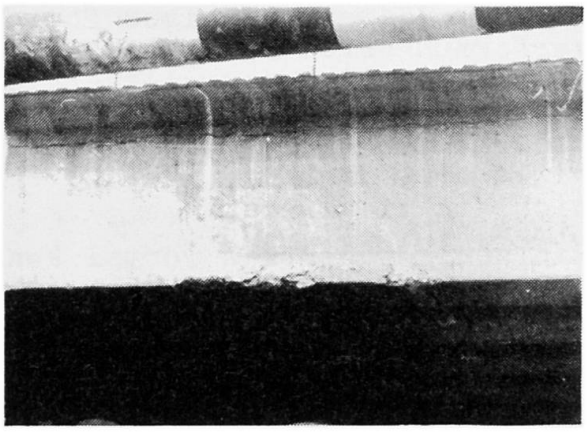

Bild 3. Beschädigter Ferzigteilträger

Eisenbahnbrücken erleiden wiederholt solche Schäden /Bild 4./ und es kommt oft vor, dass das Gleis verschoben wird. Im Ausland verursachte ein solcher Fall eine schwere Zugkatastrophe. In Ungarn war einmal die Reparatur der Brücke gerade beendet, als erneut ein hohes Fahrzeug die Konstruktion beschädigte.

3. VORBEUGUNG DER SCHÄDEN

3.1 Verkehrstechnische Massnahmen

Da die erwähnten Schäden leider sehr oft vorkommen, bemüht man sich natürlich um Massnahmen, solche Unfälle vorzubeugen. Die vorgeschriebenen Warnschilder am letzten Strassenknotenpunkt und bei der Brücke, und das auffällige Schraffieren der Konstruktion bleiben meistens erfolglos, man muss also die Brücken "mit Gewalt" schützen.

3.2 Schutzbalken

Es ist relativ einfach, die leichten Eisenbahnbrücken zu schützen,mit dem Einbau eines in der waagerechten Ebene sehr starren Balkens neben der gefährdeten Unterkante, einige Zentimeter niedriger stehend. Diese Balken sind fest in die Widerlager verankert und sind fähig, die Fahrzeuge durch Verformung abzubremsen bzw. aufzuhalten.

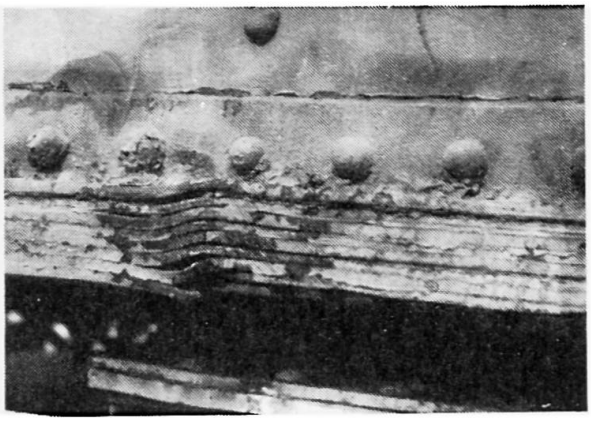

Bild 4. Beschädigter Untergurt einer Eisenbahnbrücke

3.3 Portale

Bei Mehrfeldbrücken und besonders bei den Windverbänden und Querverbänden ist es allgemein nicht möglich, solche Balken anzuordnen, in diesen Fällen sind Schutzportale nötig. Es ist aber nicht einfach, ein prinzipielles System solcher Portale auszuarbeiten.

Ein so widerstandfähiges Portal zu bauen, welches einem Anprall verformungsfrei widerstehen kann, ist praktisch unmöglich. Das Absorbieren der Anprallenergie würde eine sehr komplizierte, teuere und erhaltungsbedürftige Konstruktion benötigen, wie etwa die Prallböcke der Kopfbahnhöfe der Eisenbahn, die Anprallkraft wirkt aber hier cca viermal höher. So kommt auch diese Lösung nicht in die Frage.

Ein weniger starkes Portal kann beim Anprall umkippen. Das gefährdet die Fahrzeuge, die in der Gegenrichtung fahren. Bisher haben sich solche Portale bewährt, wo der starre waagerechte Balken viel höher liegt, als die Konstruktion, die zu schützen ist, und von diesem hängen Teile bis zur entsprechenden Höhe herunter. Diese Teile können Ketten /nur Warnung/, Doppelbleche /Warnung durch Schalleffekt/ oder deformierbare Elemente sein. Im letzten Fall wird der Fahrer durch die Deformation dieser Elemente und der Ladung /Schall- und Bremseffekt/ auf die nicht zugelassene Höhe des Fahrzeuges aufmerksam gemacht. Die Portale müssen so weit vor der Brücke aufgestellt werden, dass genügend Bremsweg vorhanden ist. Hinter dem "Warnportal" ist eine Ausweichspur zweckmässig, auf die das hohe Fahrzeug vor der kritischen Brücke ausweichen kann. Es ist aber meistens nicht möglich, diese Spur auszubauen. Wenn das Ausweichen nicht möglich ist, so kann das hohe Fahrzeug nur durch Rückwertsfahren oder - wenn die Fahrzeughöhe nur wenig grösser ist, als die lichte Höhe - durch Weiterfahren nach Verminderung des Luftdruckes in den

Reifen den Ort verlassen.

Versuchsweise wurde einmal ein solches Portal aufgestellt, wo eine abhängende, ziemlich schwere Stahlkonstruktion beim Anprall ausschlägt und dann in die ursprüngliche Lage zurückfällt /Bild 5./. Die Erfahrung zeigt, dass diese Konstruktion - neben den verhältnismässig hohen Baukosten - nicht wirksamer ist, als z. B. ein Portal mit herabhängenden Doppelblechen.

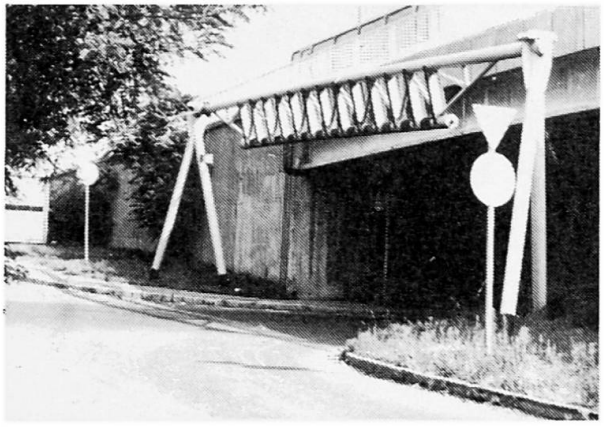

Bild 5. Portal mit ausschlagender Stahlkonstruktion

3.4 Elektrische Einrichtungen

In den letzten Jahren bemüht man sich in Ungarn mit der Konzipierung elektrischer Schutzeinrichtungen. Es bestehen aber juristische bzw. verkehrstechnische Probleme. Nach der Vorstellung sollen vor der Brücke - in einer etwas grösseren Entfernung als der Bremsweg - zewi Pfosten mit einer Lichtquelle bzw. einer Photozelle aufgestellt werden. Wenn der Lichtstrahl durch das hohe Fahrzeug unterbrochen wird, erscheint an der Brücke ein Warnlicht und ein Schild: "Einfahrt für Fahrzeuge mit der Höhe über.....m verboten".

Die Probleme sind folgende:

- ein rotes Licht ist nur dann erlaubt, wenn die Ampel im Normalfall gelbes Blinklicht ausgibt;
- die Stromversorgung ist problematisch, wenn die Brücke weit von den Ortschaften entfernt liegt;
- wie lange soll das rote Licht und das erwähnte Schild leuchten?
- das rote Licht ist auch für andere Verkehrsteilnehmer gültig;
- das Erlöschen des roten Lichtes kann als "Genehmigung" für die Weiterfahrt erklärt werden.

Die Lösung der erwähnten Probleme und im allgemeinen der Schutz der gefährdeten Brücken ist eine wichtige zukünftige Aufgabe.

4. VON DER FAHRSPUR AUSWEICHENDE FAHRZEUGE

Neben den hohen Fahrzeugen möchte ich noch kurz diejenige Fahrzeuge erwähnen, die die vorgeschriebene Fahrspur verlassen. Auf einer stählernen Langer-Konstruktion verursachte ein Fahrzeug nach einer unzulässigen Überholung schwere Schäden an einem Hängestab. An einer Fachwerkbrücke beschädigte die hohe Ladung nach dem Abbruch des Schutzportals abrutschend vom Fahrzeug einen Stab des Hauptträgers.

Das Durchbrechen der Geländer führt oft zum Absturz des Fahrzeuges, was nicht nur für das erwähnte Fahrzeug, sondern auch für die Verkehrsteilnehmer der unteren Fahrbahn eine grosse Gefahr bedeutet. Solche Unfälle können mit technischen Massnahmen

nicht verhindert werden, weil die Geländer nicht in der Lage sind, ein schweres Fahrzeug zurückzuhalten. Neben den Hängestäben ist kein Platz für eine Schutzeinrichtung vorhanden.

5. SCHLUSSWORT

Die hier diskutierten Probleme können am besten durch die Verbesserung der Verkehrsdisziplin gelöst werden. Die Veröffentlichung der Schadensfälle kann dazu beitragen.

Ausländische Erfahrungen über Details der Schadensfälle und über Schutzeinrichtungen liegen uns nicht vor.

Leere Seite
Blank page
Page vide

Leere Seite
Blank page
Page vide